University of Alberta

Radar Remote Sensing of River Ice on the Athabasca River at Fort McMurray, Alberta

by

©

Kristel Pelletier

A thesis submitted to the Faculty of Graduate Studies and Research in partial fulfillment of the requirements for the degree of Master of Science

In

Water Resources Engineering

Department of Civil and Environmental Engineering

Edmonton, Alberta
Spring 2006

Library and
Archives Canada

Published Heritage
Branch

395 Wellington Street
Ottawa ON K1A 0N4
Canada

Bibliothèque et
Archives Canada

Direction du
Patrimoine de l'édition

395, rue Wellington
Ottawa ON K1A 0N4
Canada

Your file Votre référence
ISBN: 0-494-13872-6
Our file Notre référence
ISBN: 0-494-13872-6

NOTICE:
The author has granted a non-exclusive license allowing Library and Archives Canada to reproduce, publish, archive, preserve, conserve, communicate to the public by telecommunication or on the Internet, loan, distribute and sell theses worldwide, for commercial or non-commercial purposes, in microform, paper, electronic and/or any other formats.

The author retains copyright ownership and moral rights in this thesis. Neither the thesis nor substantial extracts from it may be printed or otherwise reproduced without the author's permission.

AVIS:
L'auteur a accordé une licence non exclusive permettant à la Bibliothèque et Archives Canada de reproduire, publier, archiver, sauvegarder, conserver, transmettre au public par télécommunication ou par l'Internet, prêter, distribuer et vendre des thèses partout dans le monde, à des fins commerciales ou autres, sur support microforme, papier, électronique et/ou autres formats.

L'auteur conserve la propriété du droit d'auteur et des droits moraux qui protège cette thèse. Ni la thèse ni des extraits substantiels de celle-ci ne doivent être imprimés ou autrement reproduits sans son autorisation.

In compliance with the Canadian Privacy Act some supporting forms may have been removed from this thesis.

While these forms may be included in the document page count, their removal does not represent any loss of content from the thesis.

Conformément à la loi canadienne sur la protection de la vie privée, quelques formulaires secondaires ont été enlevés de cette thèse.

Bien que ces formulaires aient inclus dans la pagination, il n'y aura aucun contenu manquant.

Canada

Abstract

Every year during river breakup, communities across Canada are threatened by the risk of ice jam flooding, endangering both property and lives. Such events can occur quite suddenly and it is difficult to predict their occurrence and severity. Forecasters are primarily reliant on aerial reconnaissance to monitor breakup progression. However, this can be expensive and time consuming. The purpose of this investigation was to examine whether SAR (RADARSAT-1) satellite imagery could be used to complement these efforts. Its viability was explored using a case study of the Athabasca River near Fort McMurray. Data collected in 2003 and 2004 was employed to establish whether it might be possible to identify the location and length of ice jams and, further, to evaluate if information regarding ice texture or thickness could be deduced from satellite imagery. The potential of SAR to discern ice conditions and its limitations are discussed.

Acknowledgement

Funding for this study was generously provided by Alberta Environment as well as the Natural Sciences and Engineering Research Council of Canada (NSERC) through the MAGS (Mackenzie Gewex Study) Research Network. I would like to thank Chandra Mahabir and Larry Garner in particular for their help and support in the field. Furthermore, NSERC and Alberta Ingenuity generously provided scholarship funding and the Canada Centre for Remote Sensing donated satellite imagery and supported the field program. All of this support is most gratefully acknowledged.

I would also like to recognize my examiners, Dr. Thian Gan and Dr. Benoit Rivard for reviewing this thesis and providing valuable feedback. I know that this submission will be a stronger contribution because of their efforts. Joost van der Sanden at the Canada Centre for Remote Sensing proved to be a valuable resource to me throughout this project. His helpfulness and support with respect to image processing and interpretation are greatly appreciated.

An incredible team of people worked with me to collect ground truth data for this body of research. Some regularly flew the study reach of the Athabasca River to photograph and document ice conditions during river breakup while others endured the cold February weather to collect ice thickness and structure data. These individuals include Twyla Kowalczyk, Evan Friesenhan, Robyn Andrishak, Karen Dow, Claudine Robichaud, Carin Meliefste and Sheldon Lovell. Also, Perry Fedun provided technical support. This is gratefully acknowledged.

I would also like to acknowledge my supervisor, Dr. Faye Hicks, for her valuable direction and insight. She supported my selection of a somewhat unconventional topic and developed an enthusiasm for the subject which persisted even in those times when my own was lacking. Most of all, though, I am grateful for her advice, mentorship and friendship. I know that, as a result, I am taking away from this experience a positive attitude and outlook which will serve me throughout my life.

There are many who have supported me on a much more personal level throughout this crazy adventure. My friends and family continued to encourage me throughout my education and simply refused to consider that I might not succeed. To Mom and Diane, you were always there to provide a much-needed reality check: please know that I love and appreciate all that you do. To Eric, your unconditional love and support mean more than you will ever know. Thank you for your patience and understanding.

TABLE OF CONTENTS

1.0 INTRODUCTION 1

2.0 LITERATURE REVIEW 5

2.1 Introduction 5

2.2 Radar Backscatter 7
- 2.2.1 The Radar Equation 7
- 2.2.2 Speckle 8
- 2.2.3 Target Parameters Affecting Radar Return 10
- 2.2.4 Illumination Parameters Affecting Radar Return 12
- 2.2.5 Geometric Considerations 13

2.3 Introduction to River Ice Processes 14
- 2.3.1 River Ice Freezeup 14
- 2.3.2 River Ice Breakup 15

2.4 Previous Investigations 16
- 2.4.1 Burntwood River, Manitoba (LeConte and Klassen 1991) 16
- 2.4.2 St. Marys, Connecticut and White Rivers (Gatto 1993) 17
- 2.4.3 Moose River, Ontario (Murphy et al. 2001) 18
- 2.4.4 Mississippi River, Missouri and Missouri and Red Lake Rivers, North Dakota (Tracy and Daly 2003) 20
- 2.4.5 Peace River, Alberta (Weber et al. 2003; Jasek et al. 2003) 20
- 2.4.6 Saint-François River, Quebec (Gauthier et al. 2001; Gauthier et al. 2003) 22
- 2.4.7 Peace River, Alberta (Gherboudj et al. 2005) 23
- 2.4.8 Sagavanirktok River, Alaska (Duguay et al. *In press*) 25

2.5 Summary 26

3.0 MONITORING BREAKUP: QUALITATIVE ANALYSIS 39

3.1 Introduction 39

3.2 Study Area 39

3.3 Methods 40
3.3.1 Field Observations 40
3.3.2 Image Processing 40

3.4 Breakup 2003 43
3.4.1 Field Observations 43
3.4.2 Results 44
3.4.3 April 8, 2003 44
3.4.4 April 15, 2003 44
3.4.5 April 18, 2003 44
3.4.6 April 21, 2003 46
3.4.7 April 22, 2003 (07:28:45) 46
3.4.8 April 22, 2003 (18:55:28) 47
3.4.9 April 25, 2003 48

3.5 Breakup 2004 48
3.5.1 Field Observations 48
3.5.2 Results 48
3.5.3 April 9, 2004 49
3.5.4 April 12, 2004 49
3.5.5 April 15, 2004 49
3.5.6 April 19, 2004 50
3.5.7 April 26, 2004 50

3.6 Summary 51

4.0 MONITORING BREAKUP: QUANTITATIVE ANALYSIS 94

4.1 Introduction 94

4.2 Backscatter Variability Analysis 94
4.2.1 Factors affecting Radar Return 94
4.2.2 Methods 95
4.2.3 Results 95

4.3 Ice Thickness Investigation 98
4.3.1 Methods 98
4.3.2 Limitations 99
4.3.3 Preliminary Investigation, April, 2003 99
4.3.4 Field Study, February 2004 101
4.3.5 Results 102
4.4 Summary and Discussion 103
5.0 CONCLUSIONS AND RECOMMENDATIONS 123
5.1 Breakup Progression 123
5.2 Sensor Limitations 124
5.3 Image Processing 125
5.4 Future Studies 126
6.0 REFERENCES 128

LIST OF TABLES

Table 2.1 Typical bands utilized by radar systems....................................27

Table 3.1 Image acquisition schedule for 2003 Athabasca River breakup...52

Table 3.2 Image acquisition schedule for 2004 Athabasca River breakup...52

LIST OF FIGURES

Figure 2.1 Side-looking systems. 28
Figure 2.2 Schematic of Synthetic Aperture Radar. 28
Figure 2.3 Radar power density at the surface. 29
Figure 2.4 The significance of dielectric constant on backscatter. 29
Figure 2.5 The effect of ice texture on surface scatter. 30
Figure 2.6 The effect of bubbles, impurities and cracks on volume scatter. 30
Figure 2.7 Scattering model describing the effect of incidence angle on surface scatter (adapted from Farr, 2005). 31
Figure 2.8 Geometrical distortion: foreshortening. 31
Figure 2.9 Geometrical distortion: layover. 32
Figure 2.10 Geometrical distortion: radar shadow. 32
Figure 2.11 Thermal ice cover. 33
Figure 2.12 Thermal ice cover with cracks and bubbles. 34
Figure 2.13 Juxtaposed ice cover. 35
Figure 2.14 Hummocky ice surface. 36
Figure 2.15 Thermally deteriorating river ice cover. 37
Figure 2.16 Breakup ice jam. 37
Figure 2.17 Running ice after ice jam release. 38
Figure 3.1 Athabasca River study reach (adapted from Robichaud, 2003). 53
Figure 3.2 Comparison of original RADARSAT-1 image with the corresponding derived river ice information product. 54
Figure 3.3 Ice conditions in the study reach on April 15, 2003. 55
Figure 3.4 Ice conditions in the study reach on April 18, 2003. 56
Figure 3.5 Ice conditions in the study reach on April 20, 2003. 57
Figure 3.6 Ice conditions in the study reach on April 21, 2003. 58
Figure 3.7 Ice conditions in the study reach on April 21, 2003, 1200h. 59

Figure 3.8 Ice conditions in the study reach on April 22, 2003, 0930h. 60
Figure 3.9 RADARSAT image product of the full study reach captured at 6:41:23 (local time) on April 8, 2003. 61
Figure 3.10 RADARSAT image product of the full study reach captured at 7:37:13 (local time) on April 15, 2003. 62
Figure 3.11 RADARSAT image product of the full study reach captured at 19:12:09 (local time) on April 18, 2003. 63
Figure 3.12 Areas of open water lining the left bank (April 18, 2003). 64
Figure 3.13 An accumulation of ice at the Horse River confluence (April 18, 2003). 65
Figure 3.14 Open water development in the reach near G130 (April 18, 2003). 66
Figure 3.15 Open water development in the reach near G135 (April 18, 2003). 67
Figure 3.16 Open water development in the reach from G140 to Cascade Rapids (April 18, 2003).........68
Figure 3.17 RADARSAT image product of the full study reach captured at 7:57:58 (local time) on April 21, 2003. 69
Figure 3.18 RADARSAT image product of the full study reach captured at 7:28:45 (local time) on April 22, 2003. 70
Figure 3.19 Open water development downstream of Fort McMurray (April 22, 2003). 71
Figure 3.20 Downstream end (toe) of ice jam (April 22, 2003).........72
Figure 3.21 Upstream end (head) of ice jam at Mountain Rapids (April 22, 2003). 73
Figure 3.22 Residual ice at Station G140 and in Cascade Rapids (April 22, 2003). 74
Figure 3.23 RADARSAT image product of the full study reach captured at 18:55:28 on April 22, 2003 during ice run through Fort McMurray. 75

Figure 3.24 RADARSAT image product of the full study reach captured at 7:41:23 (local time) on April 25, 2003. 76
Figure 3.25 Ice conditions in the study reach on April 9, 2004. 77
Figure 3.26 Ice conditions in the study reach on April 12, 2004. 78
Figure 3.27 Ice conditions in the study reach on April 19, 2004. 79
Figure 3.28 RADARSAT image product of the full study reach captured at 7:33:02 (local time) on April 9, 2004. 80
Figure 3.29 Deteriorating ice cover from Cascade Rapids to Crooked Rapids (April 9, 2004). 81
Figure 3.30 Open lead development at Mountain Rapids and deteriorating ice cover near bridge (April 9, 2004). 82
Figure 3.31 RADARSAT image product of the full study reach captured at 19:12:11 (local time) on April 12, 2004. 83
Figure 3.32 Deteriorating ice cover from G135 to G140 (April 12, 2004). 84
Figure 3.33 Ice accumulation at Mountain Rapids (April 12, 2004). 85
Figure 3.34 RADARSAT image product of the full study reach captured at 7:57:57 (local time) on April 15, 2004. 86
Figure 3.35 Open leads developing in study reach from G135 to G150 (April 15, 2004). 87
Figure 3.36 Open water and accumulations developing in study reach (April 15, 2004). 88
Figure 3.37 RADARSAT image product of the full study reach captured at 7:41:22 (local time) on April 19, 2004. 89
Figure 3.38 Remnant ice from Cascade Rapids to Crooked Rapids (April 19, 2004). 90
Figure 3.39 Deteriorating accumulation at Mountain Rapids (April 19, 2004). 91
Figure 3.40 Open water and remnant ice downstream of the townsite (April 19, 2004). 92

Figure 3.41 RADARSAT image product of the full study reach captured at 7:37:12 (local time) on April 26, 2004. 93

Figure 4.1 RADARSAT-1 S1 mode image acquired on April 21, 2003 with the locations of zones in which mean radar backscatter was tracked. 105

Figure 4.2 Mean radar backscatter (σ^0 in dB) during 2003 Athabasca River breakup. 106

Figure 4.3 Daily mean temperature during 2003 Athabasca River breakup 107

Figure 4.4 Estimated daily snowfall during 2003 Athabasca River breakup 107

Figure 4.5 Mean radar backscatter (σ^0 in dB) during 2004 Athabasca River breakup. 108

Figure 4.6 Daily mean temperature during 2004 Athabasca River breakup 109

Figure 4.7 Estimated daily snowfall during 2004 Athabasca River breakup 109

Figure 4.8 Drilling a hole to determine ice thickness. 110

Figure 4.9 Ice thickness gauge. 110

Figure 4.10 Hummocky ice surface at freeze-up jam location 111

Figure 4.11 RADARSAT image product of the full study reach acquired at 6:41:23 on April 1, 2003 112

Figure 4.12 RADARSAT image product of the upper study reach, 22 days before breakup (April 1, 2003). 113

Figure 4.13 Ice conditions at four locations just upstream of Fort McMurray (April 1, 2003). 114

Figure 4.14 Large extent of water present at G130 compared to the more intact ice cover at G135 (April 1, 2003). 115

Figure 4.15 Ice thickness and texture at five locations in the upper portion of the study reach (April 1, 2003). 116

Figure 4.16 RADARSAT image product of the full study reach captured at 6:41:22 (local time) on February 07, 2004 117
Figure 4.17 Locations of transects examined during February field study...... 118
Figure 4.18 Estimated and measured ice thicknesses vs. backscatter coefficient. 119
Figure 4.19 Ice thickness data plotted by transect. 120
Figure 4.20 Averge cross-sectional ice thickness vs. backscatter coefficient. 121
Figure 4.21 Thickness data plotted by ice type. 122

1.0 INTRODUCTION

In cold climates, the presence of ice on rivers and waterways is a reality which has far-reaching implications; it can restrict industrial activity, cause property damage and even threaten human life. The most fundamental hazard of river ice is likely the risk of ice jam flooding. Each spring when northern rivers break up, there is a risk for ice jams to form and cause flooding. The severity of this risk is primarily dependent on whether thermal or dynamic factors dominate breakup processes. In the case of a "thermal" breakup, the ice cover essentially melts in place and there is very little danger of either ice jam formation or ice jam related flooding. Rather, ice jams tend to occur when mechanical processes are predominant. A large runoff event can bring about rising water levels which lift and crack the ice cover, sending large floes downstream in often lengthy ice runs. If an ice run such as this is arrested, the floes will build up and form an ice jam; incoming floes will serve to lengthen and further consolidate this accumulation.

Once an ice jam has formed, there is a significant flood risk to property both upstream and downstream of the accumulation. While it is in place, the accumulation can drastically obstruct the flow, creating a backwater condition upstream. As water levels rise, water and ice can inundate land neighbouring the jam and potentially endanger both property and lives. Further, the increasing pressure within the accumulation (especially if there is no outlet to a local flood plain) combined with a weakening ice cover downstream creates the risk of an ice jam release. The result of such a failure can be a life threatening wave of ice and water, placing downstream communities at severe risk and often causing millions of dollars in flood damage. Who can forget Badger, Newfoundland where a 2 metre high wave flooded the town in 2003? Many other Canadian communities are also at risk due to the nature of breakup on northern rivers: historically, the Hay River in the Northwest Territories, the Saint John River in New Brunswick and the Athabasca River at Fort McMurray, Alberta have all experienced repeated ice jam-induced flooding.

The Athabasca River in Alberta frequently experiences ice jams which have previously caused flooding within the Fort McMurray townsite (Kowalczyk 2005). Fort McMurray is located at the confluence of the Clearwater and Athabasca Rivers and the town site floods if there is an ice jam on the Athabasca River hindering outflow of the Clearwater River, causing it to back up. The history of such events in this region have been well documented. In more recent years, 1977 and 1997 both mark significant ice jam floods which essentially submerged the downtown sector. However, the most devastating event is likely that which occurred in 1875. It was documented by Henry J. Moberly in the archives of the Hudson's Bay Company (Moberly and Cameron 1929):

> *"On the 20 Instant about 2 hours after daylight, the river suddenly gave sign of breaking up and in half an hour from that time the water had risen about 60 feet, and the whole place was flooded – the water and ice passing with fearful rapidity and carrying off everything before them. We had just enough time to escape to the hill, in our immediate vicinity, with the families, bedding and a little Provisions and Ammunition, and to throw up stairs the Furs and most of the valuable property, when the water was already rushing through the Fort. From the time the river first gave signs of starting hardly half an hour elapsed before there was 5 feet of water in the highest building in the Fort, and the Interpreter's house was carried bodily away and dashed to pieces in the Woods; the Workshop and Men's houses have been almost destroyed."*

It would be highly beneficial to provide reliable forecasting of these dramatic floods in order to protect the lives and property of those who occupy flood-prone areas. Increasingly effective numerical models are currently being developed to model even the most dynamic ice jam release waves (She and Hicks 2005). However, this is an exceedingly complex challenge involving the interaction of ice and water as well as dynamic flow hydrodynamics. Previous studies have demonstrated that ice effects are hydraulically significant and cannot be neglected (Kowalczyk and Hicks 2003). Therefore, these need to be incorporated into such models to provide realistic predictions of events of this nature. This necessitates that accurate data with respect to ice conditions be obtained. At a minimum, the location and length of any jams **need** to be known, but an approximation of ice roughness or thickness would also be desirable.

Unfortunately, data acquisition remains the greatest hurdle to be overcome in this field. Collecting consistent ice information is a challenging undertaking due to both the hardship and inherent risk of working on an ice cover as well as the isolated sites at which reaches of interest are often located. During the winter months, harsh conditions make it unpleasant to conduct field studies and many electronic devices doe not operate reliably. As breakup progresses, the ice cover becomes unpredictable, making it impractical to manually collect data. Once an ice jam has actually formed, it is completely unsafe to even attempt any sort of meaningful data collection.

For river reaches not accessible by road or foot, information regarding ice conditions must routinely be gathered via aerial reconnaissance. This is currently the most effective means for flood forecasters to document river breakup progression but it has several substantial limitations. First, the prohibitive cost and time commitment of such an undertaking means that only a relatively short reach of river can be documented on a daily basis (~50 kilometres). It is also highly dependent on weather conditions and only features visible to the naked eye (and from a high altitude) can be identified; it is not feasible to discern ice thickness or roughness with any degree of reliability. Thus, the potential for extracting information from satellite imagery is becoming an increasingly attractive alternative.

The remote sensing of sea ice and icebergs has already received widespread use for such purposes as detecting ice hazards, determining the spatial extent of sea ice and even studying climate change (Haykin *et al.* 1994). In recent years, due in part to increasing improvements in sensor resolution, the remote sensing of river ice has come under investigation. While some optical sensors have been addressed (Gatto 1990), studies have focused primarily on radar imaging systems. Synthetic Aperture Radar (SAR) likely shows the most promise in this field due to the data acquisition benefits it provides. It is particularly appealing because provides its own illumination and operates in the microwave range of the electromagnetic spectrum. This allows for imaging at any time of day or night and minimizes contributions from haze or cloud cover. Most systems also have a repeat cycle that facilitates numerous imaging opportunities within a relatively brief time frame.

This investigation focused on the use of RADARSAT-1 imagery to examine river breakup progression and facilitate flood forecasting efforts. The potential for employing SAR imagery as a remote sensing tool was examined using the Athabasca River at Fort McMurray as a case study. The objectives of this study include:

1. to determine if it is possible to identify the length and locations of ice jams from SAR (RADARSAT-1) satellite imagery;
2. to explore if more detailed information of the ice cover, specifically regarding ice texture or thickness, at breakup can be deduced from SAR satellite imagery;

A literature review, comprised of two major components is provided in Chapter 2. A brief introduction to radar is followed by summaries of the more significant studies relating to the remote sensing of river ice (dating back to 1991) that have been conducted. Chapter 3 contains a qualitative analysis of the satellite imagery collected during spring breakup on the Athabasca River at Fort McMurray. The type of information which can be gathered from a simple visual assessment is examined. A more quantitative analysis of the image data is provided in Chapter 4. This includes an examination of the variation in the backscatter coefficient during the breakup period and an evaluation of the potential for extracting ice thickness or structure data from satellite imagery. Chapter 5 summarizes major findings of this investigation and outlines several key recommendations for future research in this area.

2.0 LITERATURE REVIEW

2.1 INTRODUCTION

RADAR is an acronym for **RA**dio **D**etection **A**nd **R**anging. Imaging radars as discussed herein are *active* microwave remote sensing systems which provide their own illumination. Essentially, they function by transmitting a signal, illuminating the surface and recording the response returned from the target. *Active* systems can easily be differentiated from *passive* systems because passive systems do not transmit any energy toward the target. Rather, *passive* microwave sensors detect the small amounts of microwave energy that are naturally emitted from all objects. As depicted in Figure 2.1, imaging radars are side-looking systems. Microwave energy is transmitted toward the target, and the sensor measures both the strength of the reflected energy and the round-trip time for a given pulse to return from the surface. Recognizing that a radar pulse travels at the speed of light, the distance or range to a reflecting target is calculated from the measured return time. In this manner, the radar only "looks" to one side, since looking in both directions would result in identical return times for two separate locations (i.e., one from each side).

Radars utilize the microwave portion of the electromagnetic spectrum, beyond the visible and thermal infrared regions. Also, rather than covering a wide band of frequencies as optical sensors generally do, imaging radars use a single, specific wavelength in the microwave region (narrow bandwidth with a central frequency/ wavelength). A relatively long wavelength (~1-30 centimetres) is employed by most systems. This provides superior signal penetration, effectively removing atmospheric contributions and providing the sensor with "all-weather" sensing capabilities. In fact, it is considered to be virtually unaffected by the presence of haze or cloud cover (Henderson and Lewis 1998). Water clouds can have an effect on the signal but this is only significant at wavelengths less than 2 cm and the effects of rain are relatively inconsequential at wavelengths greater than 4 cm (Henderson and Lewis 1998). Additionally, since imaging radars provide their own illumination, sensors are independent of the sun conditions, allowing for imaging at any time of day or night. Such versatility is especially useful for imaging northern rivers since polar regions undergo long periods of darkness in the winter. However, it is important to note that, while the actual radar return is unaffected by sunlight, surface conditions may be highly sensitive to the diurnal cycle and the resultant images will reflect this.

There are relatively standardized bands within the microwave region of the electromagnetic spectrum within which a selected wavelength normally falls. These include X, C, L, and K bands, among others. A listing of bands and their corresponding wavelength ranges is available in Table 2.1. This alphabetic nomenclature was initially established by the military during the initial stages of radar research and, though other identification schemes have been proposed, this system is still used almost universally today (Henderson and Lewis 1998).

Synthetic aperture radar (SAR) is currently the primary means of remote sensing applied to river ice monitoring. SAR is an imaging radar that utilizes microwave radiation to observe a scene. It is differentiated from real aperture radar (RAR) because its azimuthal (along-track) resolution is not determined by the physical length of the antenna (Raney 1998). Rather, a very long antenna is synthesized by combining signals which the radar receives as it moves along its flight track. As depicted in Figure 2.2, a pulse is transmitted at each position along the radar's path. The echoes generated by each pulse are recorded and, because the sensor is moving relative to the ground, each is Doppler-shifted. Hence, the Doppler-shifted frequencies can be compared to a reference frequency, enabling many signals to be focused on a single point. This effectively increases the antenna length imaging that point and contributes to SAR's being capable of generating radar images in which very fine detail can be resolved. RADARSAT-1, the Canadian satellite launched in November of 1995, can provide fine beam images at an approximate resolution of 8 metres. This is a distinct advantage when viewing rivers which are commonly only on the order of tens to hundreds of metres in width.

The frequency of image acquisition has also contributed to the popularity of SAR. Though the repeat cycle of RADARSAT-1 is technically 24 days, it is actually possible to obtain images much more frequently by working with different image modes and recognizing that not exactly the same total area will always be captured. Additionally, imaging opportunities are increased at locations further from the equator since the overlap between subsequent imaging strips increases with an increase in latitude (van der Sanden 2004). This makes it ideal for northern locations; at Fort McMurray, past experience has shown that images can be obtained approximately 2 out of every 3 days. Such regular acquisition is absolutely essential for operational river breakup monitoring and makes SAR far superior to many visible and infrared systems which commonly have repeat cycles greater than 10 days (Tracy and Daly 2003).

2.2 RADAR BACKSCATTER

2.2.1 The Radar Equation

A brief examination of the radar equation provides insight into what is meant by "radar backscatter" and the parameters from which it is determined. A space-borne SAR utilizes an antenna which transmits energy towards the earth's surface. This energy is transmitted into space in all directions. Hence, the power density (power per unit area) at the target is defined by the power transmitted (P_t) divided by the surface area of a hypothetical sphere with radius equal to the range distance (R), as depicted in Figure 2.3. However, side-looking imaging radars actually direct or concentrate the emitted energy such that the power is focused or increased in a desired direction (i.e., toward the target). This increase is referred to as the gain of the transmitting antenna (G_t). Accordingly, the power density at the surface is described by Equation 2.1:

$$\frac{power}{area}=\frac{G_t P_t}{4\pi R^2}$$

Equation 2.1

At the surface, some of the incoming flux is absorbed while some is transmitted and some is scattered (reflected). The power scattered back toward the antenna, P_s, is described by Equation 2.2:

$$power = P_s = \sigma\frac{G_t P_t}{4\pi R^2}$$

Equation 2.2

where σ represents the radar cross-section. It has units of area and corresponds to the area that when multiplied by the incident irradiance produces the observed amount of power scattered back toward the antenna. The backscatter microwave energy described in Equation 2.3 must travel the range distance (R) from the target to the radar in order to return to the receiver. Hence, the power density at the receiver is determined by dividing the scattered power (as described in Equation 2.2) again by the area of a sphere with radius R.

$$\text{power density at receiver} = \sigma \frac{G_t P_t}{4\pi R^2}\left(\frac{1}{4\pi R^2}\right) = \sigma \frac{G_t P_t}{16\pi^2 R^4} \qquad \textbf{Equation 2.3}$$

As a result, the total power received at the sensor (P_r) is the power density (Equation 2.3) multiplied by the antenna receive area, A_r (see Equation 2.4).

$$\text{power received at sensor} = P_r = \sigma \frac{G_t P_t A_r}{16\pi^2 R^4} \qquad \textbf{Equation 2.4}$$

Note that the effect of range distance on power received at the sensor is inverse and to the fourth power. Thus, the large distances characteristic of spacecraft observations (as compared to airborne SAR) require a very powerful antenna in order to obtain detailed observations.

The radar cross-section (σ) is divided by the area (A) of the illuminated surface (resolution cell) to produce a term called the differential radar cross-section (σ^0). The backscatter coefficient[1] is commonly expressed in terms of this dimensionless parameter. Typically, it is modeled to study interactions with surface materials and is often expressed in decibels since surfaces can have orders of magnitude differences in scattered power from place to place. In decibels, the differential radar cross-section is described by Equation 2.5.

$$\sigma^0 = 10\log_{10}(\sigma/A) \qquad \textbf{Equation 2.5}$$

2.2.2 Speckle

An important characteristic of SAR's is that they provide coherent scene illumination. The illumination provided by each pulse is monochromatic and emitted from a point source. Hence, the radiating field basically consists of structured (spherical) phase fronts centred at the radar. As a result, the input returned to an imaging radar from a scene is a linear summation of contributions from reflecting elements illuminated by this coherent wave field (Raney 1998). When reflections from more than one scene element are combined through vector addition, local constructive and destructive interference can occur. This creates bright and dark spots within an image, a phenomenon termed *speckle*, which results in an overall grainy looking appearance.

---

[1] Because the term "cross-section" is ambiguous in a river engineering context, "backscatter coefficient" or "scattering coefficient" are primarily used to describe the differential radar cross-section.

Speckle affects an important image characteristic, *texture*. Texture is a second order spatial average of brightness over a feature in an image; it describes variation in *tone*. Tone refers to the first order spatial average, or mean, of a feature's brightness (Raney 1998). Essentially, SAR image texture is comprised of both scene texture and speckle. Scene texture is an attribute of the surface and refers to the variation in image tone as a result of changes in a feature's reflectivity. In contrast, speckle is the component of image texture which is solely a result of SAR and its processing system.

The effects of speckle are most pronounced in fine beam imagery. Though fine beam data provides the best resolution, it only utilizes one look and is characterized by a greater amount of speckle than multi-look image modes (Weber *et al.* 2003). Multi-look processing is a technique performed in the SAR processor. It effectively reduces speckle by averaging over different sub-images of the same scene. *Looks* refers to the sub-images formed during SAR processing. The number of statistically independent sub-images used in the average controls image speckle variance (Raney 1998). However, though the effects of speckle are less significant under these conditions, it is a process requiring averaging and therefore reduces spatial resolution.

In order to effectively analyze radar data, speckle reduction is usually an essential step (most notably for single-look data). This is normally completed via image processing with the application of a specialized speckle filter. The Kuan filter (Weber *et al.* 2003) and the enhanced Lee filter (Murphy *et al.* 2001) are two such examples, but many others exist with each providing a distinct result. All of these filters employ an averaging process of sorts. However, this is done at the expense of spatial resolution (CCRS 2003) and can blur thin image details such as textural or structural features (Lopes *et al.* 1993). A gamma filter, which preserves lineal features fairly effectively, was employed in the course of this study.

2.2.3 Target Parameters Affecting Radar Return

The interpretation of SAR imagery for studying river ice is a complex and challenging undertaking. There are various possible interactions of the radar signal with river ice which complicate image analysis. Specifically, some factors that affect the backscatter coefficient include the dielectric constant of the target, surface roughness and the effect of these factors on surface scatter and volume scatter.

Dielectric Properties

The dielectric properties of a material are predominantly responsible for the dissipation of radar energy as heat at frequencies above 1 GHz. For ice, the dielectric constant (ε_r) is nearly entirely dependent on free-water content. This has major implications regarding the expected penetration depth of a radar signal, especially during times of thermal change. Ice that is "dry" will have a lower dielectric constant (ε_r), absorb less energy and allow for a greater penetration depth. Conversely, ice with a high moisture content will have a high dielectric constant and lower penetration depth. When dry, the potential penetration depth into freshwater ice ranges from 100 m to 10 m at 1 to 10 GHz, respectively (Hallikainen and Winebrenner 1992). Both RADARSAT-1 and ENVISAT/ASAR operate in the C band at approximately 5.3 GHz. Thus, the potential penetration depth actually exceeds typical ice thicknesses on Canadian rivers. It follows that the radar return is not necessarily limited to the response of the uppermost ice layers, suggesting that scattering within the medium and interactions at secondary interfaces may have a significant effect. In the reverse circumstance, the presence of a wet snow cover can reduce the penetration depth dramatically, making the recorded backscatter largely a response to snow parameters rather than the underlying ice (Drinkwater 1989). In fact, for frequencies in the C band, as little as 5% water in a snow pack can reduce the penetration depth to less than a centimetre (Hallikainen and Winebrenner 1992). This indicates that when a wet snow cover is present, backscatter is dominated by surface scatter at the air-snow interface.

The issue of penetration depth has implications for the nature of the radar signal's interaction with the target surface. Energy is reflected when there is a change in dielectric constant. With sufficient penetration depth, this can mean that it is scattered by dielectric discontinuities located in the medium and/or secondary interfaces with which it may come in contact. In fact, as depicted in Figure 2.4, when the ice surface is dry, the ice-water interface may actually control the radar response to a greater extent than the air-ice interface (Elachi and Bryan 1976). This is attributable to the drastic change in dielectric constant at the ice-water interface (from 3.2 to 81) as compared to that at the air-ice interface (from 1 to 3.2) (Weber *et al.* 2003).

Surface and Volume Scatter

Essentially, there are two types of interaction with a target which may scatter a radar signal: surface scatter and volume scatter. Surface scatter is a result of the reflection that occurs when a radar signal contacts an interface at which there is a change in dielectric constant. As depicted in Figure 2.5, this has implications for the effect of ice texture on the radar return. Smooth surfaces tend to reflect in a *specular* manner, directing most of the energy away from the sensor in a single direction while rough ice surfaces (at the scale of the wavelength) tend to cause *diffuse* scattering, reflecting the energy nearly uniformly in all directions and directing more radiation back toward the sensor. Hence, rougher surfaces tend to generate greater surface scatter.

In contrast, volume scattering refers to the behaviour of radar waves within a medium. Upon penetrating the surface of an ice cover, the radar signal may be scattered by dielectric discontinuities within the ice itself. Therefore, cracks, bubbles, liquid water pockets and impurities may increase the backscatter coefficient. As indicated in Figure 2.6, this suggests that highly inhomogeneous ice covers will generate a higher radar return due to volume scatter than ice covers that are more uniform in composition. This difference can be ascribed to a considerable volume scattering component. However, the mixture constituents need to be of a scale similar to that of the radar wavelength to effectively scatter the signal.

2.2.4 Illumination Parameters Affecting Radar Return

Apart from the properties of the target surface which influence SAR imagery, there are also a number of system parameters which can have a substantial effect on radar return. Among these are wavelength, incidence angle and polarization. Depending upon the desired application, it may be possible to minimize the impact of these parameters by repeatedly selecting the same image mode and polarization. In this manner, any assessment of changes between successive images is simplified since the surface condition will be the primary variable under consideration. However, for monitoring purposes, it is necessary to use multiple image modes in order to maximize acquisition. This provides more data but complicates analysis since there are more variables that may need to be taken into account.

Wavelength

For a given radar system, the nominal wavelength of the transmitted pulses is predetermined and generally falls within one of standard bands as listed in Table 2.1. The wavelength of the transmitted signal is important since, at the target surface, it governs the scale of textural elements which will scatter the radiation. Hence, a radar system operating in the C band with a nominal wavelength of 5.4 centimetres would not be affected by small impurities and/or textural features at the millimetre scale.

Beam and Incidence Angle

The primary distinctions between the various RADARSAT-1 image modes are the image resolution and incidence angle. Fine beam images are denoted with an F (e.g. the "F" in F5) and have a resolution of approximately 8 m whereas standard beam images are denoted with an S (e.g. the "S" in S1) and have a resolution of approximately 25 m. The numerical portion of the image mode title is indicative of its range of incidence angles (RADARSAT International 2000). For fine images, F1 has the steepest range of incidence angles at 37-41° while F5 has the shallowest range at 45-47°. With standard images this disparity is greater: S1 uses a range of incidence angles of 24-31° while for S7 it is 39-42°. Additionally, the position can either be shifted closer to or further away from Nadir (the locus of points directly beneath the flight path) for fine beam images. The resulting positions are denoted by either an N (Near) or F (Far).

As stated, changes in the selected beam (e.g. fine versus standard) affect the resolution of the resultant image. While it may seem that the only "real" difference this could cause is the ability to distinguish smaller scale features, its impact on image texture should also be considered. Standard beam images utilize multi-look processing which reduces speckle. These images cannot be straightforwardly compared to fine beam images.

Incidence angle is also an important factor as it can have a significant effect on the amount of surface scatter. Figure 2.7 presents a model of scattering behaviour as a function of incidence angle (adapted from Farr, 2005). Note that, for an equally rough surface, the surface scatter becomes greater as incidence angle is reduced. This is because object surfaces naturally tend to become more normally aligned with the incoming radar at steeper angles of incidence, producing increasingly more normal reflections where the energy is reflected directly back toward the sensor. This effect is more pronounced for smoother surfaces due to the more specular nature of surface scatter.

Polarization

Some SAR systems are capable of operating in multiple polarizations. This means that it can transmit radar waves in one polarization and receive in the same or a different one. When more scattering occurs at the surface, the echo will be more depolarized. Up to four different combinations of polarizations are possible: HH (transmit and receive in horizontal), HV (transmit in horizontal, receive in vertical), VV (transmit and receive in vertical) and VH (transmit in vertical, receive in horizontal). According to the reciprocity principal (Raney 1998) the results from each case should theoretically be identical. However, this may not be true in practice, complicating image analysis. For instance, it can be difficult to assess surface changes using HH/HV images from one date and VH/VV images from another date.

2.2.5 Geometric Considerations

Geometric distortions are commonly found in SAR imagery due to sensor viewing geometry and image generation. Because radar measures distance in slant range (see Figure 2.1), terrain can cause elevation displacement in the form of foreshortening, layover and radar shadow.

Foreshortening

Foreshortening occurs along terrain slopes facing the sensor. It has the effect of mapping the slope on a compressed scale relative to its appearance if the same terrain were level. Figure 2.8 demonstrates an example of foreshortening which would occur when a radar attempts to image feature abc. Because "b" is at a higher elevation than points "a" and "c", the wave front will reach this location sooner than otherwise would have occurred. Thus, when these points are mapped in the image plane, slope "ab" is *foreshortened.* In this manner, the radar "sees" points a, b, and c at a', b' and c', respectively. This effect is more pronounced for steeper slopes and steeper incidence angles.

Layover

An extreme case of foreshortening occurs when the top of a reflecting feature is closer to the radar (in slant range) than the base of the feature. For example, Figure 2.9 demonstrates how the wave front reaches the top (b) of feature "abc" before the base (a). Hence, the radar detects that points a, b, and c are located at a', b' and c' accordingly. Once imaged, this gives the appearance that the feature has "fallen over" toward the radar. This effect is more pronounced at small incident angles.

Radar Shadow

Radar shadow is another form of geometric distortion. It occurs when regions are not illuminated by radar energy, generally due to being hidden behind an elevated feature. Figure 2.10 depicts radar shadow. The geometry is such that when feature "abc" is imaged, the backslope is not illuminated. Thus, slope "bc" and area "cd" are in shadow and therefore remain undetected by the radar. With virtually no reflectivity, this region will appear as small digital numbers, or as a dark region in the image.

2.3 INTRODUCTION TO RIVER ICE PROCESSES

2.3.1 River Ice Freezeup

River ice is classified primarily according to formation process (Michel and Ramseier 1971). When calm water surfaces freeze (as seen with border ice and during backwater conditions) a smooth thermal ice cover forms. For this structure type, skim ice initially forms on the surface and a columnar crystal structure develops as the crystals grow downward. An example of this ice type is shown in Figure 2.11. The characteristically smooth ice surface is evident in the left photo and the large columnar crystal structure is evident in the right photo of a thin section taken under polarized light. In some cases, bubbles and large cracks can form in thermal covers. Figure 2.12 depicts an example of this occurrence.

In rivers, highly turbulent flow occurs in the main channel, especially if the channel slope is at a significant gradient. In this case, frazil ice (small ice discs) nucleate at the surface and are quickly entrained throughout the flow depth in supercooled water. Because supercooled frazil is very adhesive, it flocculates and forms balls of slush which eventually float to the surface to form "pans". These pans can freeze together, forming large "rafts" and as the surface concentration of ice approaches 100%, the flow becomes congested and bridging becomes likely. Once arrested, rafts and pans accumulate edge to edge to form a "juxtaposed" ice cover. Subsequently, ice grows thermally downward from the frozen frazil cover. The typical surface texture and crystal structure of a juxtaposed ice surface is as depicted in Figure 2.13. Note that the frazil ice surface has a fine grained texture as compared to the underlying columnar crystals.

In some cases, a juxtaposed ice cover will collapse, forming a hummocky ice cover or freezeup jam. Covers of this type can exhibit varying degrees of severity. For example, in Figure 2.14, the photo taken at transect "I" shows a significantly rougher surface than taken at transect "F". Both would be categorized as "hummocky" ice covers.

2.3.2 River Ice Breakup

River breakup is influenced by both thermal and dynamic processes and it is the relative magnitude of these factors which dictates the nature and severity of river ice breakup. In the case of a thermal breakup, river ice deteriorates in place (Figure 2.15). Meteorological conditions are of primary importance and breakup tends to start with melting (and sometimes ponding) of snow on the ice surface, which reduces the surface albedo. This is generally followed by the development of open leads, allowing heat to enter the flow.

In contrast, dynamic breakups are strongly influenced by hydraulic factors and are often associated with a large runoff event. Before any significant thermal deterioration of the ice cover has taken place, it can be lifted by rising water levels, breaking it up and carrying ice floes downstream with the flood flow. Ice jam formation (Figure 2.16) will result if such an ice run is arrested. Ice jams can be very thick (on the order of metres) and normally appear quite "dry" as a significant portion of the ice rests above the phreatic surface. However, there are often unpredictable dangers associated with these accumulations, making manual data collection unsafe.

Ice jams remain a major concern because of the flood risk they pose to nearby communities. Essentially there are two mechanisms by which an ice jam can cause flooding. The jam itself can severely obstruct the flow and cause water to back up in the channel, flooding areas upstream. Alternatively, if and when an ice jam releases, it can send a life-threatening wave of ice and water down the channel. The result is running ice (Figure 2.17) accompanied by drastically increasing water levels in the downstream reach.

2.4 PREVIOUS INVESTIGATIONS

2.4.1 Burntwood River, Manitoba (LeConte and Klassen 1991)

The value of synthetic aperture radar for river ice monitoring was investigated with airborne SAR systems prior to any satellite observations. LeConte and Klassen (1991) were among the first to undertake a study of this nature in their work on the Burntwood River in northern Manitoba. In April 1989 and January 1990, C- and X-band data were collected along an 80 km stretch of the Burntwood River. Originating northeast of Flin Flon and discharging into Split Lake, the study area is found at an approximate latitude of 55° north. Its flows have increased dramatically since 1976 due to diversion from the Churchill River system, altering the hydraulic regime. During the week of the SAR flights, ground truthing efforts were undertaken including reconnaissance helicopter flights and visits to ground calibration sites to collect ice, snow and water data.

A total of six flight passes were flown on April 5, 1989 and 7 passes on January 4, 1990. System parameters were selected such that different sections of the study area were imaged under a number of viewing geometries, polarizations, look directions and frequencies. This facilitated, to some extent, an exploration of the effects of these parameters on resulting imagery. However, the majority of analysis focused on the C band HH data taken at narrow swath mode (incidence angle, 45-76 degrees). This is because this data would be most comparable to that from Canadian satellite RADARSAT-1 and also because airborne narrow swath imagery would not suffer from severe image distortions in the near range.

For the Burntwood River, most of the channel within the study area was generally characterized by high backscatter (bright returns). This is attributed primarily to the structure of the ice cover. With an extremely jagged surface, the ice on the Burntwood downstream of First Rapids was essentially comprised of massive juxtapositioned ice overlying deep slush. In fact, cores taken at the time revealed as many as 8 layers of rafted plates and slush ice. This could generate increased volume scatter. In contrast, the ice on Split Lake produced generally dark radar signatures due to the typically smooth ice/water interface. Though some unexpectedly bright radar responses were noted on the lake surface, these were attributed predominantly to the presence of slush ice from the Burntwood River. Ice cores taken from these areas confirmed the occurrence of a two layer ice cover similar to that found in the channel.

2.4.2 St. Marys, Connecticut and White Rivers (Gatto 1993)

The utility of spaceborne SAR first came under investigation (in a river ice context) in the early nineties. During the 1992-1993 winter, Gatto obtained fifteen SAR images (~30 m resolution) using European Remote Sensing Satellite-1 (ERS-1). These images covered reaches of the St. Marys, Connecticut and White Rivers, thereby facilitating a comparison of ice conditions from three distinct regimes. Connecting Lake Superior to Lake Huron, the St. Marys River is easily the largest of these three waterways. It is a very wide flat channel with a significant gradient change (from 0.7×10^{-5} to 0.3×10^{-5}) at St. Marys Falls near Sault Ste. Marie. Comparatively, the Connecticut River is intermediate in size. It has a width of about 100-500 metres and an average gradient of 0.3×10^{-3}. In contrast, the White River is at the opposite end of the spectrum. At an average slope of 0.12×10^{-2} and width ranging from 50-150 metres, it was the smallest and steepest of the rivers investigated.

Simple image processing was performed to remove speckle from the images and optimize brightness and contrast. This was sufficient to provide promising preliminary results which indicate that satellite-borne SAR's are capable of providing valuable data for managing river navigation and evaluating the potential for ice jams and ice erosion along the banks of many rivers. The St. Marys River ice cover was very evident in the SAR imagery, clearly showing open water, snow ice, clear ice, cracks and the associated ice ridges through the narrow reach upstream of the Soo Locks. Encouraging results were also obtained along the Connecticut River. Upstream of the Wilder Dam, the ice was smooth in the centre of the channel while the near shore ice was rough, with snow ice at the surface. Consequently, the near shore ice produced a brighter signature than that in mid-channel. Further, the open water downstream of the dam appeared black in the image due to the very low backscatter it generated.

Unfortunately, results from the SAR data were of limited utility along the White River. During one acquisition, approximately half the channel was open with frazil pans floating in the water but this was not apparent in the SAR image. Additionally, in another instance, it was difficult to even distinguish the presence of an ice jam on the river which formed near an island. This suggests that there are major limitations for using SAR to monitor ice on smaller scale rivers. Gatto (1993) commented that for rivers less than 30-35 metres in width, the spatial resolution is likely too small to adequately describe the ice cover. In this circumstance, the backscatter from the ice cover is integrated with that of surrounding terrain, obscuring the ice-unique information. He also acknowledged that using only a single radar band and polarization may have limited the differentiation capabilities of SAR.

2.4.3 Moose River, Ontario (Murphy et al. 2001)

Murphy et al. (2001) further investigated the applicability of SAR in a river ice monitoring capacity during the late nineties. Using Canadian satellite RADARSAT-1, five fine resolution mode images (~9 m resolution) were obtained of the estuarine reaches of the Moose River in northern Ontario just prior to breakup in 1997. That year, river breakup was dominated by thermal rather than dynamic processes. Breakups of this nature are generally preceded by highly variable ice conditions (Michel 1971) and ice-surface flooding may occur through cracks or shore leads (which can re-freeze at night). This can occur at different parts of the river at different times, possibly producing inconsistent backscatter. In the Moose River basin, spring thaw occurred relatively early with above freezing temperatures in mid-April gradually weakening the river ice cover. High water levels were not characteristic during this period and only the lowest areas of the islands and mainland experienced any flooding.

For verification purposes, groundtruth data was obtained from information reported by officials of the Ontario Ministry of Natural Resources as well as direct observations made during the critical spring period. The SAR data was proven effective in determining the location and development of ice-cover "macro-characteristics" (Murphy *et al.* 2001). Various ice types were visible including rubbly offshore ice in James Bay, shorefast ice along the coast and in the delta, and the dark grey to black river ice. Also, brighter zones (higher backscatter) were noted in some areas; in some of the smaller channels, the ice was brighter than in the main channel and the location of an ice road was clearly visible.

As breakup advanced, a number of clear changes in the ice cover could be noted from the SAR imagery. Within James Bay, the shorefast ice exhibited increasing erosion of its seaward edge. Additionally, a progressive increase of ice push ridges (bright spots) and shear zones near the banks (and in some cases across the river) were evident. Visible dark patches were associated with areas which became flooded with fluvial water while patches with light rims and darker central zones appeared to be indicative of submerged bars. Broken reaches developed and were characterized by rubbly ice on a dark (water surface) background. Overall, breakup initiated upstream and progressed swiftly toward the mouth of the river.

Murphy et al. (2001) notes that another factor which should be considered when analyzing imagery of this type is the effect of incidence angle. Due to the limited data set in this case, it was unfortunately impractical to draw any clear conclusions regarding its effect on backscatter. However, it was found that any changes attributable to incidence angle were not significant enough to mask the overall environmental changes.

2.4.4 Mississippi River, Missouri and Missouri and Red Lake Rivers, North Dakota (Tracy and Daly 2003)

Tracy and Daly (2003) investigated the efficacy of SAR on rivers of varying size and ice cover, acquiring six RADARSAT-1 images at three different sites in the winters of 2002 and 2003. A reach of the Mississippi River near St. Louis ranging from 500-2000 metres in width was selected as the largest scale site, while the Missouri River was intermediate (400-1000 wide) and the Red Lake River was the smallest at only 40-75 metres wide. Similar to Gatto's findings (Gatto 1993), results from this study indicated that scale is certainly a limiting factor on the utility of SAR for remotely sensing river ice. For the Mississippi River, it was relatively straightforward to identify and classify the ice as either brash or border ice. Likewise, for the reach of the Missouri River which was examined, the imagery was deemed suitable to delineate river ice and approximate the fraction of the channel with ice in the flow. However, for the Red Lake River, the narrowness of the channel complicated the delineation of channel boundaries. Even though ice surveys confirmed the presence of river ice within the study reach, it was indistinguishable in the SAR imagery.

2.4.5 Peace River, Alberta (Weber et al. 2003; Jasek et al. 2003)

The Peace River was extensively utilized throughout 2000 to 2003 as a study site for investigating the viability of radar remote sensing of river ice; it is of particular interest because it is a regulated river. In order to minimize the risk of ice jam flooding during freezeup, BC Hydro must assess when the ice downstream is strong enough to resist secondary consolidation (Weber *et al.* 2003). Traditionally, this decision has been based on information gathered via aerial reconnaissance and from local residents living along the Peace River. However, the use of satellite imagery could be a valuable addition to this monitoring program.

Weber et al. (2003) examined the potential for classifying ice types by performing both a supervised and unsupervised classification and comparing this to results obtained from a simple visual analysis. To streamline this process, the focus was placed on an unsupervised approach since less user intervention is required, and the Fuzzy K-means algorithm appeared to generate the most promising results. Using this procedure, seven classes were identified: open water, frazil pans with two levels of concentration, juxtaposed ice, an intermediate juxtaposed/consolidated ice type and consolidated covers at two levels of consolidation. The resultant "ice maps" are useful for dam operations as indicators of ice strength (large areas with heavy consolidation) and weakness (large areas of open water) could easily be spotted. Because of the relative flexibility of scheduling ice observation flights (and the high cost of acquiring RADARSAT-1 images), they found it unlikely that SAR would replace the existing protocol at this time. However, they did find it provided a valuable supplement to current monitoring efforts.

In addition, efforts have also been made to locate ice frozen to the river bed and/or indirectly infer ice thickness and strength information from SAR imagery. It is expected that ice frozen to the bed would produce a lower backscatter coefficient because soil has a much lower dielectric constant than water (ε_r(soil)=8 vs. ε_r(water)=81). An extensive field campaign was launched in 2002 and 2003. In 2002, data was gathered on three separate field trips which approximately coincided with image acquisition dates. These dates were selected to capture the ice cover soon after formation (Jan 24), one week subsequent to this when the biggest changes to ice cover properties occur (Jan 30) and one repeat cycle (24 days) after the second acquisition (Feb 23). Because there were 24 days between the second and third acquisition, the same beam position and orbit was utilized, thereby removing any effect of look angle and/or look direction. A study site was chosen and a 25 m x 75 m grid of 96 points was laid out covering three different ice types: thermal border ice, shore-fast frazil and consolidated ice. At each point, solid ice thickness, slush ice thickness, air/ice and ice/water roughness and ice stratigraphy were documented. In 2003, the campaign was slightly different. Instead of a grid, ice cross sectional surveys were conducted at 8 locations on three occasions during the ice season. Each section consisted of 12 to 16 measurement points with 10 to 15 of them falling between the outer shear lines.

Unfortunately, subsequent data analysis has not yielded conclusive results. Since the border ice did not actually freeze to the bed at any of the study sites, the hypothesis that the backscatter should decrease could not be supported. Additionally, the effects of incidence angle and look direction made it difficult to assess whether an overall decrease in backscatter could be attributed to a decrease in the solid ice/slush ice interface roughness. A relationship between total ice thickness (solid ice and slush ice thickness) and backscatter coefficient was evident. The best correlation was found for images taken soon after ice cover formation while data taken later in the season showed degradation in the correlation coefficient, possibly due to the redistribution of frazil slush underneath the ice cover.

However, contributions from slush are not yet confirmed and it is uncertain whether its presence makes a measurable difference. It is possible that the high water content in slush ice (~50%) may severely limit the penetration depth of the radar signal, minimizing its potential contribution.

2.4.6 Saint-François River, Quebec (Gauthier et al. 2001; Gauthier et al. 2003)

Gauthier et al. (2001) were among the first to analyze the effect of seasonal changes on the backscatter coefficient in SAR imagery. During the winter of 2000-2001, thirteen fine mode RADARSAT images were obtained to monitor the evolution of the ice cover on a stretch of the Saint-François River in Quebec. The time frame extended from November 24 when the river was free of ice until April 19 when deterioration of the ice cover was essentially complete. The study reach was approximately 70 kilometres in length and varied in width from 100 to 400 metres. With three dams and 8 bridges, the river's natural flow regime has clearly been disturbed, and this provided a variability of ice conditions ideal for research of this nature.

Temporal changes in the scattering coefficient were investigated by extracting the signal amplitude along a mid-channel vector extending the length of the reach. This provided a helpful indication of the nature and magnitude of change expected for a developing ice cover. For example, the lowest backscattering occurred on November 24 and April 17 when the river was almost entirely free of ice. Low returns could also be noted for moderately wet, smooth ice covers. In both cases, it was expected that the wet surface would reduce penetration depth and generate high signal losses, causing surface scatter to dominate. Since the surface is smooth, energy was predominantly reflected away from the sensor in a specular manner. In contrast, when the surface was wet but rough (as occurred on April 10), backscattering is increased because much of the energy reflected at the surface returns to the sensor. Increased backscattering was also noted in December due to the occurrence of ice jams and floating ice in the upper reaches of the study area.

A number of other interesting features were documented throughout this study as well. The scattering coefficient showed a decrease in late February for which the cause was uncertain. Gauthier et al. (2001) comment that this may have been related to dam operations and/or changes in ice thickness. At the dam location, a distinctive break in the strength of backscatter coefficient was also apparent. Upstream of the dam where the river is slow, the ice produced relatively low backscattering while the ice downstream (in the vicinity of rapids) generated higher backscattering. Additionally, increased backscattering was also received from an ice road and from the shear walls remaining after a surge passed through the channel.

Gauthier et al. (2003) later used this data set in combination with imagery from 2002 and 2003 to develop a classification approach using contextual analysis. In this vein, two homogeneous reaches were selected upon which texture analyses were performed. The first reach was a gradually sloped, relatively straight, slow moving section while the second was a narrow, steep reach with shallow waters and nested between two islands. Though the result from each reach was inherently different, both demonstrated that this approach has a great deal of promise. The use of texture parameters provided significantly better discrimination of ice types than consideration of the backscattering coefficient alone.

2.4.7 Peace River, Alberta (Gherboudj et al. 2005)

In a recent study of the Peace River in Alberta, Gherboudj et al. (2005) examined the effect image mode can have on backscatter and proposed an algorithm to standardize the received signal. This is a significant advancement for river ice monitoring purposes since factors such as incidence angle can have a considerable effect on backscatter, and images acquired during a study generally do not all use the same image mode.

The algorithm was developed using two pairs of RADARSAT-1 fine beam images. The pairs were selected such that they were acquired under similar environmental conditions but used different image modes and orbits. After the pixel values were converted to backscatter, the images were each orthorectified. Homogeneous zones of river ice were subsequently selected from which the average backscatter coefficient and incidence angle could be extracted.

In developing the method, it was assumed that the received backscatter was primarily influenced by surface scatter occurring at the ice-water interface. Accordingly, the angles of refraction (angle formed between the normal and the ray refracted into the ice) for each acquisition were calculated according to Snell's Law. This information was then used to establish a relationship between the difference in backscatter and the difference in refracted angle.

Applications of this empirical algorithm showed that it holds promise but there are disadvantages which should be acknowledged. First of all, it is based on real radar data. Thus, any error in the values can be propagated in the values of the estimated results. Another complication is the selection of training sites; it is challenging to choose zones which are homogeneous (with respect to depth, flow conditions and discharge) and have the same type of ice. Additionally, the deduced standardization parameter cannot be effective for backscatter data which is outside of the data range used for its calculation. Overall, further validation with more data sets is required.

The second stage of Gherboudj's work consisted of applying the empirical algorithm to sets of images acquired under similar environmental conditions but with two different sensors (RADARSAT-1 and ASAR). However, the backscatter of the signal acquired with RADARSAT-1 was generally found to be lower than that acquired with ASAR. In fact, there actually appeared to be a common skew between the backscatter of the two sensors. One aspect which could explain this observation is the difference in the calibration of the two sensors. Hence, the assumptions considered for the standardization of the images acquired with the same sensor are not considered to be transferable to image data gathered with different sensors.

2.4.8 Sagavanirktok River, Alaska (Duguay et al. *In press*)

Duguay et al. (*in press*) examined the potential of SAR for identifying fish habitat in rivers of the Arctic coastal plain in their study along the Sagavanirktok River in Alaska. Anadromous fish (fish that spawn in freshwater but live part of their lives in salt water) require deep locations and/or areas influenced by groundwater for the purposes of overwintering. However, deep pools during open water conditions are not necessarily suitable for habitat since large hanging dams may form there subsequent to freezeup. Therefore, the use of synthetic aperture radar to identify floating ice in low gradient river reaches would be a valuable practical application. Discrimination of this type has already been realized for lake ice and is attributed to the signal interaction which takes place at the secondary interface. If ice is underlain by water, a large dielectric discontinuity occurs, reducing penetration depth, increasing reflection and generating a high amount of backscatter. If frozen to the ground, though, the ice is underlain by soil rather than water; this increases penetration depth and reduces backscatter.

Eighteen ERS-1/2 images were acquired during the late April to early May period from 1992 to 2003. This imagery was geocoded, filtered and analyzed to facilitate recognition of areas where the ice cover was likely to be floating or grounded. Subsequently, six ASAR alternating polarization (AP) images were acquired in April 2004. Obtained at various polarizations, incidence angles and orbits, this imagery was collected during a time frame which corresponded closely to a field campaign which was carried out in that year. In total, 164 sites were available to confirm which areas were afloat and/or grounded. Field data included measurements of limnological parameters as well as snow and ice thicknesses.

A thresholding approach was applied to distinguish between floating and grounded ice. This necessitated the identification of training areas through visual inspection upon which means and standard deviations could be calculated. From this data, suitable threshold values of -10 dB and -19 dB were selected for like-polarizations (HH and VV) and cross-polarizations (HV and VH) respectively. When applied to the remaining data set, encouraging (but by no means conclusive) results were obtained: correspondence between SAR data and field observations ranged from

54% to as high as 67%. Duguay et al. (*in press*) ascribe some of this inconsistency to image resolution. As the field data was comprised of point measurements and resolution is approximately 30 metres, it is possible that a single pixel could be composed of both floating and grounded ice (mixed pixel), thereby complicating analysis.

2.5 SUMMARY

Previous research indicates that there is significant potential in the application of Synthetic Aperture Radar (SAR) imagery for river ice monitoring. It has been found to be a particularly valuable means of data acquisition for a number of reasons. Not only can it achieve relatively fine resolution (~8 m) but it is capable of acquiring images regardless of light or weather conditions. Additionally, the repeat cycle often allows SAR satellite sensors to obtain images more frequently than their visible and infrared counterparts. Its usefulness has already been demonstrated on several North American watercourses including the Mississippi (Tracy and Daly 2003), Peace (Weber *et al.* 2003; Jasek *et al.* 2003) and Saint-François Rivers (Gauthier *et al.* 2001; Gauthier *et al.* 2003).

Table 2.1 Typical bands utilized by radar systems.

Band Name	Wavelength Interval (cm)
Ka	0.8-1.1
K	1.1-1.7
Ku	1.7-2.4
X	2.4-3.8
C	3.8-7.5 (often 5.4)
S	7.5-15
L	15-30 (often 24)
P	50-100 (often 64)

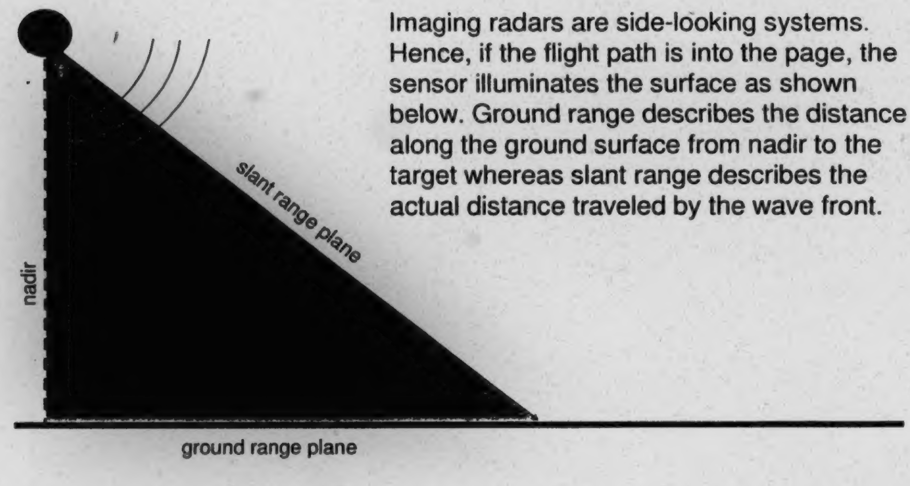
slant range plane
nadir
ground range plane

Imaging radars are side-looking systems. Hence, if the flight path is into the page, the sensor illuminates the surface as shown below. Ground range describes the distance along the ground surface from nadir to the target whereas slant range describes the actual distance traveled by the wave front.

Figure 2.1 Side-looking systems.

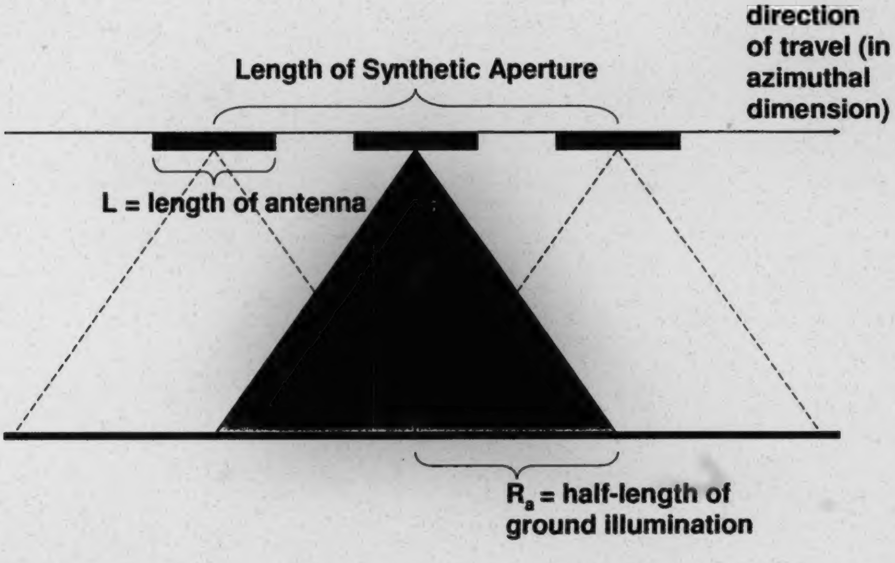
Length of Synthetic Aperture
direction of travel (in azimuthal dimension)
L = length of antenna
R_a = half-length of ground illumination

Figure 2.2 Schematic of Synthetic Aperture Radar.

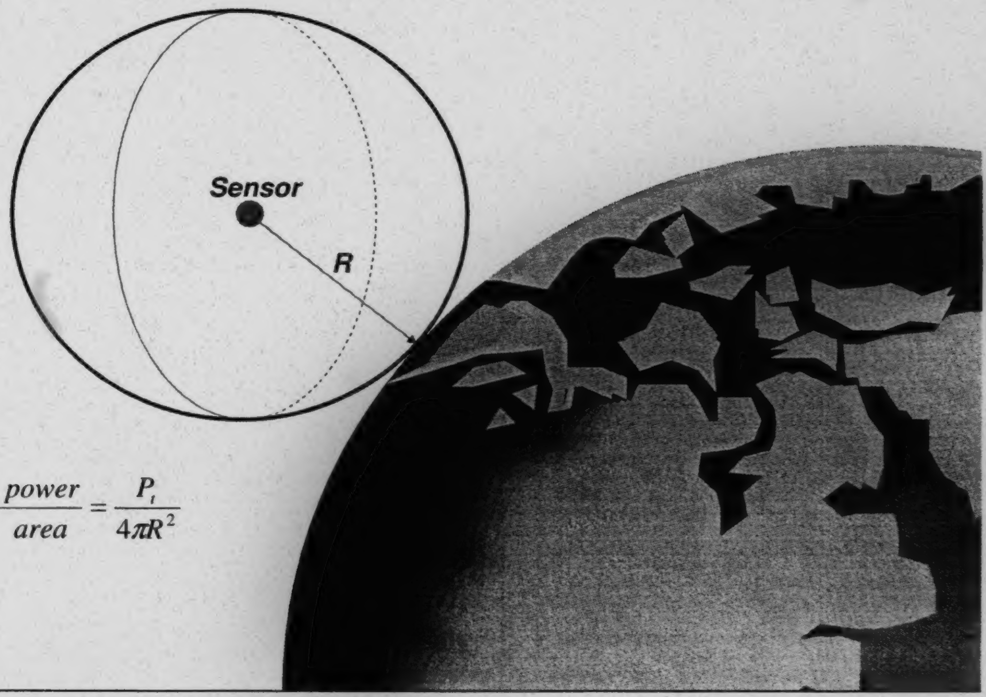

$$\frac{power}{area} = \frac{P_t}{4\pi R^2}$$

Figure 2.3 Radar power density at the surface.

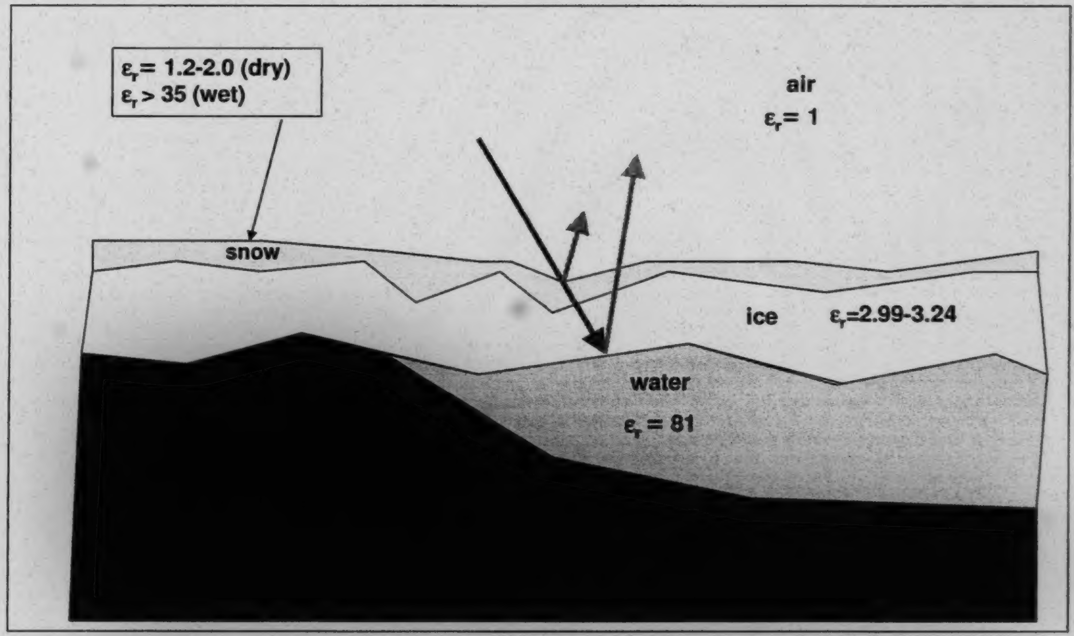
ε_r = 1.2-2.0 (dry)
ε_r > 35 (wet)
snow
air
ε_r = 1
ice
ε_r = 2.99-3.24
water
ε_r = 81

Figure 2.4 The significance of dielectric constant on backscatter.

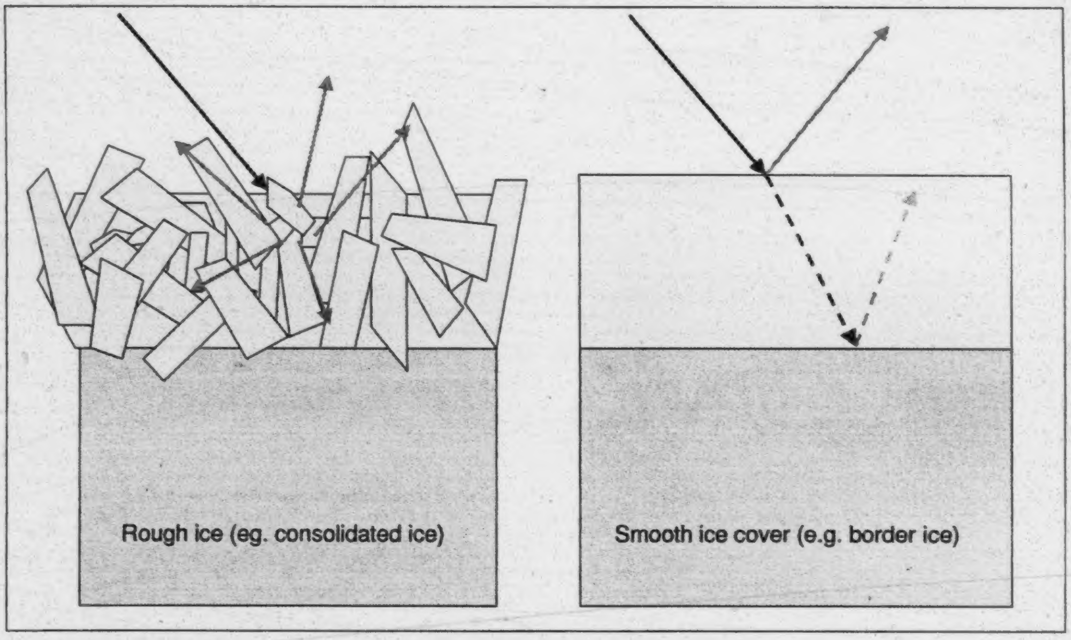
Rough ice (eg. consolidated ice)
Smooth ice cover (e.g. border ice)

Figure 2.5 The effect of ice texture on surface scatter.

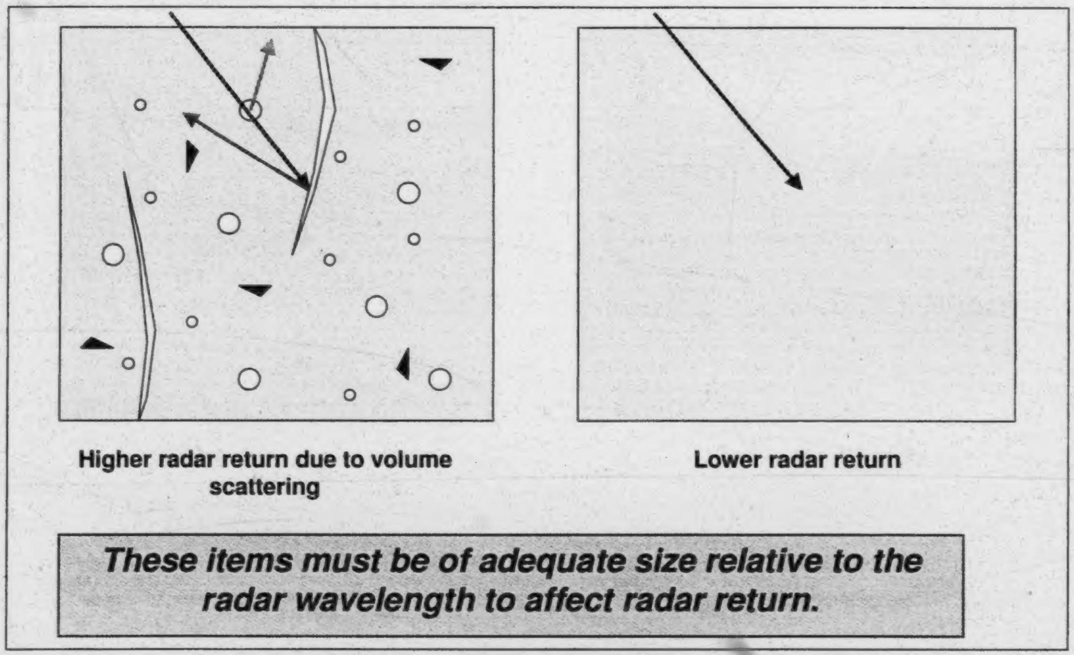
Higher radar return due to volume scattering
Lower radar return
These items must be of adequate size relative to the radar wavelength to affect radar return.

Figure 2.6 The effect of bubbles, impurities and cracks on volume scatter.

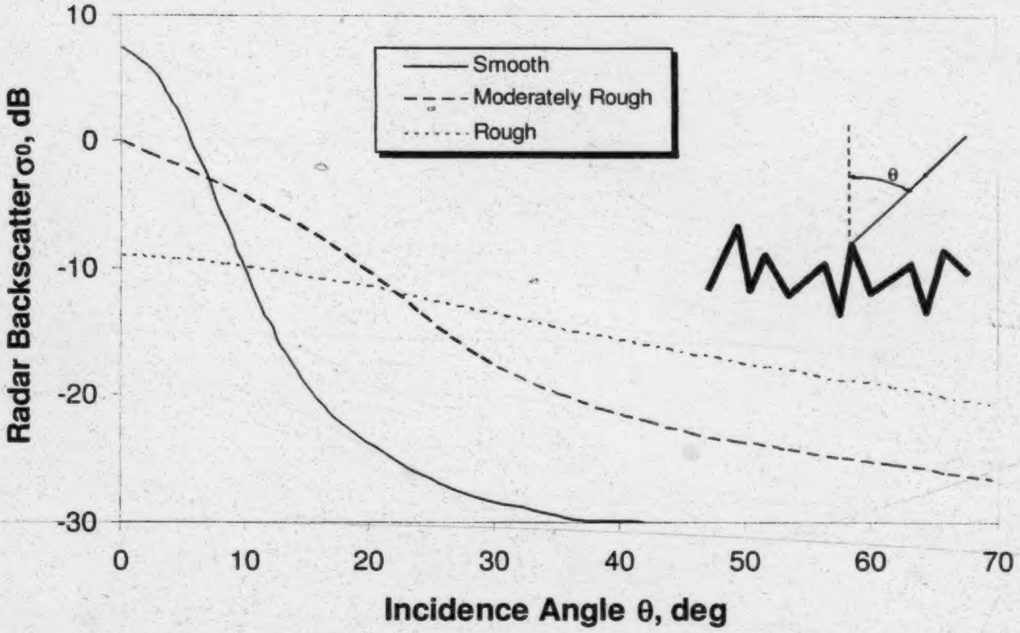

Figure 2.7 Scattering model describing the effect of incidence angle on surface scatter (adapted from Farr, 2005).

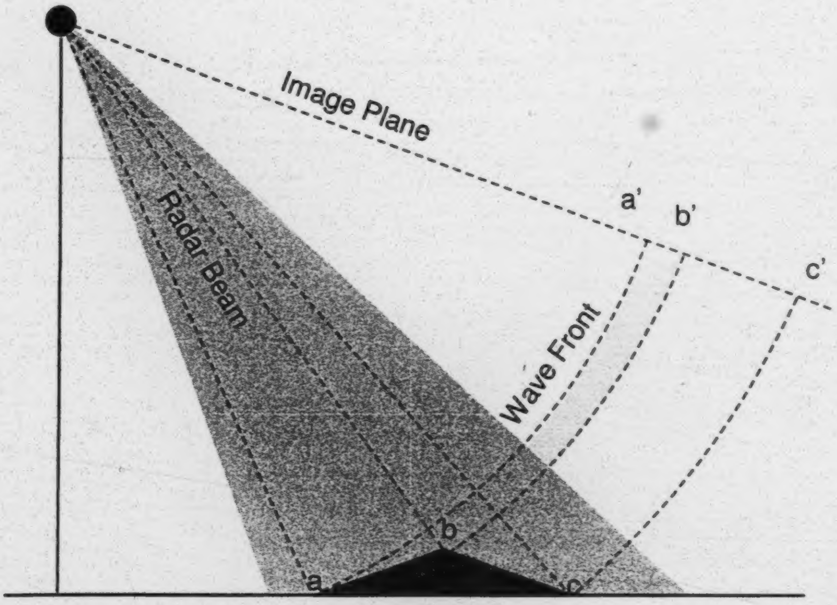
Image Plane
a'
b'
c'
Radar Beam
Wave Front
a
b
c

Figure 2.8 Geometrical distortion: foreshortening.

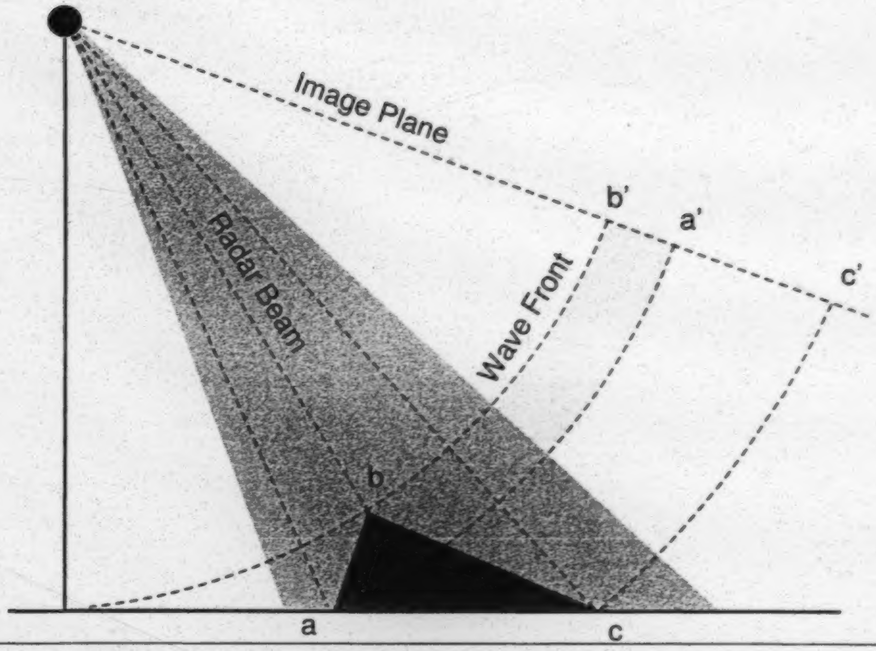
Image Plane
b'
a'
c'
Radar Beam
Wave Front
b
a
c

Figure 2.9 Geometrical distortion: layover.

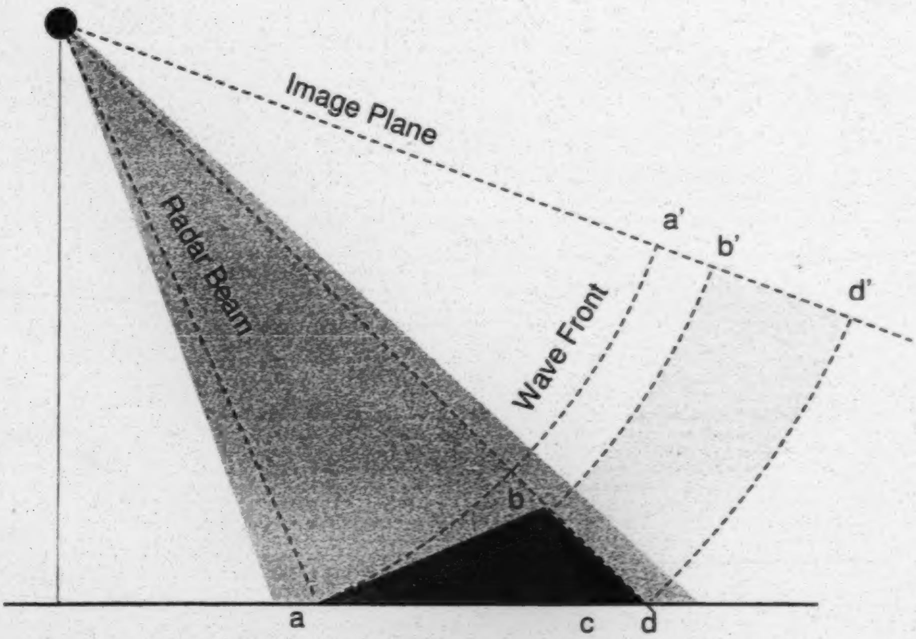
Image Plane
a'
b'
d'
Radar Beam
Wave Front
b
a
c
d

Figure 2.10 Geometrical distortion: radar shadow.

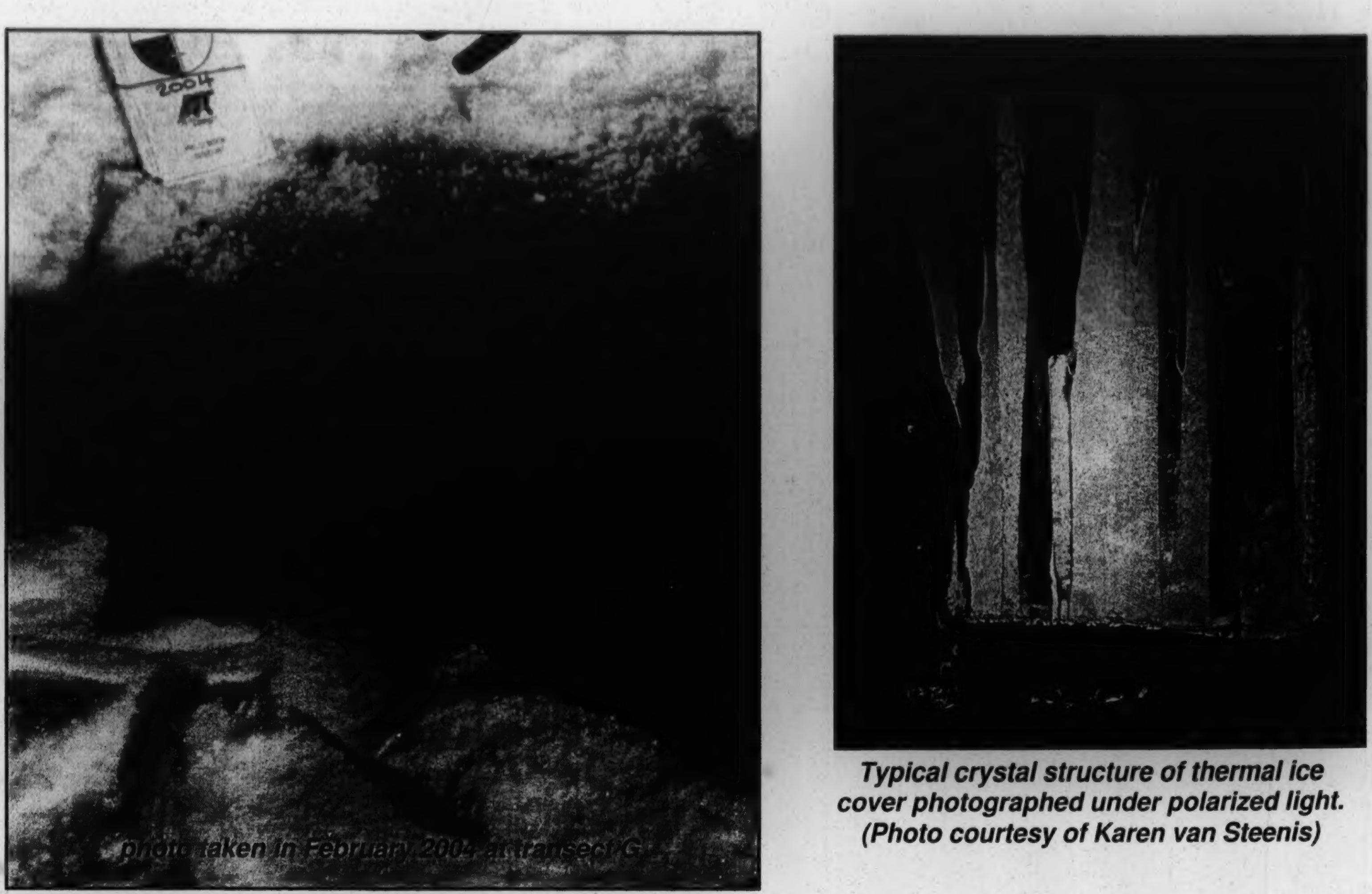

photo taken in February 2004 at transect G

Typical crystal structure of thermal ice cover photographed under polarized light. (Photo courtesy of Karen van Steenis)

Figure 2.11 Thermal ice cover.

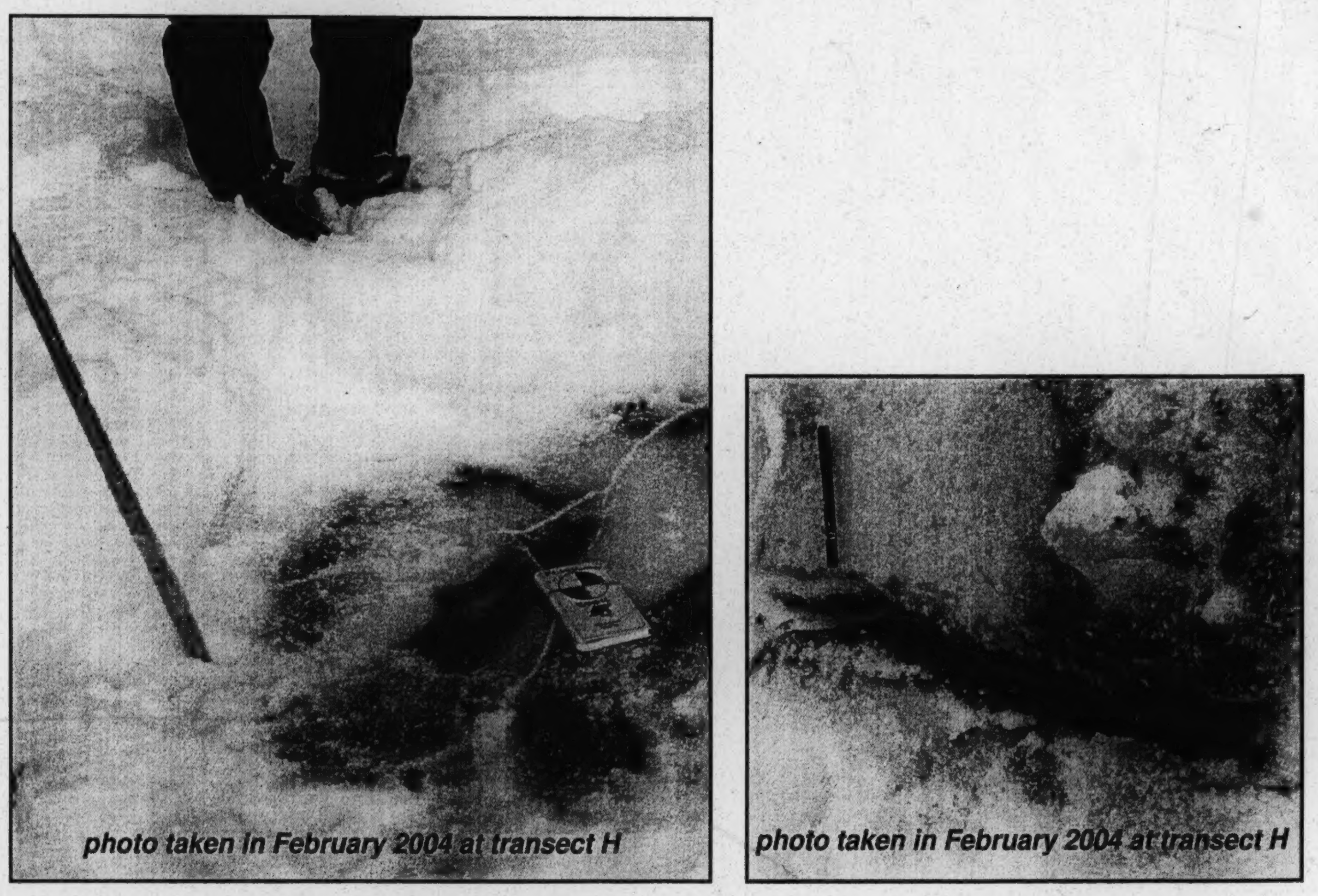

photo taken in February 2004 at transect H

photo taken in February 2004 at transect H

Figure 2.12 Thermal ice cover with cracks and bubbles.

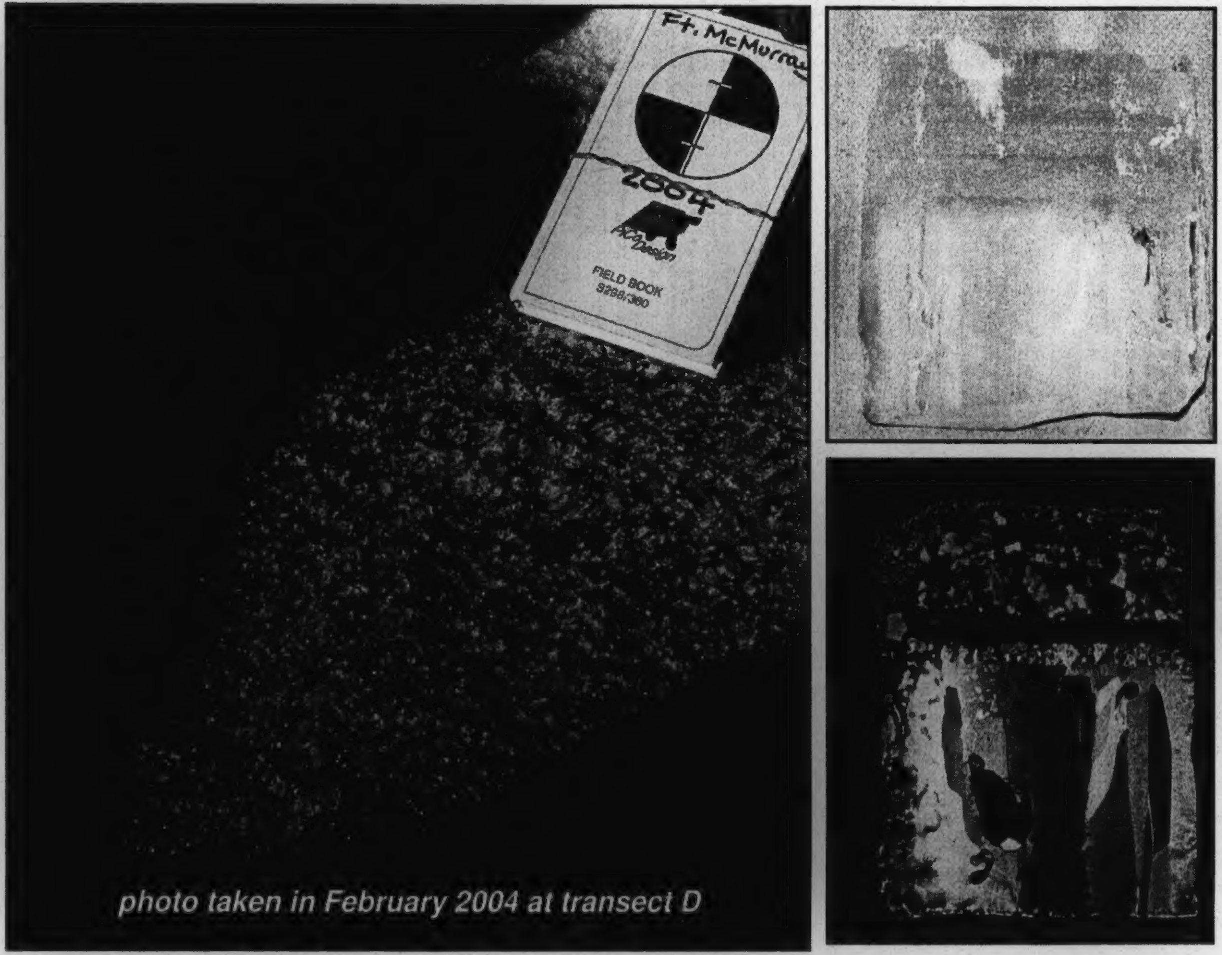
Ft. McMurray
2004
FIELD BOOK
S298/360

photo taken in February 2004 at transect D

Juxtaposed ice cover, in profile. (Photo courtesy of Karen van Steenis)

Typical crystal structure of a juxtaposed ice cover photographed under polarized light. (Photo courtesy of Karen van Steenis)

Figure 2.13 Juxtaposed ice cover.

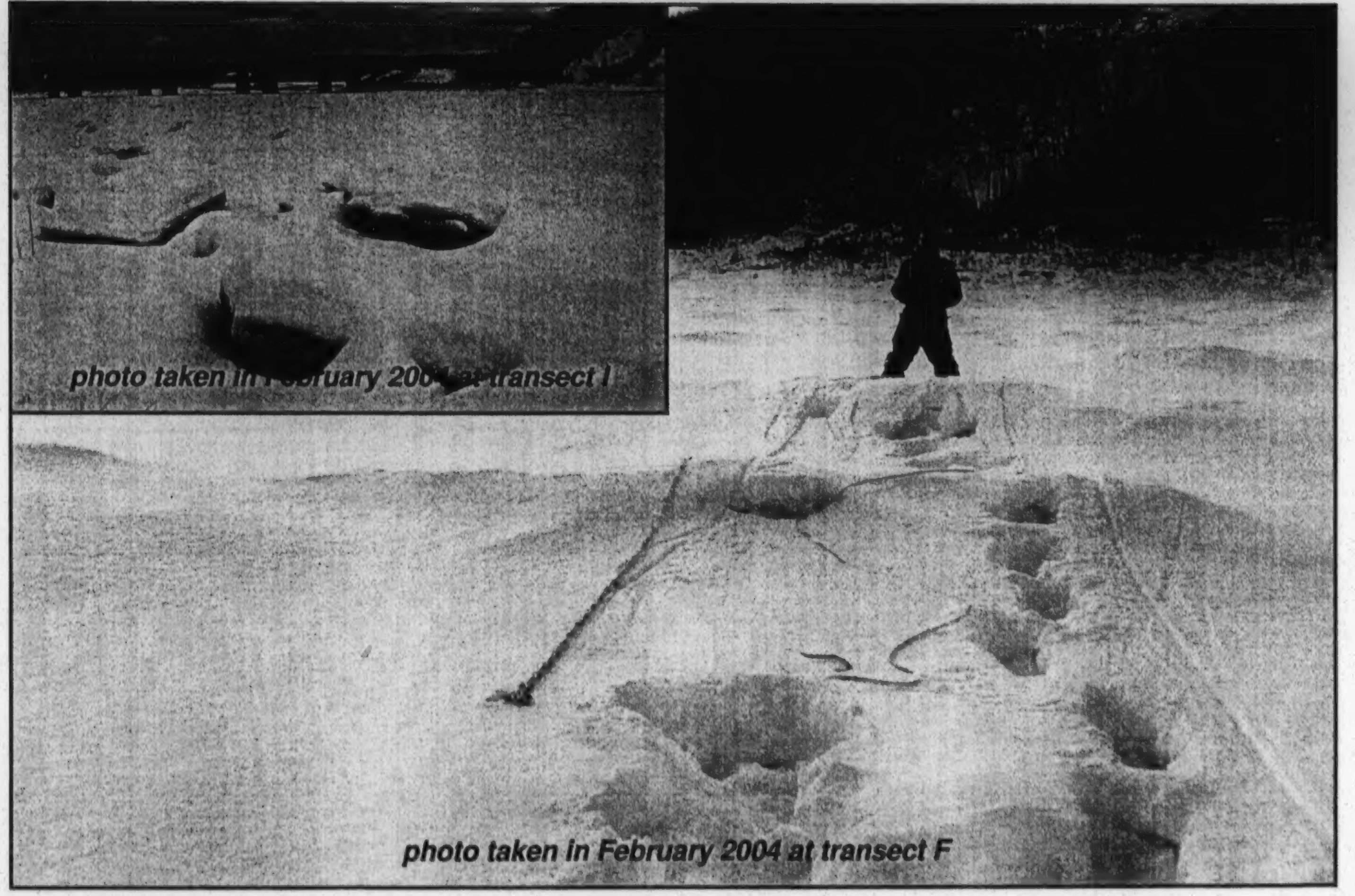
photo taken in February 200 at transect I
photo taken in February 2004 at transect F

Figure 2.14 Hummocky ice surface.

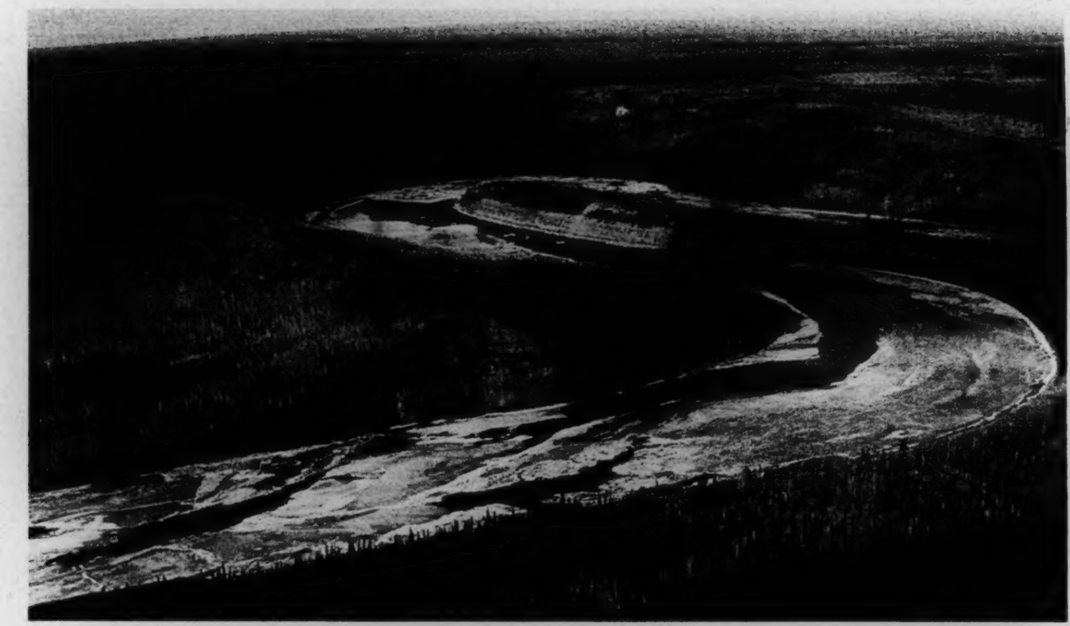

Figure 2.15 Thermally deteriorating river ice cover.

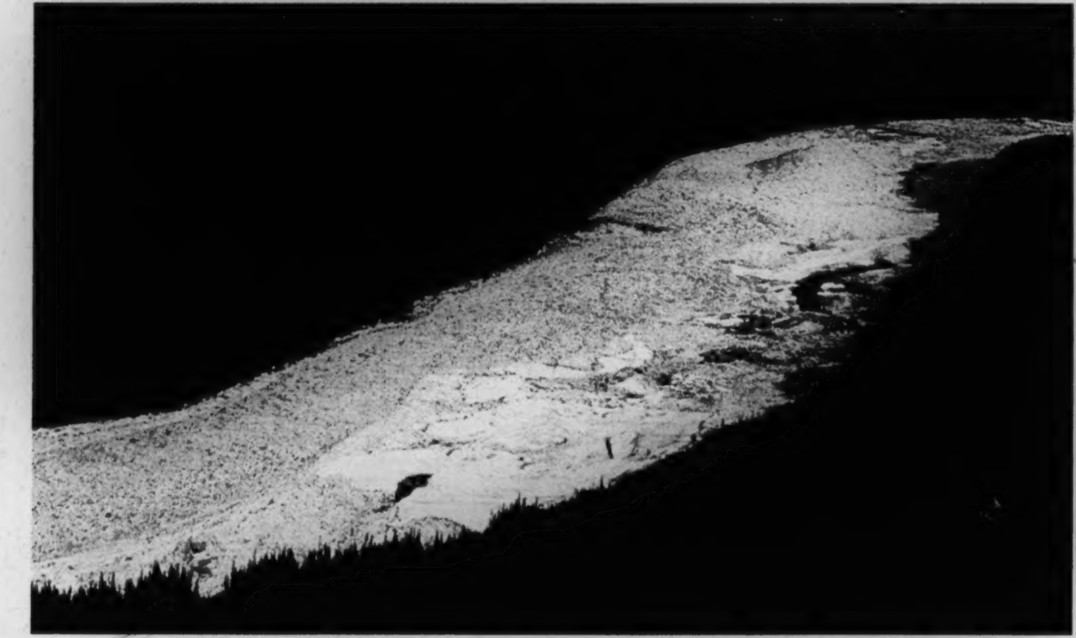

Figure 2.16 Breakup ice jam.

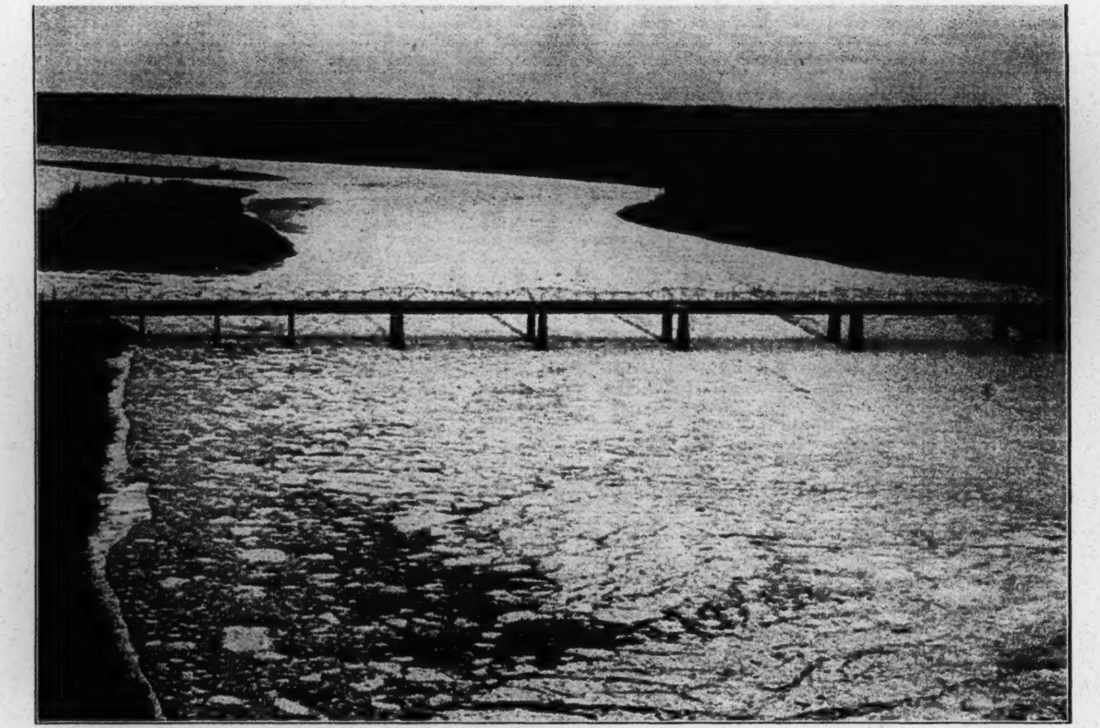

Figure 2.17 Running ice after ice jam release.

3.0 MONITORING BREAKUP: QUALITATIVE ANALYSIS

3.1 INTRODUCTION

For flood forecasting purposes, a primary goal of any breakup monitoring program is to detect the occurrence of ice jams which may threaten a community with flooding. To determine whether it might be possible to observe an ice jam from SAR data, a qualitative analysis was conducted on imagery obtained during the 2003 and 2004 breakup seasons on the Athabasca River. As a "first look", this portion of the analysis examines the extent of information which can be extracted by visually comparing the processed imagery to observed field conditions and ground truth data. Information of this type is incredibly valuable since it will be the primary resource in the field when satellite information is available but there is little time for extensive analysis.

3.2 STUDY AREA

For this project, the Athabasca River near Fort McMurray, Alberta was selected as the study area. As depicted in Figure 3.1, the selected reach extends from Crooked Rapids 35 kilometres upstream of the city to 10 kilometres downstream, near Inglis Island. The locations of staff gauges in this reach are noted in the figure. These are used to describe locations at which breakup developments occur.

Upstream of Fort McMurray, the river's gradient is approximately 0.001 m/m but it flattens out dramatically near the townsite to about 0.0002 m/m. The nature of breakup on the Athabasca River near Fort McMurray is generally quite dynamic and its start is typically marked by the development of a series of ice jams in the reach upstream of the community. As breakup progresses, the ice jams tend to release as a cascade through this steep reach and subsequently reform in the vicinity of Fort McMurray. Since this can cause severe flooding it is highly desirable, from an emergency preparedness perspective, to have prior knowledge of incoming ice runs. Consequently, an objective of the flood monitoring program during breakup is to determine the location and length of ice jams in the reach upstream of Fort McMurray.

Because of the extent of the reach contributing to these ice runs (nearly two hundred km) it is impractical and expensive to fly the river daily to identify incoming events. This investigation was initiated to determine if it would be possible to use Synthetic Aperture Radar (SAR) images, as acquired by the Canadian RADARSAT-1 satellite, to monitor the progression of breakup in an effort to aid flood forecasting efforts. Further, due to the susceptibility to ice jam flooding and the flood risk posed to the community, a comprehensive monitoring program was already in place at Fort McMurray. This facilitated ground-truth efforts and afforded an excellent opportunity to assess the usefulness of satellite SAR imagery.

3.3 METHODS

3.3.1 Field Observations

Ground referencing data were obtained throughout the breakup periods in 2003 and 2004 in order to assess the viability of using satellite SAR for river ice characterization. During the primary breakup period, water surface profiles were measured and ground-truth data for ice conditions were documented via digital still and video photography obtained during daily reconnaissance flights. This information was utilized to generate maps depicting the progression of breakup throughout the study reach.

3.3.2 Image Processing

Satellite imagery was obtained from the Canadian satellite RADARSAT-1 as detailed in Table 3.1 and Table 3.2. Following acquisition, the received RADARSAT-1 image data were converted to river ice information products by means of a series of image processing techniques. The image processing procedure adopted is comprised of SAR speckle filtering, image geocoding, and the generation of colourized ice information products. Finally, to facilitate interpretation and emphasize ice covered areas, a landmask overlay was applied. Figure 3.2 shows a subset of an original RADARSAT-1 image and the corresponding derived river ice information product, respectively.

Images were primarily taken in fine beam mode (8 m resolution) but, for some days, it was necessary to utilize the standard beam (25 m resolution). Apart from resolution, the primary difference between these two image types is that standard beam images are a product of multi-look processing and fine beam images utilize single look data. For multiple look images, measurements from adjacent resolution cells (cells that adjoin in the azimuth direction) are linearly averaged. A measurement from a single resolution cell is denoted as a "look" and standard beam imagery uses 3.2 "looks." The application of image filters for the purpose of speckle reduction is another averaging process which can effectively increase the "number of equivalent looks" (NEQ) in an image. The NEQ is not a determined by the SAR processing system but, rather, is a measure of the resultant textural variance after processing.

A protocol was adopted for processing all of the images. This procedure primarily involved filtering (for speckle reduction) and geocoding but consists of the steps outlined below.

1. **Backscatter:** the original image data was brought into PCI and the backscatter coefficient (σ^0) was calculated for each pixel.
2. **Cropping:** to streamline subsequent processing, each image was cropped such that only the bounds of the study reach were included. The information for the area of interest was then transferred to a new file using the image transfer command (III) in Xpace.
3. **Speckle Reduction:** the procedure for removing speckle was developed by Joost van der Sanden at the Canada Centre for Remote Sensing and involved the application of a gamma filter (FGAMMA) in a 2-step process.
    a. Fine beam imagery: a 5x5 pixel window was used in each application of the gamma filter.
        i. The first application was performed on the original image data (0.9 looks).
        ii. A second application was performed on the resultant data (6.60 NEQ).
    b. Standard beam imagery: a 3x3 pixel window was used in each application of the gamma filter.

    i. The first application was performed on the original image data (3.2 looks).
    ii. A second application was performed on the resultant data (6.97 NEQ).

   After processing, both the standard and fine beam imagery had approximately 10 NEQ.

4. **Convert to decibels:** after the gamma filters were applied, the image data was converted to express the backscatter coefficient (σ^0) in decibels.
5. **Geocoding:** rivers vectors and a georeferenced Landsat image were used with GCPWorks to geocode the images. For each image, no less than thirteen ground control points were selected and these were concentrated along the river. Selecting points in this manner likely reduced the level of accuracy in other parts of the image but achieved the best results in the vicinity of the river. Other features were really not a concern for the purposes of this project. A second order polynomial transformation (requiring a minimum of 7 ground control points) was utilized and nearest neighbour was selected as a resampling mode.

The 32-bit filtered, geocoded image plane was exported as an ASCII file so that it could be brought into ArcView. A colour scale was then applied over the dynamic range of the data (-5 dB to -25 dB) such that relatively high backscatter was displayed in the yellow/orange/red colour range and relatively low backscatter was displayed in the cyan/blue colour range. Then, in order to display the surrounding terrain in a clear and effective manner, a black and white overlay of the "land" was added to the imagery. This overlay was constructed using stitched panchromatic data from Landsat acquisitions. Islands and sand bars located within the river were excluded from the overlay because the exposed portion of islands can vary widely depending on water level.

3.4 BREAKUP 2003

3.4.1 Field Observations

Daily observations of ice conditions and measurements of water surface profiles commenced on April 16, 2003 and continued until April 23, 2003. Figure 3.3 through Figure 3.8 present maps depicting the progression of breakup through the study reach, based on the digital still and video photography obtained during reconnaissance flights.

Open leads at the rapids, some border flow, and slight thermal deterioration of the ice downstream of the bridges were observed on April 15 (Figure 3.3). Conditions changed little until April 21 (Figure 3.6), when the AENV observers at G140 reported the commencement of an ice run at 08:15. Water levels rose by about 3 m in 25 minutes, and the ice run continued for about 45 minutes. An observational flight documented the ice run stalling approximately 30 km upstream of the city. At 10:00 this ice started to move again and by 11:45 the ice run was about 20 km upstream of the city. By 15:15, a 10 km long ice jam had formed about 10 km upstream of the city (Figure 3.7).

By April 22 at 08:00, the jam had not moved and water levels were dropping in the city (as would be expected since water was being stored within the jam upstream). By 12:30 the jam had increased in length to 12-15 km. The daily observational flight revealed that a second ice run was on the way, and by timing its rate of travel, it was determined that it should reach the ice jam poised upstream of the city at about 16:00. By 15:00, the AENV observers at station G140 reported the river running full of ice and an associated 2 m rise in water level.

The arrival of this wave of ice and water at the head of the ice jam caused it to release. The resulting wave release passed station 90 at 18:06. Based on manual measurements at this station, a peak magnitude of over 4 m was documented. Manual water level measurements were also taken at station G75 where the peak wave height was about 3 m. The automated measurements at the Water Survey of Canada gauge (Station G57) discontinued part way through this event. The ice run passed through Fort McMurray without jamming; however, it did leave residual ice obstructing outflow from the Clearwater River. The resulted in a rapid and significant (>2 m) rise in water level, which persisted for more than 48 hours.

3.4.2 Results

The processed images were qualitatively compared to ground referencing photos obtained to assess their value for categorizing the nature of the breakup ice cover. In particular, an attempt was made to distinguish open water (which would have the lowest backscatter), intact ice (which would generate moderate backscatter) and rough ice, indicating ice jams, which would be expected to cause the highest backscatter.

3.4.3 April 8, 2003

A fine beam (F3F) RADARSAT-1 image was taken at 07:37:13 on April 8, 2003. There was little ground truth data available for this date but the river ice image product is included (Figure 3.9) for the sake of documenting breakup progression as fully as possible. It should be noted that the ice cover appears visibly brighter along the reach from the town site to the vicinity of G110. This is suspected to be the result of a freeze-up ice jam which had formed in the reach.

3.4.4 April 15, 2003

A fine beam (F5) RADARSAT-1 image was taken at 07:33:02 on April 15, 2003. Due to weather conditions, photographic data could not be utilized to validate radar data. However, the development of open leads as noted from field observations (Figure 3.3) corresponds well to areas of low backscatter in the river ice image product (Figure 3.10).

3.4.5 April 18, 2003

A fine beam (F2N) RADARSAT-1 image of the study reach taken five days before breakup is shown in Figure 3.11. The satellite image was taken during an evening overpass at 19:12:09 on April 18, 2003 and photographs taken between 17:00 and 18:00 of the same day were used to support inferences made from the satellite image. It is interesting to note that on this day, the reach downstream of G110 no longer exhibited significantly higher backscatter than the rest of the river. This is most likely due to changes in the ice cover (i.e. the wetting of the ice due to thermal deterioration). As the wetness increases, more of the incident microwave energy is reflected at the ice-air interface (i.e. the ice surface) thereby allowing less energy to penetrate the ice volume. Consequently, the radar return signal of a wet ice cover is governed to a greater extent by the cover's surface roughness. The effect of any change in viewing geometry (i.e. ascending rather than descending acquisition), is likely negligible since the overall backscattering properties of the ice cover are highly omnidirectional.

A close-up of the region downstream of the town site is presented in Figure 3.12. Although overall the satellite image indicated only moderate backscatter across the river, it was still possible to discern several areas of relatively lower backscatter (darker blue in colour) lining the left bank near the sewage lagoons. As can be confirmed by the photographs, these areas corresponded to open water. It should be noted that those areas appearing red or orange (high backscatter) represent the islands in the river. Land tends to generate substantially higher backscatter than ice and is therefore quite apparent. Note also that this can generate masking errors as the delineation of bank features obviously varies with water level. This variation was not taken into account at this stage of the investigation.

Figure 3.13 presents an enlarged view of the reach immediately upstream of the Grant MacEwan Bridge. In this image an accumulation of ice at the Horse River confluence shows up clearly as yellow (higher backscatter) amidst the overall moderate return of the surrounding ice (green and cyan). The thin borders (in red) along the eastern bank at both the golf course and the water treatment plant are due to masking error, as discussed above.

In some instances it was possible to delineate the shape and location of long open leads. As shown in Figure 3.14, a large open lead lined the left bank near the upstream extremity of the reach. There were also two areas of open water immediately upstream of G130. Another example of the clear delineation of open water could be noted in Figure 3.15. Just downstream of G135, a large triangular-shaped area of open water visible in the satellite image corresponded very closely to that in the photograph. In Figure 3.16, the ice cover at Cascade Rapids exhibited somewhat higher backscatter than the surrounding area in the satellite image. Also, areas of open water were visible near G140; note the segment lining the left bank and the area upstream of the island.

3.4.6 April 21, 2003

As presented in Figure 3.17, a standard beam (S1) RADARSAT-1 image was taken at 07:57:58 on April 21, 2003. As with the April 8 image, though, ground truth data was unavailable on this date.

3.4.7 April 22, 2003 (07:28:45)

A standard beam (S7) RADARSAT-1 image was taken during a descending overpass on April 22, 2003 at 07:28:45, shortly after the formation of an ice jam. The image product presented in Figure 3.18 clearly reveals the jam length and location. The jam extends from the toe, occurring downstream of G110, to the head, located upstream of G130. The jam itself generated higher backscatter than the intact ice downstream of G110. This increase can be explained by the extreme surface roughness of the highly consolidated ice cover that makes up the jam.

Figure 3.19 provides a closer look at the ice cover downstream of the Grant MacEwan Bridge. The ice cover was still partially intact, but the image indicated open water around the perimeter of the islands and along the right bank of the main channel downstream of the Clearwater confluence, as confirmed by the photograph. The reach of river from G110 to Mountain Rapids is presented in Figure 3.20. Near G110, the toe of the jam could be distinguished, having a higher backscatter than the intact ice cover downstream. Some intact ice and open water along the right bank upstream of G110 could also be noted on the image. Figure 3.21 shows the upstream end of the ice jam in the vicinity of G130.

The areas of higher backscatter near the head of the jam (red in colour) would seem to indicate the presence of a locally rougher ice cover. However, the associated photograph and ground truth observations did not support this interpretation. In fact, the ice cover near the head of the accumulation was less consolidated, compared to that in the main body of the jam downstream, with water visible near the top of the ice. The heavy consolidation within the body of the jam is indicative of a much thicker accumulation (> several meters thick). Since the ice mass is known to float with about 10% of its thickness above the water level, the rough exposed ice above the water can be of substantial thickness itself and thus appears dry. The result then was a dry rough surface with textural elements in the order of metres. It follows that the increased backscatter observed near the head could be attributed to the increased surface scatter as a result of the surface wetness.

Another feature that could be easily discerned from the satellite image was "residual ice," as presented in Figure 3.22. As used here, residual ice refers to both the shear walls and the intact sheets (predominantly border ice) which remain after the ice cover has broken up. Large sheets of unbroken ice were recognizable along the left bank near G140 and at Little Cascade Rapids. As well, there was residual intact ice along the right bank near Cascade Rapids and residual consolidated ice around the island.

3.4.8 April 22, 2003 (18:55:28)

A standard beam (S1) RADARSAT-1 image was acquired at 18:55:28 on April 22, 2003 shortly after the release of the ice jam. Again, due to swath limitations, it was not possible to obtain a fine beam image at this time. Upon release, a wave of ice and water propagated through town and continued downstream, marking the start of a major ice run. Note that once a jam releases, its structure changes dramatically. An in-place jam is a static accumulation of ice floes, the total thickness of which is on the order of metres. This results in a significant depth of the jam resting well above the phreatic surface, making it appear very dry. In contrast, a jam that has released spreads out longitudinally making it both longer and thinner. This also means that there is less ice above the phreatic surface, making the surface of the ice run wetter. Figure 3.23 shows the image product for this date taken shortly after this release. The running ice was clearly visible on the image, as was the leading edge of the ice run, located near Stony Island. This correlated well with video photography obtained from a helicopter at this time (also shown in Figure 3.23). Also visible is in the image is an apparent "open channel" along most of the reach. Because running ice tends to be more concentrated where flow is the fastest, this likely corresponds to an area of lower concentration (as can be noted in Figure 2.17).

3.4.9 April 25, 2003

On this date, a fine beam (F2N) image was taken at 7:41:23. By the time of acquisition, the ice run had fully moved through the river and there was open water throughout the entire extent of the study reach. As is clear in the satellite data (Figure 3.24), only some residual ice remained. This can be noted near G140, G110 and immediately downstream of the twin bridges where the ice is still attached to the banks in some areas.

3.5 BREAKUP 2004

3.5.1 Field Observations

Daily observations of ice conditions and measurements of water surface profiles commenced quite early in April of 2004. Figure 3.25 through Figure 3.27 present maps depicting the progression of breakup throughout the study reach, based on the digital still and video photography obtained during reconnaissance flights.

The ice cover began to thermally deteriorate near the start of the month and, by April 6, the ice was noticeably darker and open leads were beginning to develop (Hicks 2004). This decay continued and on April 12 small accumulations were documented at Mountain Rapids, Little Cascade Rapids and Crooked Rapids. On April 15, however, intermittent snow started and notably slowed breakup progression. In the subsequent days, little change was visible and even with rain on several days, no major changes were noted. A small ice run was reported at Cascade Rapids, though, and apparently some minor shoves occurred downstream of Mountain Rapids on April 21st and April 22nd. By this point, though, the sustained thermal decay throughout the reach had essentially eliminated the risk of a threatening dynamic event. Melt continued and by the time of the last image (on April 26), the study reach was free of ice.

3.5.2 Results

The processed images were qualitatively compared to ground referencing photos obtained to assess their value for categorizing the nature of the breakup ice cover. As with the data from 2003, special attention was paid to try and distinguish open water, intact ice and rough (jammed) ice.

3.5.3 April 9, 2004

A fine beam (F5) RADARSAT-1 image of the study reach taken at 07:33:02 on April 9, 2004 is shown in Figure 3.28. The portion of the study reach upstream of Cascade Rapids is presented with available aerial photo data in Figure 3.29. In this figure, segments of open water near Crooked Rapids are quite visible in the radar data. Additionally, the ice in the vicinity of Cascade Rapids corresponds to an area in the image product which exhibits a significantly higher backscatter (red/orange) coefficient than the surrounding ice.

Figure 3.30 provides a closer look at the reach extending from Mountain Rapids to the Grant MacEwan Bridge at the townsite. Open leads just upstream of Mountain Rapids were noted on this date and aerial photography closely matches satellite data in this area. Another feature of note in the radar data is the patch of ice immediately adjacent to the water treatment plant (G90). This area generated significantly higher backscatter (red/orange) than ice upstream and downstream. Though not obvious in the photo taken from the plane, this was actually the location of a substantial freeze-up accumulation, making the ice incredibly rough (on the order of metres) here.

3.5.4 April 12, 2004

A fine beam (F2N) RADARSAT-1 image of the study reach taken at 19:12:11 on April 12, 2004 is shown in Figure 3.31. The upstream portion of the study reach (from G140 to G135) is shown in Figure 3.32 with digital stills taken the same day. Note the deterioration in the reach downstream of the island and the large open lead at G135.

Several accumulations were noted on this day, and the one at Mountain Rapids was likely the most obvious. Figure 3.33 provides a view of this feature as detected by the satellite. The accumulation itself has a higher backscatter (yellow/orange) while the water upstream of it generates a much lower backscatter (dark blue). Two separate photographs of the accumulation are also included for comparison purposes.

3.5.5 April 15, 2004

A standard beam (S1) RADARSAT-1 image of the study reach taken at 07:57:57 on April 15, 2004 is presented in Figure 3.34. Both the radar image and digital stills were acquired prior to the onset of snow which occurred later this day, slowing the progression of breakup. Figure 3.35 depicts the upstream portion of the study reach. Small ice runs had started to occur resulting in accumulations (with open water upstream). Several of these such accumulations can be noted in the image product. Similarly, Figure 3.36 also shows several accumulations caused by small upstream ice runs. Note that the accumulation near Mountain Rapids has increased in length.

3.5.6 April 19, 2004

Figure 3.37 provides a river ice image product for the scene captured at 07:41:22 on April 19 by the fine beam (F2) sensor aboard RADARSAT-1. Though breakup had slowed significantly by this time, thermal deterioration was still occurring and there were notable changes between this acquisition and the one on April 15th. As can be noted in Figure 3.38, the meander at Crooked Rapids had completely broken up, essentially leaving only open water and a relatively minor accumulation downstream. While some intact ice was remaining near G140 and at Cascade Rapids, there were large extents of open water and even a large open lead running through the centre of Cascade Rapids.

Figure 3.39 shows the deteriorating accumulation at Mountain Rapids. While it is still present and there is clearly still intact ice downstream, it is much shorter by this date, as evidenced by the photographs. The reach downstream of the townsite is presented in Figure 3.40. In contrast to the upstream portions of the study reach, this segment of the river has a very slight gradient, and its deterioration can likely be almost wholly attributed to thermal factors. As a result, no accumulations were noted, but expanses of intact ice and open water could be delineated quite precisely.

3.5.7 April 26, 2004

The final image acquired during this breakup season was taken at 7:37:12 on April 26, 2004. It was captured with the RADARSAT-1 fine beam (F3F) sensor and the corresponding image product is presented in Figure 3.41. By this date, the river was essentially completely free of ice (with the exception of some residual ice). Dark blue areas are indicative of open water and the image product is certainly validated by the observed conditions.

3.6 SUMMARY

Approaching the analysis of SAR imagery from a purely qualitative standpoint has proven to be a valuable means of researching breakup progression. Straightforward image processing techniques were employed to enhance the RADARSAT-1 images and these were compared to aerial photographs and observations made during the breakup period. With regard to utilizing SAR as a forecasting tool, it appears that the greatest benefit may be realized by its demonstrated effectiveness in classifying types of ice cover.

Using this methodology, it was possible to identify various features present in the images (from both 2003 and 2004) which are indicative of specific stages of river breakup. At the onset of breakup, the development of open leads was quite evident; open water and border flow could be located and clearly delineated. As the ice cover continued to deteriorate, it was also possible to discern accumulations of consolidated ice. Ice jams are especially obvious due to the significantly higher backscatter generated in these reaches of the river as compared to intact ice. Furthermore, if an ice run is captured during an image acquisition, this can also be visually discriminated from other ice types.

Table 3.1 Image acquisition schedule for 2003 Athabasca River breakup.

Date (UTC)	Time (UTC)	Date (Local)	Time (Local)	Mode	Incidence Angles (degrees)
1-Apr-03	13:41:23	1-Apr-03	6:41:23	F2N	39-42
8-Apr-03	13:37:13	8-Apr-03	7:37:13	F3F	41-44
15-Apr-03	13:33:02	15-Apr-03	7:33:02	F5	45-47
19-Apr-03	1:12:09	18-Apr-03	19:12:09	F2N	39-42
21-Apr-03	13:57:58	21-Apr-03	7:57:58	S1	24-31
22-Apr-03	13:28:45	22-Apr-03	7:28:45	S7	39-42
23-Apr-03	0:55:28	22-Apr-03	18:55:28	S1	24-31
25-Apr-03	13:41:23	25-Apr-03	7:41:23	F2N	39-42

Table 3.2 Image acquisition schedule for 2004 Athabasca River breakup.

Date (UTC)	Time (UTC)	Date (Local)	Time (Local)	Mode	Incidence Angles (degrees)
9-Apr-04	13:33:02	9-Apr-04	7:33:02	F5	45-47
13-Apr-04	1:12:11	12-Apr-04	19:12:11	F2N	39-42
15-Apr-04	13:57:57	15-Apr-04	7:57:57	S1	24-31
19-Apr-04	13:41:22	19-Apr-04	7:41:22	F2	39-42
26-Apr-04	13:37:12	26-Apr-04	7:37:12	F3F	41-44

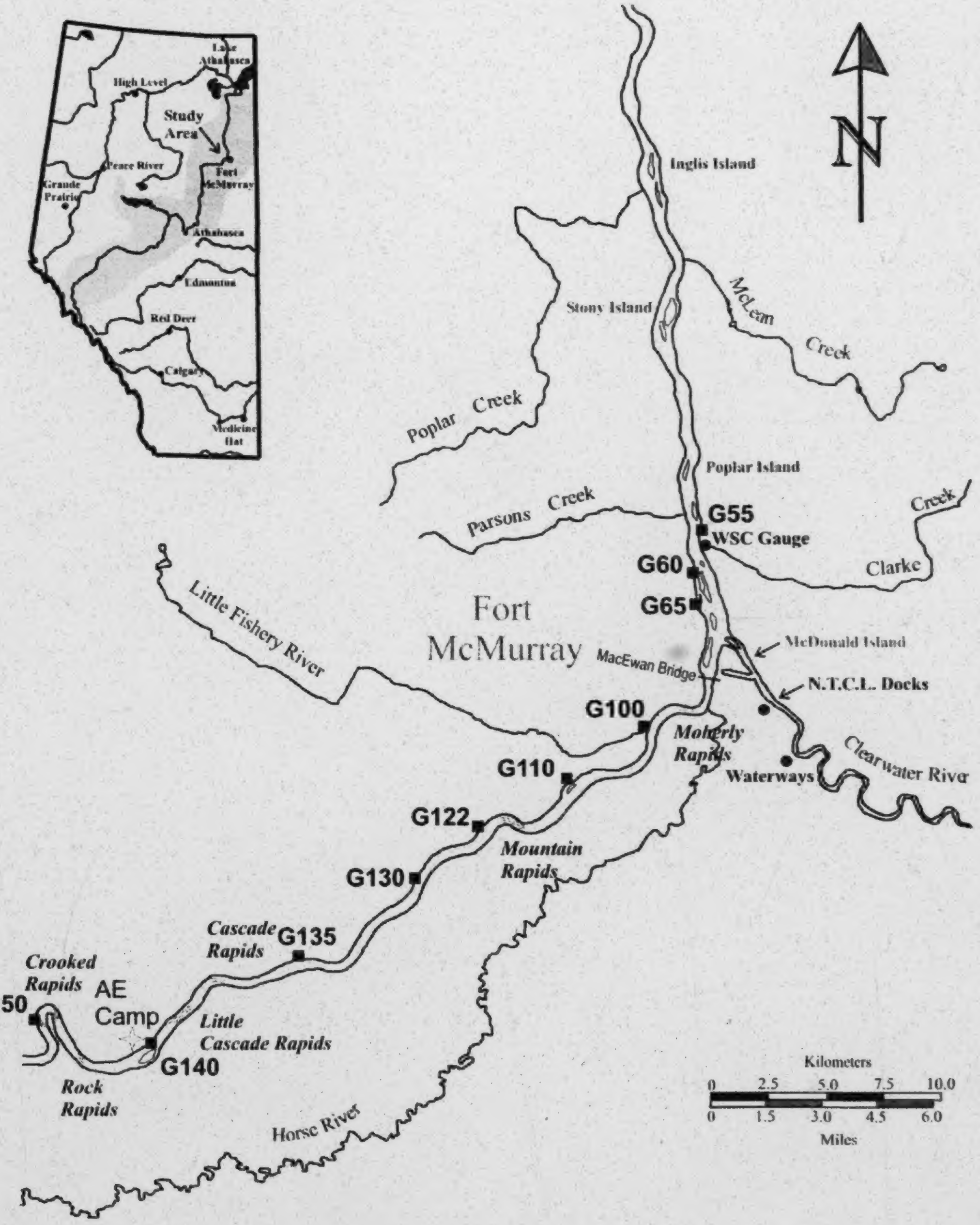
Lake Athabasca
High Level
Study Area
Peace River
Fort McMurray
Grande Prairie
Athabasca
Edmonton
Red Deer
Calgary
Medicine Hat
N
Inglis Island
Stony Island
McLean Creek
Poplar Creek
Poplar Island
Parsons Creek
G55
WSC Gauge
Clarke Creek
G60
G65
Fort McMurray
McDonald Island
MacEwan Bridge
N.T.C.L. Docks
Little Fishery River
G100
Moberly Rapids
Waterways
Clearwater River
G110
G122
Mountain Rapids
G130
Cascade Rapids
G135
Crooked Rapids
AE Camp
G150
Little Cascade Rapids
G140
Rock Rapids
Horse River
Kilometers
0 2.5 5.0 7.5 10.0
0 1.5 3.0 4.5 6.0
Miles

Figure 3.1 Athabasca River study reach (adapted from Robichaud, 2003).

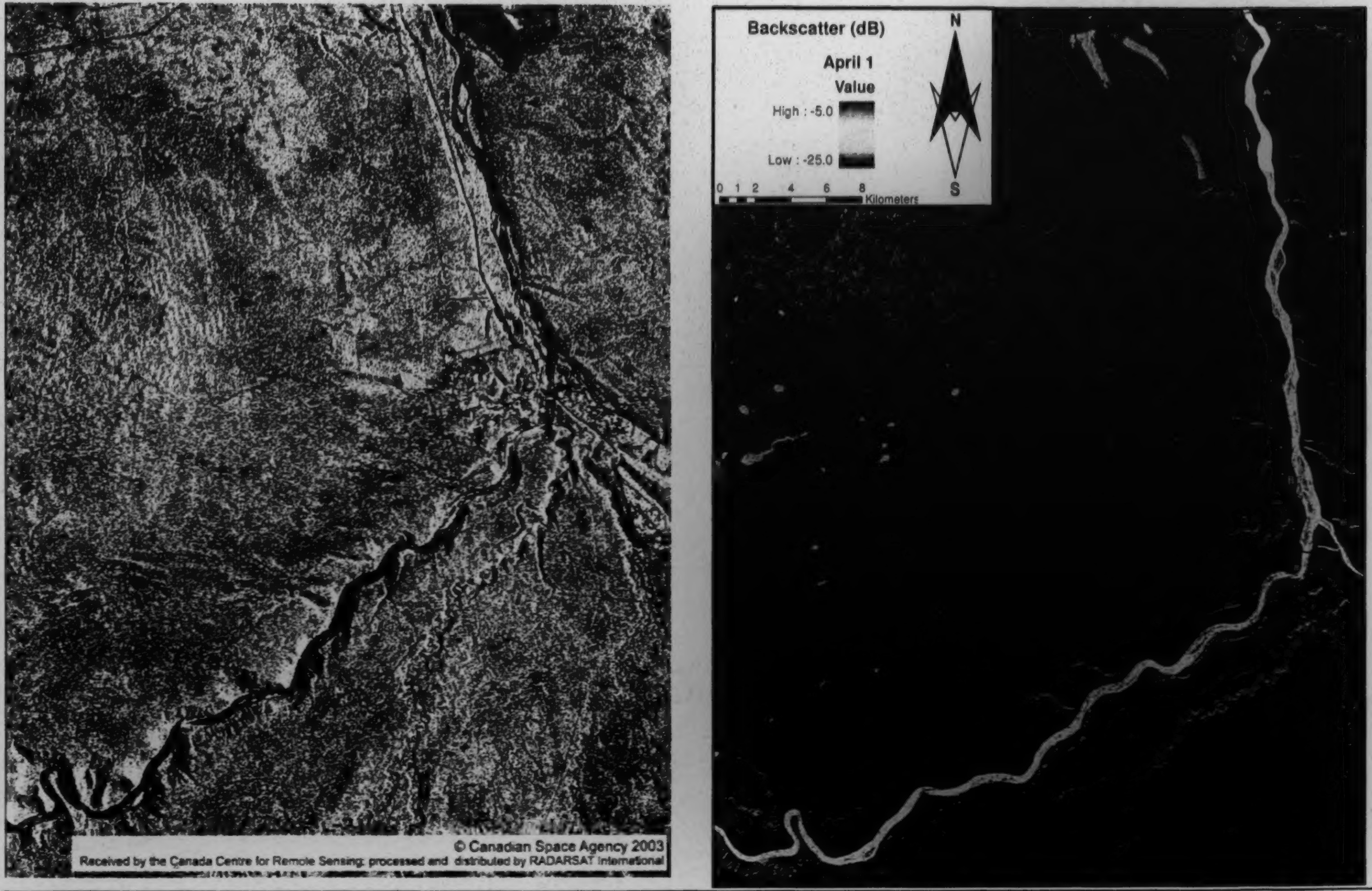
© Canadian Space Agency 2003
Received by the Canada Centre for Remote Sensing: processed and distributed by RADARSAT International
Backscatter (dB)
April 1
Value
High : -5.0
Low : -25.0
0 1 2 4 6 8
Kilometers
N
S

Figure 3.2 Comparison of original RADARSAT-1 image with the corresponding derived river ice information product.

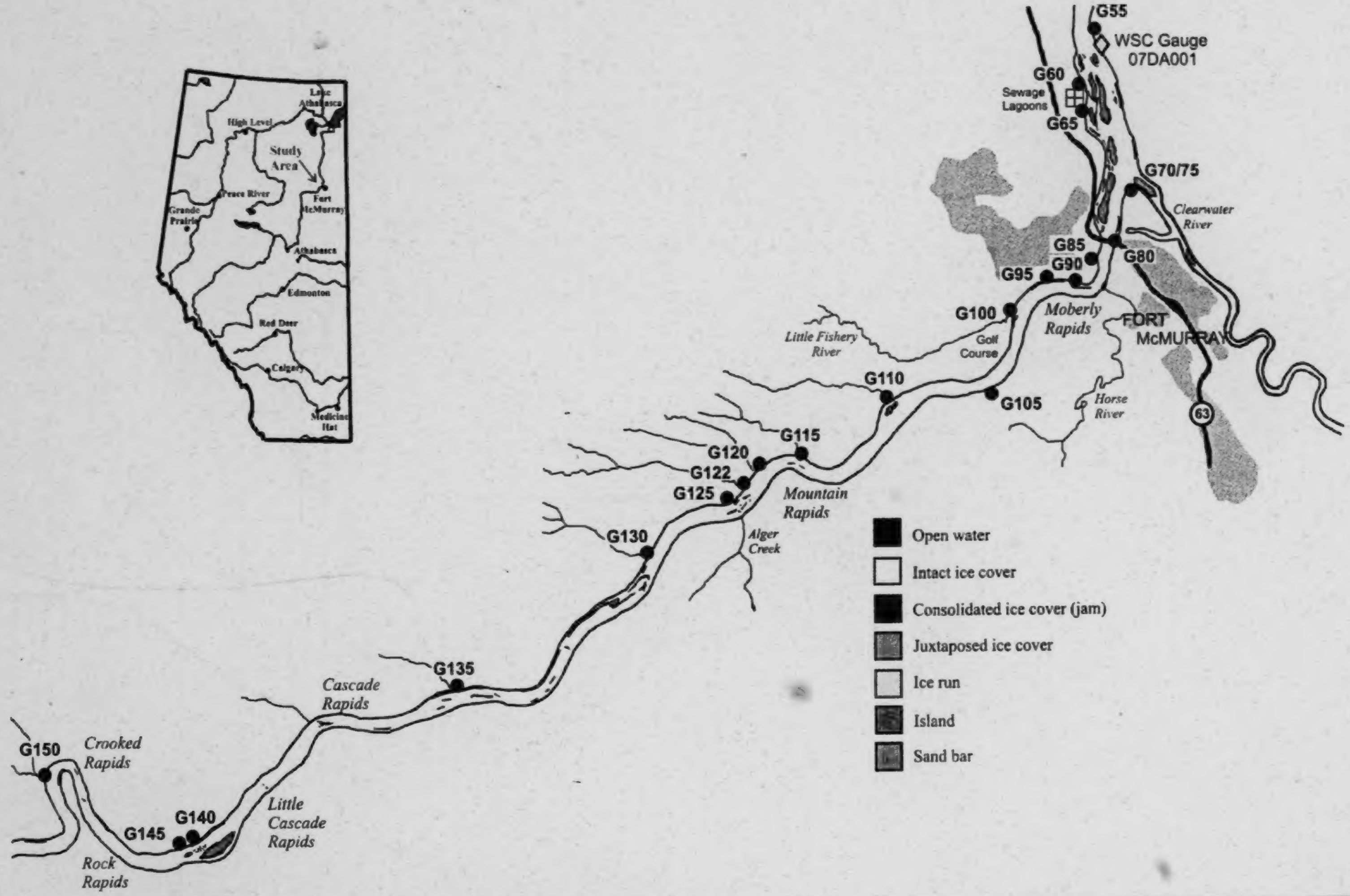
G55
WSC Gauge
07DA001
G60
Sewage Lagoons
G65
G70/75
Clearwater River
G80
G85
G90
G95
G100
Golf Course
Moberly Rapids
FORT McMURRAY
63
Little Fishery River
G105
Horse River
G110
G115
G120
G122
G125
Mountain Rapids
Alger Creek
G130
G135
Cascade Rapids
G140
G145
Little Cascade Rapids
G150
Crooked Rapids
Rock Rapids
Lake Athabasca
High Level
Study Area
Peace River
Grande Prairie
Fort McMurray
Athabasca
Edmonton
Red Deer
Calgary
Medicine Hat
Open water
Intact ice cover
Consolidated ice cover (jam)
Juxtaposed ice cover
Ice run
Island
Sand bar

Figure 3.3 Ice conditions in the study reach on April 15, 2003.

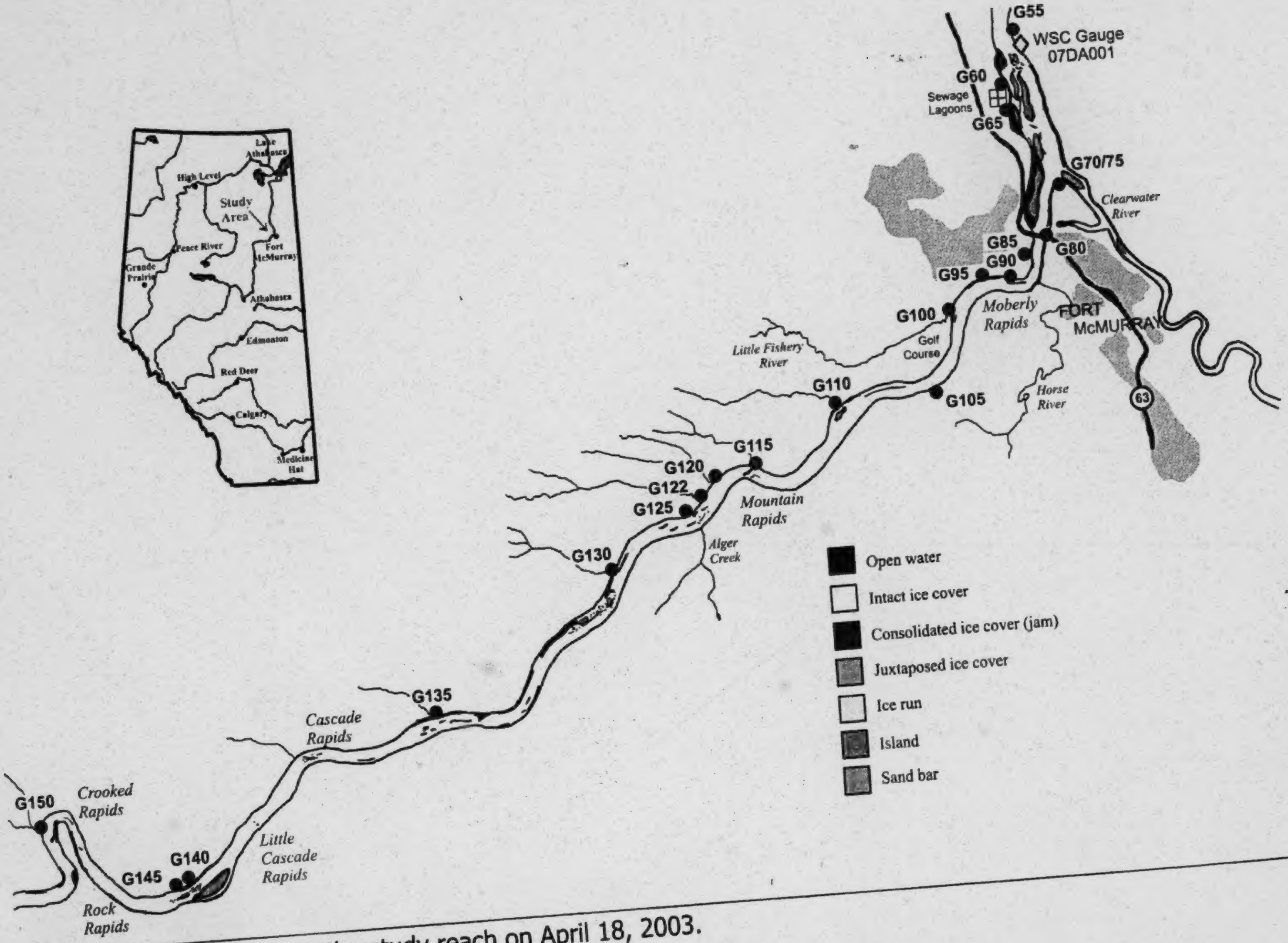
G55
WSC Gauge
07DA001
G60
Sewage
Lagoons
G65
G70/75
Clearwater
River
G80
G85
G90
G95
Moberly
Rapids
FORT
McMURRAY
63
G100
Golf
Course
Little Fishery
River
Horse
River
G105
G110
G115
G120
G122
G125
Mountain
Rapids
Alger
Creek
G130
G135
Cascade
Rapids
Little
Cascade
Rapids
G140
G145
Rock
Rapids
G150
Crooked
Rapids
Lake
Athabasca
High Level
Study
Area
Peace River
Fort
McMurray
Grande
Prairie
Athabasca
Edmonton
Red Deer
Calgary
Medicine
Hat
■ Open water
☐ Intact ice cover
■ Consolidated ice cover (jam)
▨ Juxtaposed ice cover
☐ Ice run
▨ Island
▨ Sand bar

Figure 3.4 Ice conditions in the study reach on April 18, 2003.

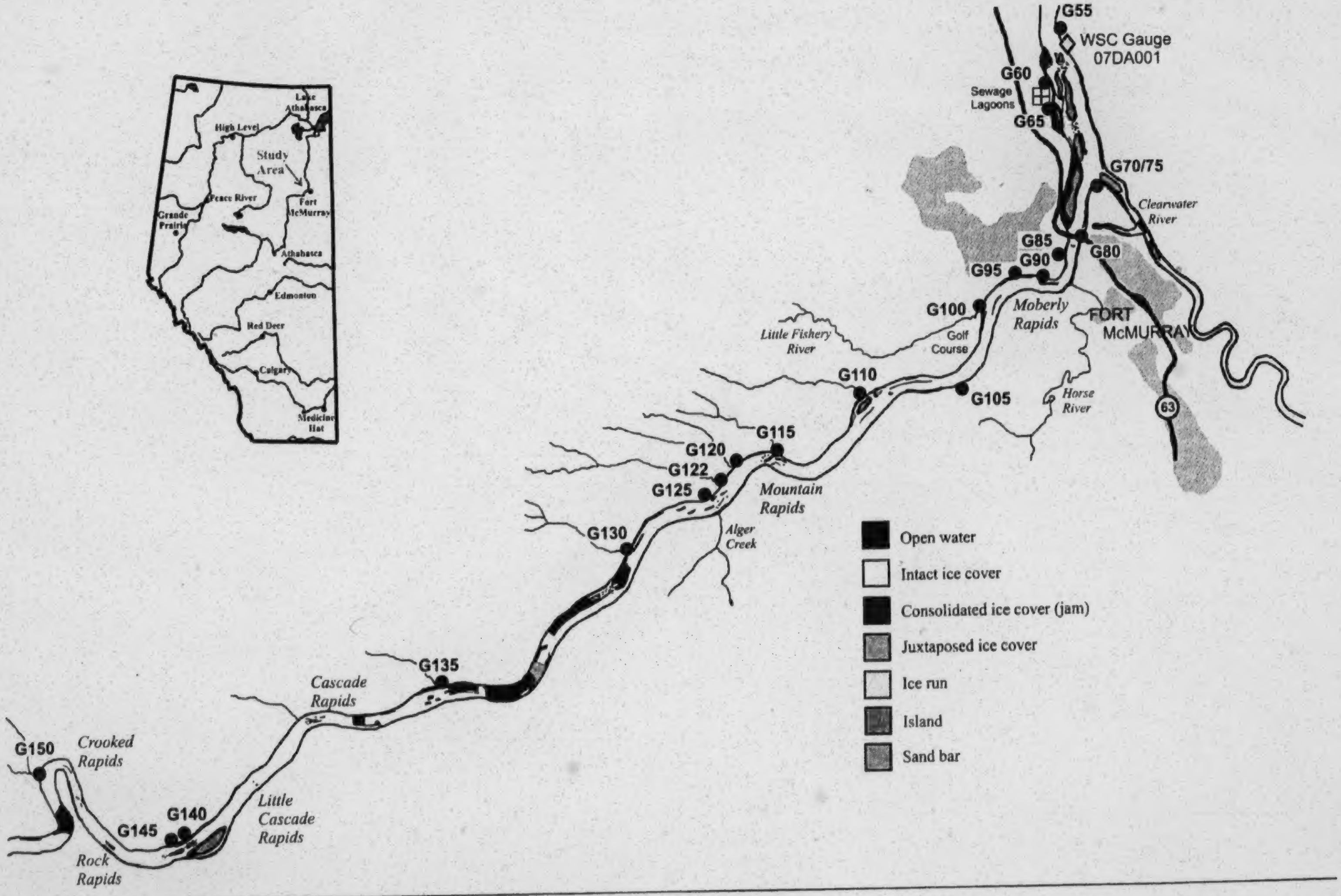

G55
WSC Gauge
07DA001
G60
Sewage
Lagoons
G65
G70/75
Clearwater
River
G85
G90
G80
G95
G100
Golf
Course
Moberly
Rapids
FORT
McMURRAY
Little Fishery
River
G110
G105
Horse
River
63
G115
G120
G122
G125
Mountain
Rapids
G130
Alger
Creek
G135
Cascade
Rapids
G150
Crooked
Rapids
G140
G145
Little
Cascade
Rapids
Rock
Rapids
Lake
Athabasca
High Level
Study
Area
Peace River
Fort
McMurray
Grande
Prairie
Athabasca
Edmonton
Red Deer
Calgary
Medicine
Hat
Open water
Intact ice cover
Consolidated ice cover (jam)
Juxtaposed ice cover
Ice run
Island
Sand bar

Figure 3.5 Ice conditions in the study reach on April 20, 2003.

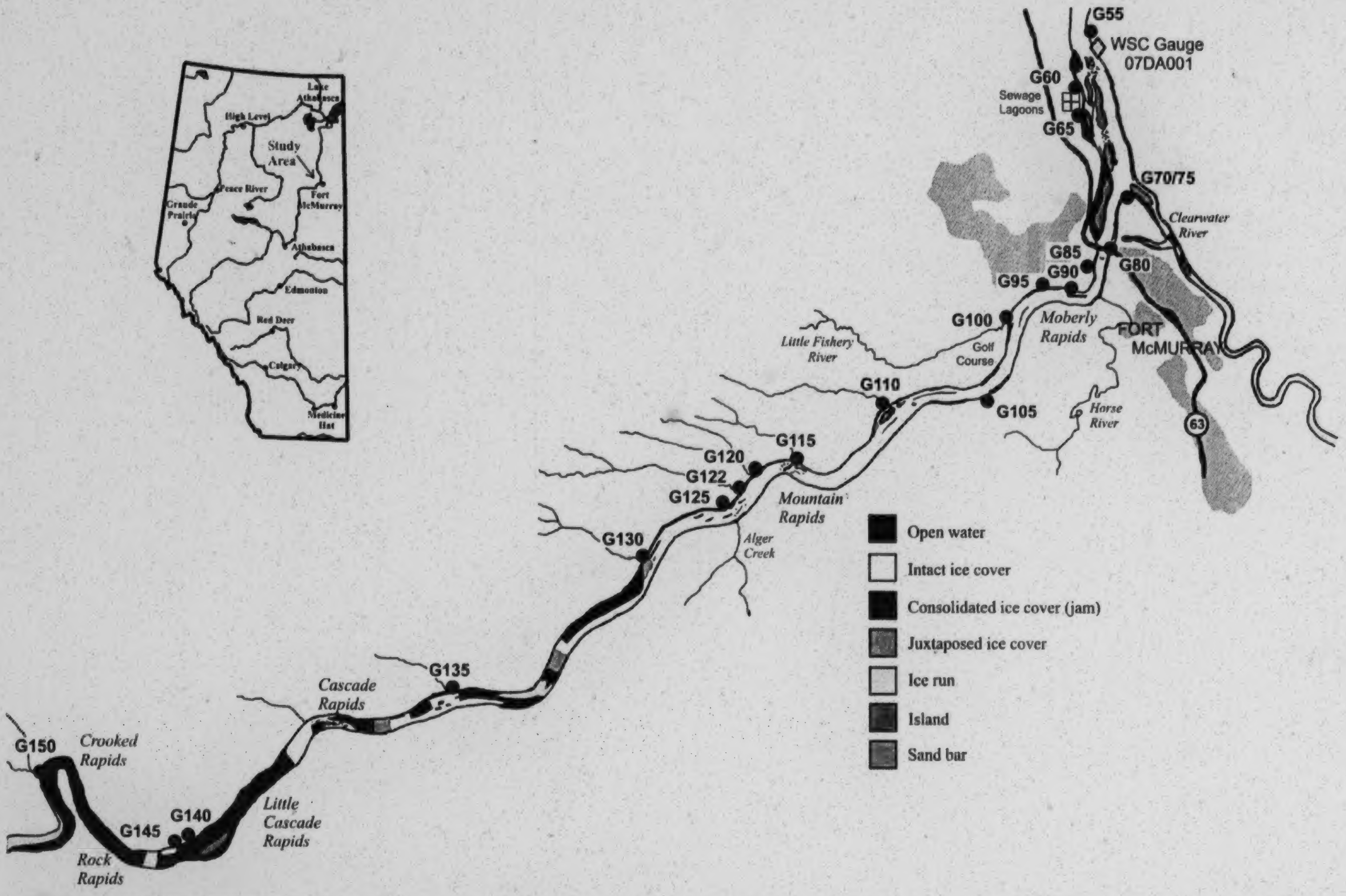
Lake Athabasca
High Level
Study Area
Peace River
Grande Prairie
Fort McMurray
Athabasca
Edmonton
Red Deer
Calgary
Medicine Hat
G55
WSC Gauge 07DA001
G60
Sewage Lagoons
G65
G70/75
Clearwater River
G85
G90
G80
G95
G100
Moberly Rapids
FORT McMURRAY
Little Fishery River
Golf Course
G110
G105
Horse River
63
G115
G120
G122
G125
Mountain Rapids
Alger Creek
G130
Open water
Intact ice cover
Consolidated ice cover (jam)
Juxtaposed ice cover
Ice run
Island
Sand bar
G135
Cascade Rapids
G150
Crooked Rapids
G140
G145
Little Cascade Rapids
Rock Rapids

Figure 3.6 Ice conditions in the study reach on April 21, 2003.

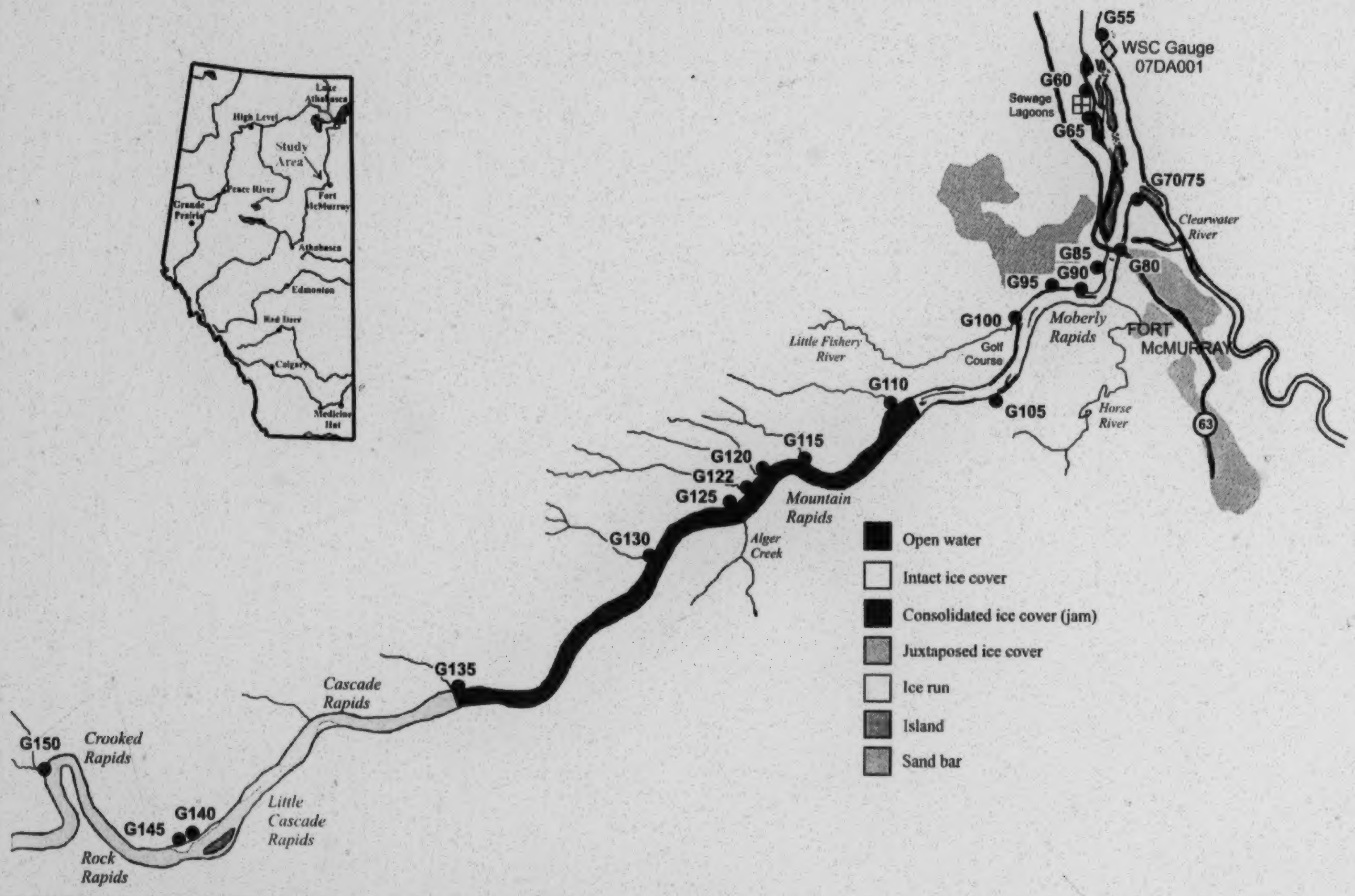
G55
WSC Gauge
07DA001
G60
Sewage
Lagoons
G65
G70/75
Clearwater
River
G85
G80
G90
G95
G100
Moberly
Rapids
FORT
McMURRAY
Golf
Course
Little Fishery
River
G110
G105
Horse
River
63
G115
G120
G122
G125
Mountain
Rapids
G130
Alger
Creek
G135
Cascade
Rapids
G150
Crooked
Rapids
G145
G140
Little
Cascade
Rapids
Rock
Rapids
Lake
Athabasca
High Level
Study
Area
Peace River
Fort
McMurray
Grande
Prairie
Athabasca
Edmonton
Red Deer
Calgary
Medicine
Hat
■ Open water
□ Intact ice cover
■ Consolidated ice cover (jam)
▨ Juxtaposed ice cover
□ Ice run
▨ Island
▨ Sand bar

Figure 3.7 Ice conditions in the study reach on April 21, 2003, 1200h.

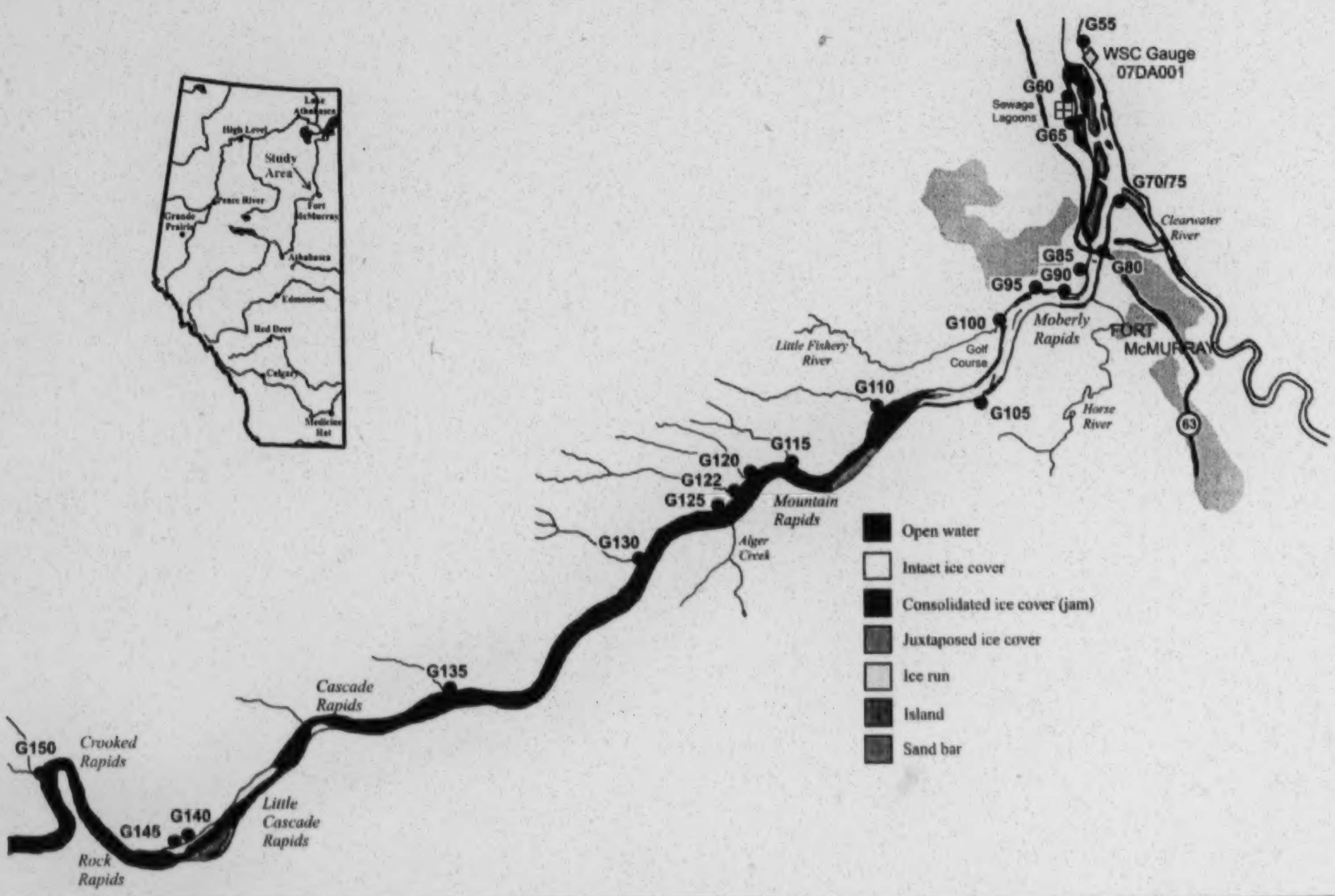
G55
WSC Gauge
07DA001
G60
Sewage Lagoons
G65
G70/75
Clearwater River
G85
G80
G90
G95
G100
Moberly Rapids
FORT McMURRAY
Golf Course
Little Fishery River
G110
G105
Horse River
63
G115
G120
G122
G125
Mountain Rapids
Alger Creek
G130
G135
Cascade Rapids
G150
Crooked Rapids
G140
G145
Little Cascade Rapids
Rock Rapids
Open water
Intact ice cover
Consolidated ice cover (jam)
Juxtaposed ice cover
Ice run
Island
Sand bar
Lake Athabasca
High Level
Study Area
Peace River
Fort McMurray
Grande Prairie
Athabasca
Edmonton
Red Deer
Calgary
Medicine Hat

Figure 3.8 Ice conditions in the study reach on April 22, 2003, 0930h.

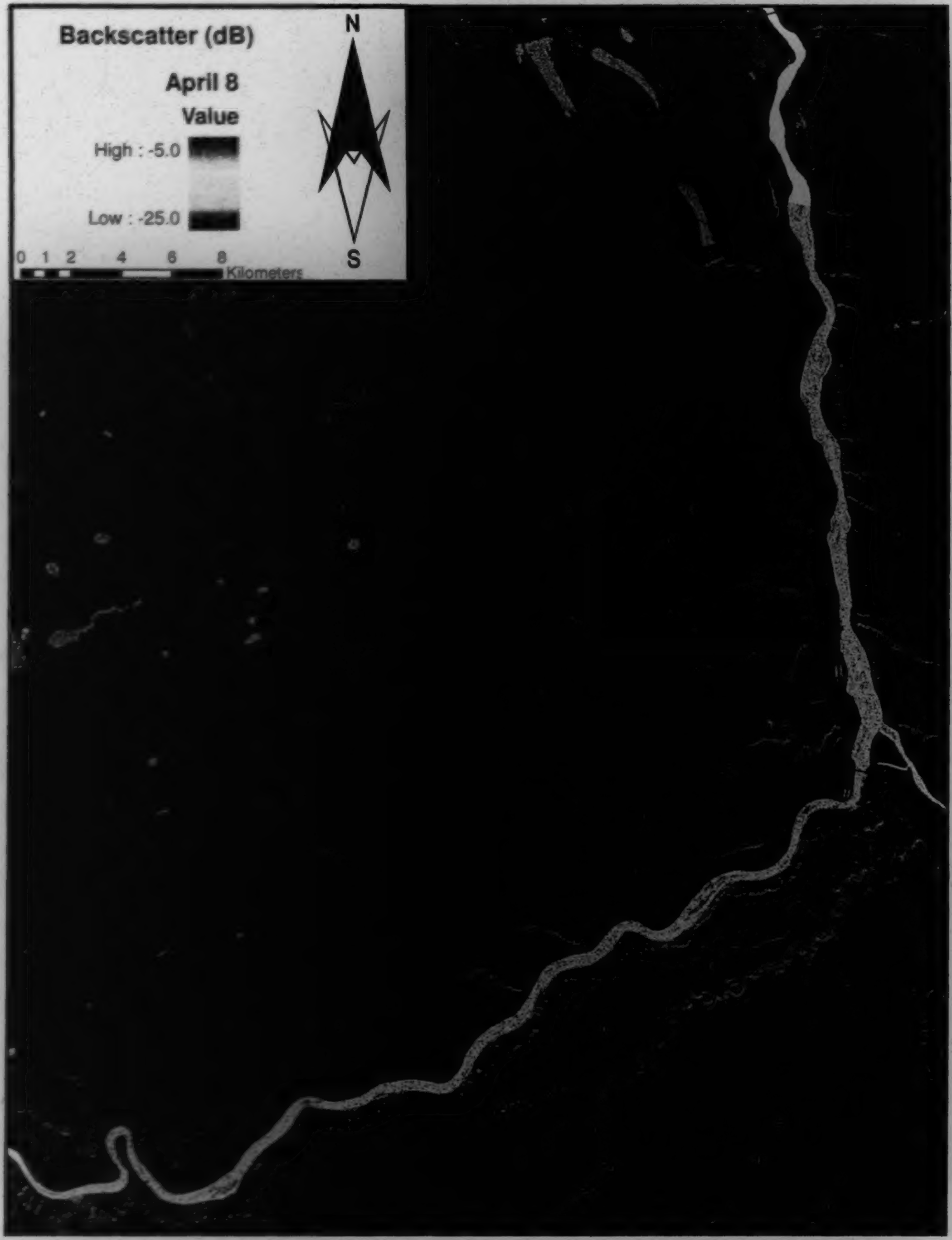
Backscatter (dB)
April 8
Value
High : -5.0
Low : -25.0
0 1 2 4 6 8
Kilometers
N
S

Figure 3.9 RADARSAT image product of the full study reach captured at 6:41:23 (local time) on April 8, 2003.

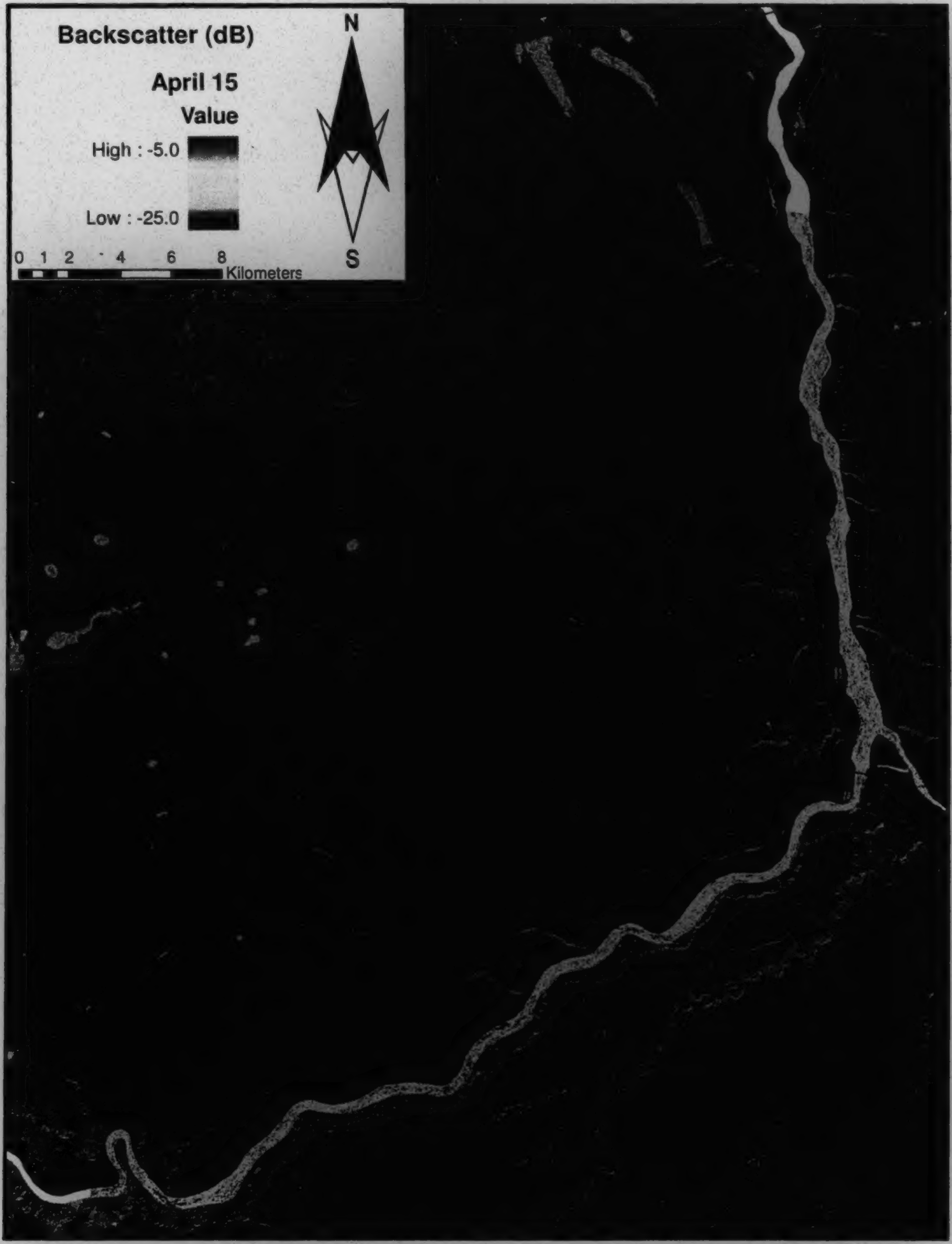
Backscatter (dB)
April 15
Value
High : -5.0
Low : -25.0
0 1 2 4 6 8
Kilometers
N
S

Figure 3.10 RADARSAT image product of the full study reach captured at 7:37:13 (local time) on April 15, 2003.

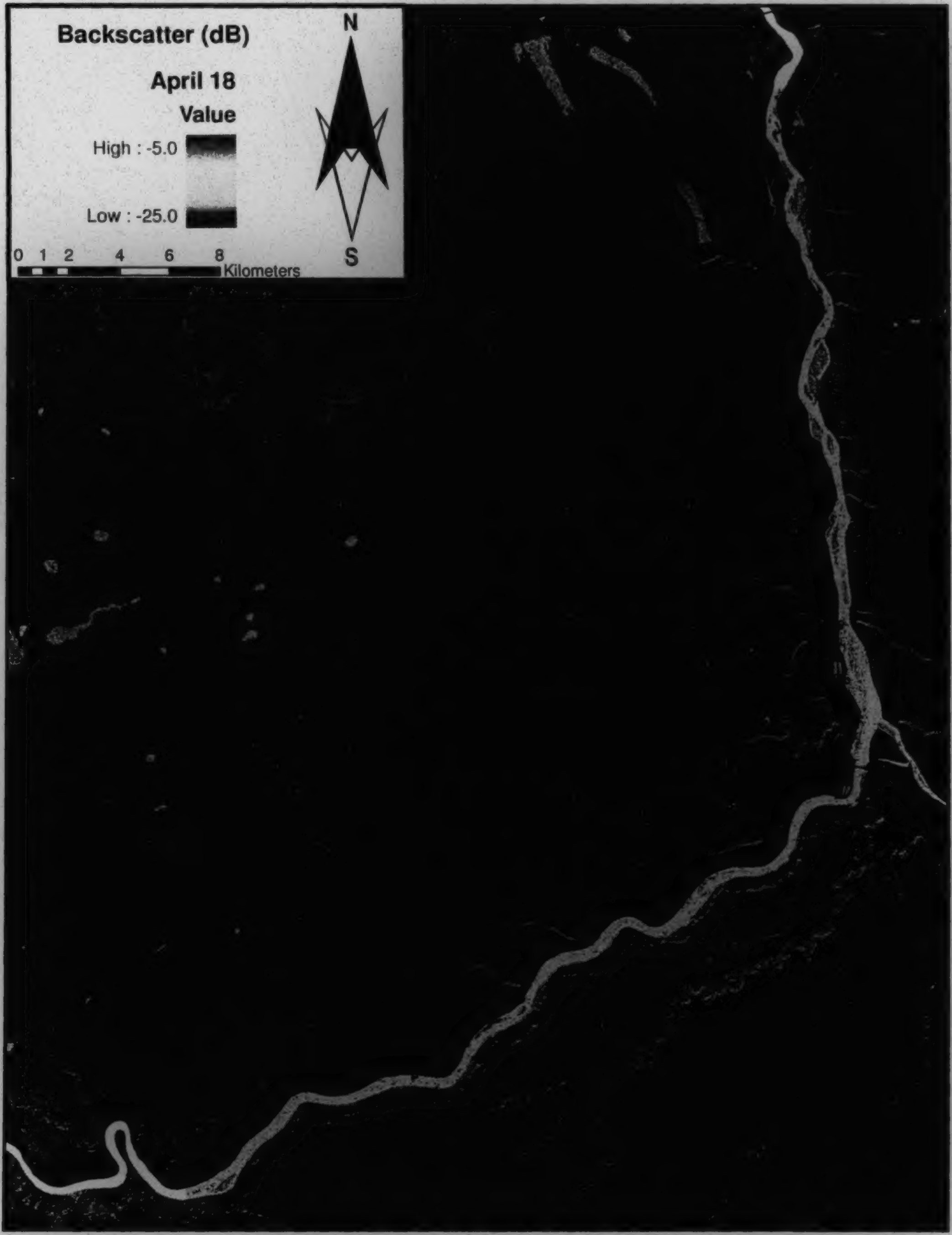
Backscatter (dB)
April 18
Value
High : -5.0
Low : -25.0
N
S
0 1 2 4 6 8
Kilometers

Figure 3.11 RADARSAT image product of the full study reach captured at 19:12:09 (local time) on April 18, 2003.

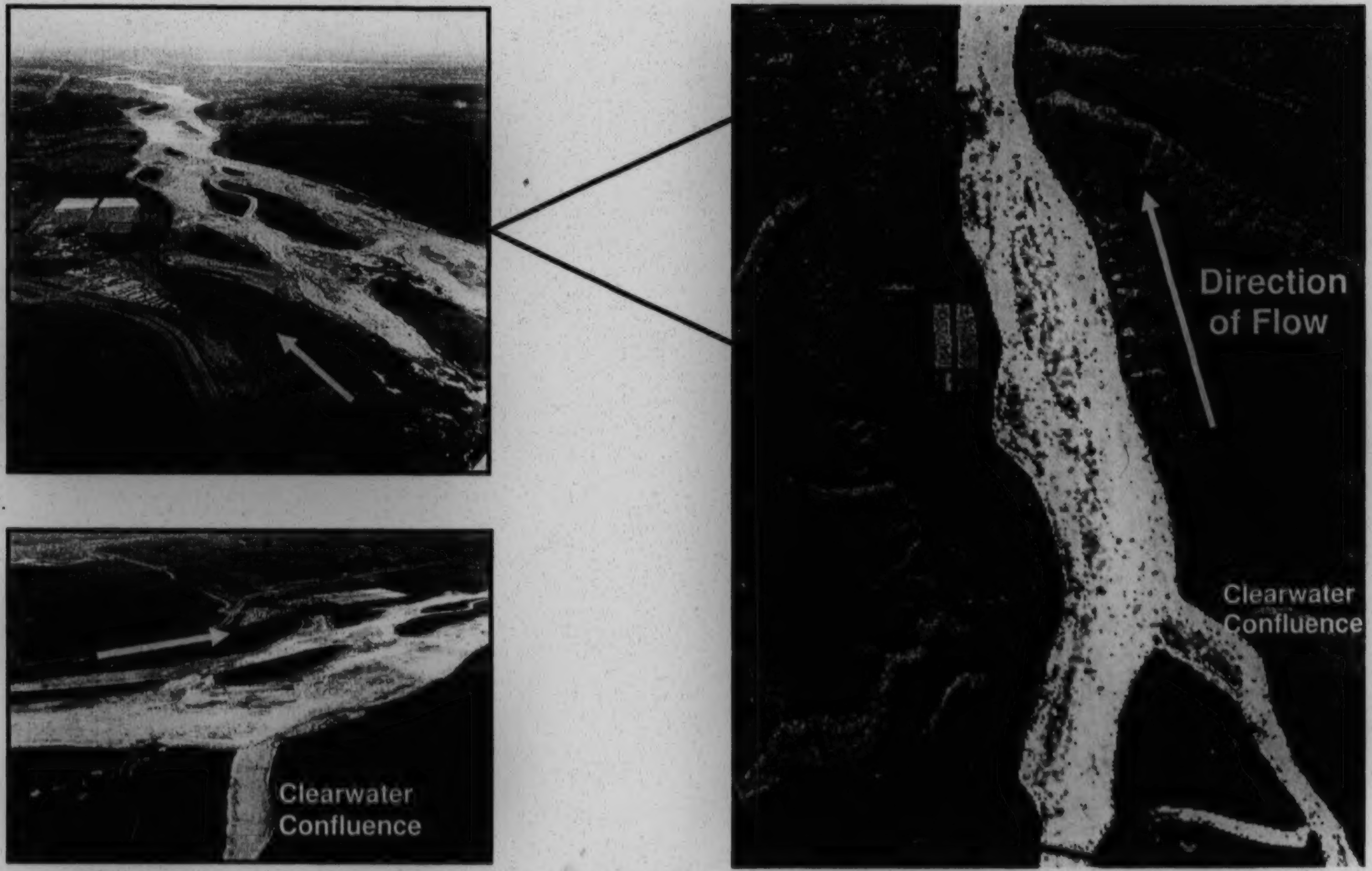
Direction
of Flow
Clearwater
Confluence
Clearwater
Confluence

Figure 3.12 Areas of open water lining the left bank (April 18, 2003).

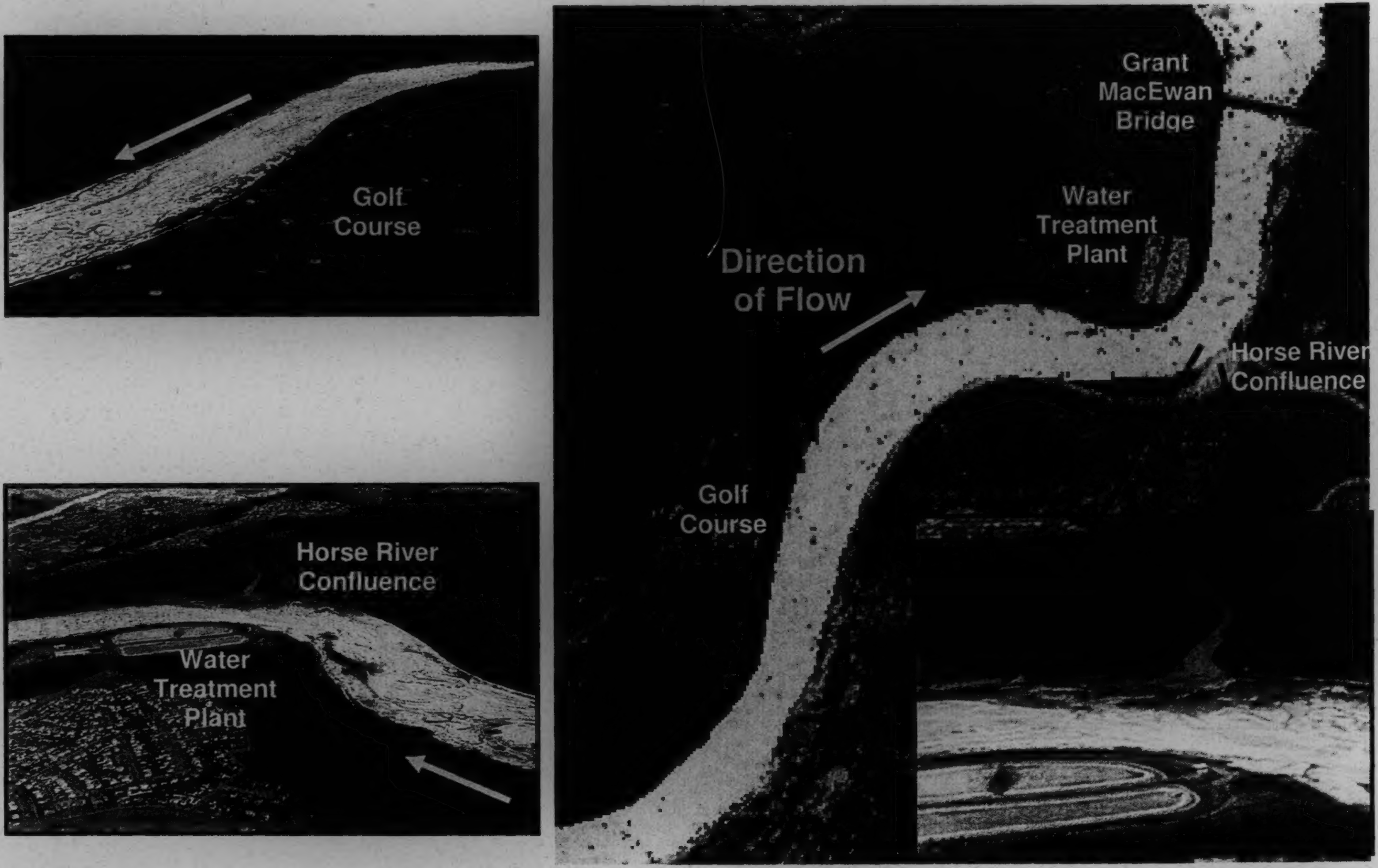
Golf
Course
Horse River
Confluence
Water
Treatment
Plant
Grant
MacEwan
Bridge
Water
Treatment
Plant
Direction
of Flow
Horse River
Confluence
Golf
Course

Figure 3.13 An accumulation of ice at the Horse River confluence (April 18, 2003).

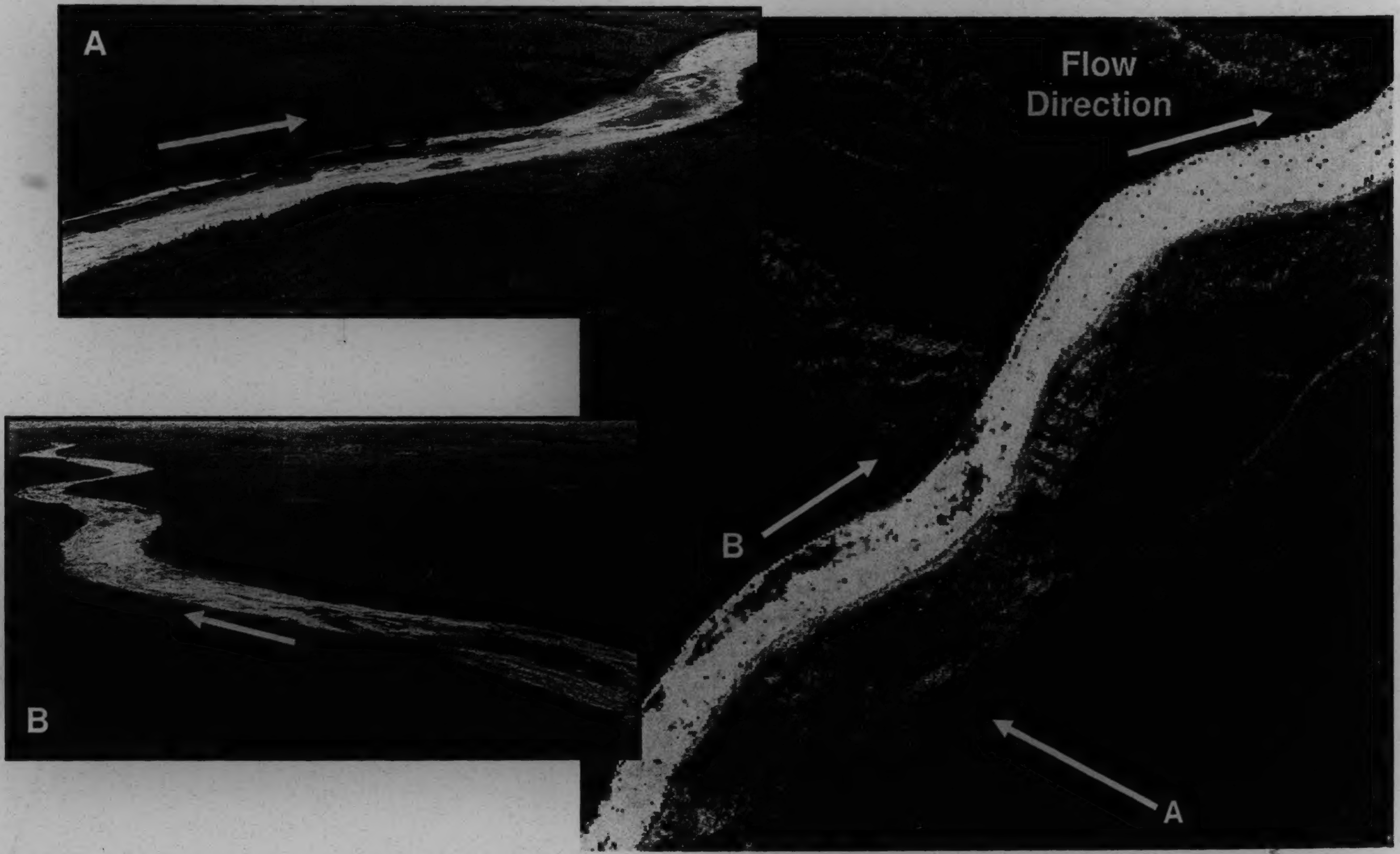
A
B
Flow
Direction
B
A

Figure 3.14 Open water development in the reach near G130 (April 18, 2003).

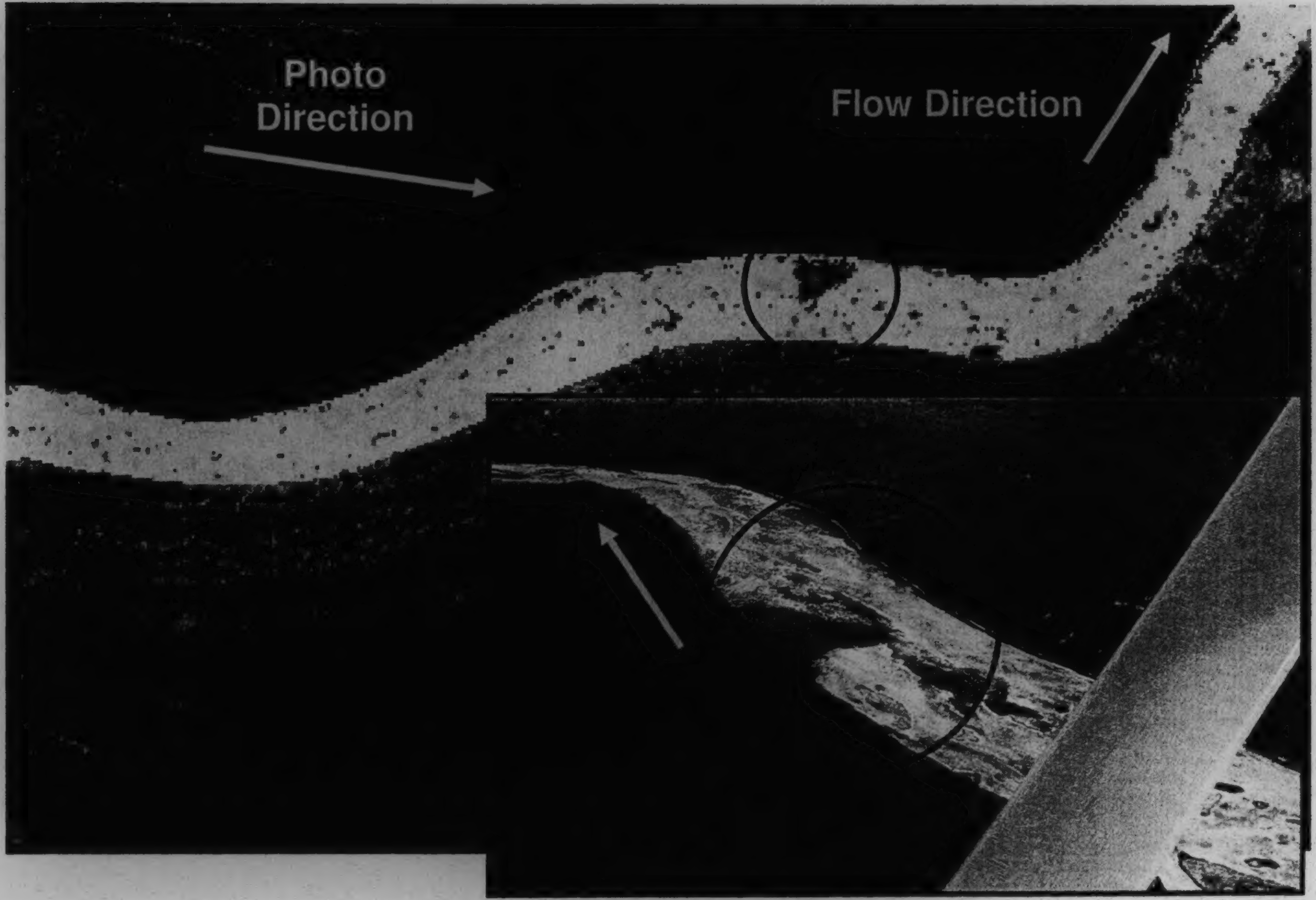
Photo Direction
Flow Direction

Figure 3.15 Open water development in the reach near G135 (April 18, 2003).

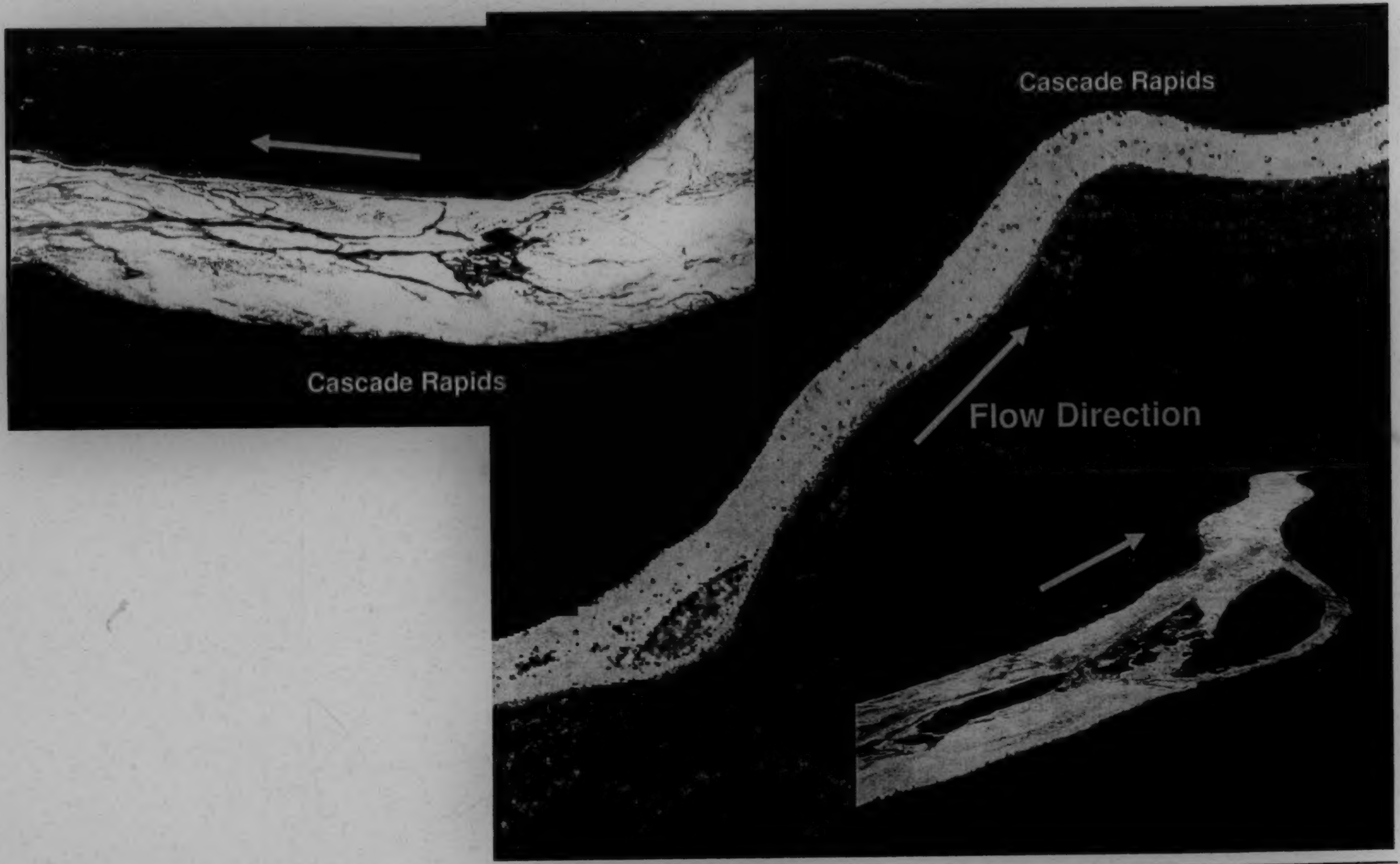
Cascade Rapids
Cascade Rapids
Flow Direction

Figure 3.16 Open water development in the reach from G140 to Cascade Rapids (April 18, 2003).

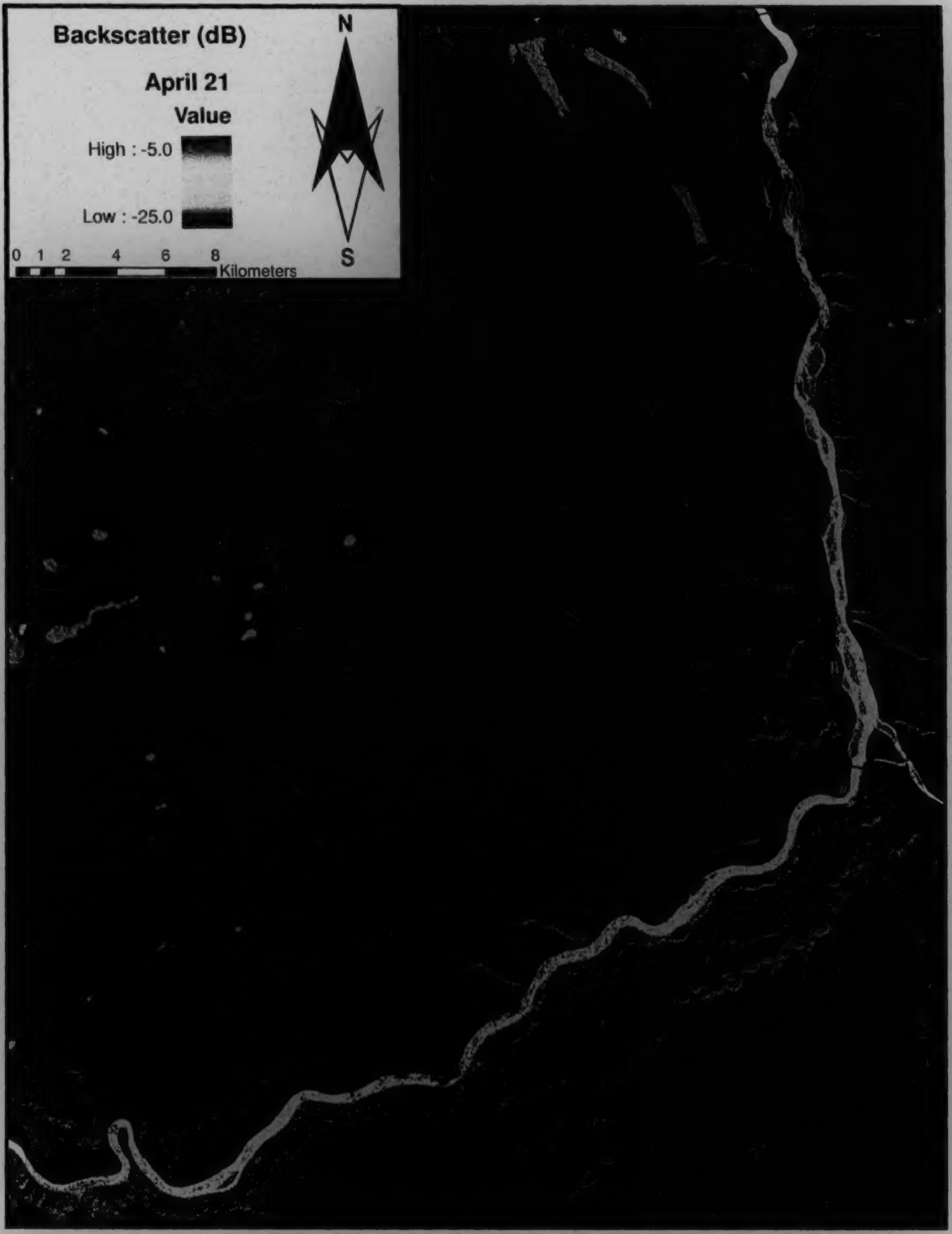
Backscatter (dB)
April 21
Value
High : -5.0
Low : -25.0
N
S
0 1 2 4 6 8
Kilometers

Figure 3.17 RADARSAT image product of the full study reach captured at 7:57:58 (local time) on April 21, 2003.

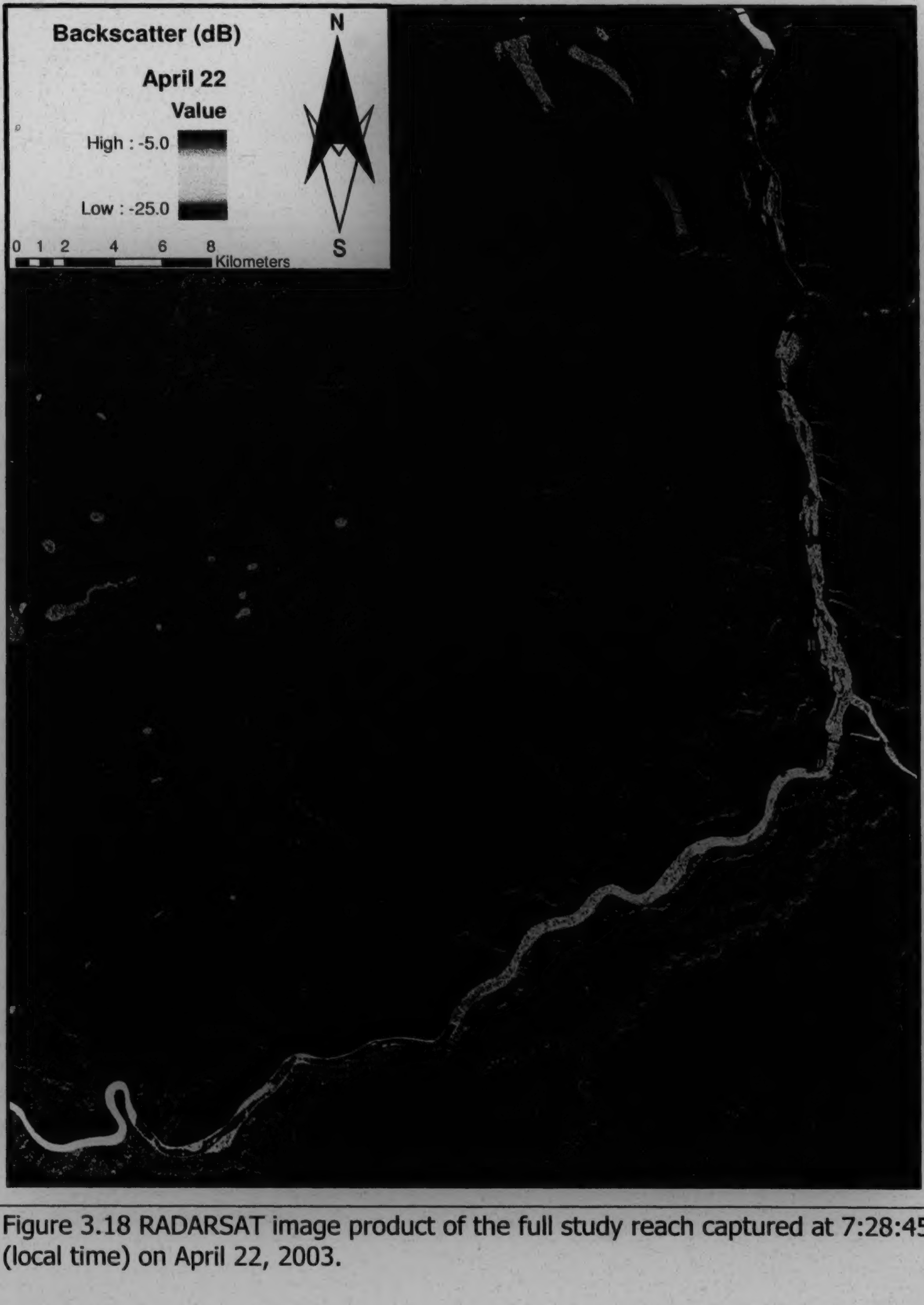
Backscatter (dB)
April 22
Value
High : -5.0
Low : -25.0
0 1 2 4 6 8
Kilometers
N
S

Figure 3.18 RADARSAT image product of the full study reach captured at 7:28:45 (local time) on April 22, 2003.

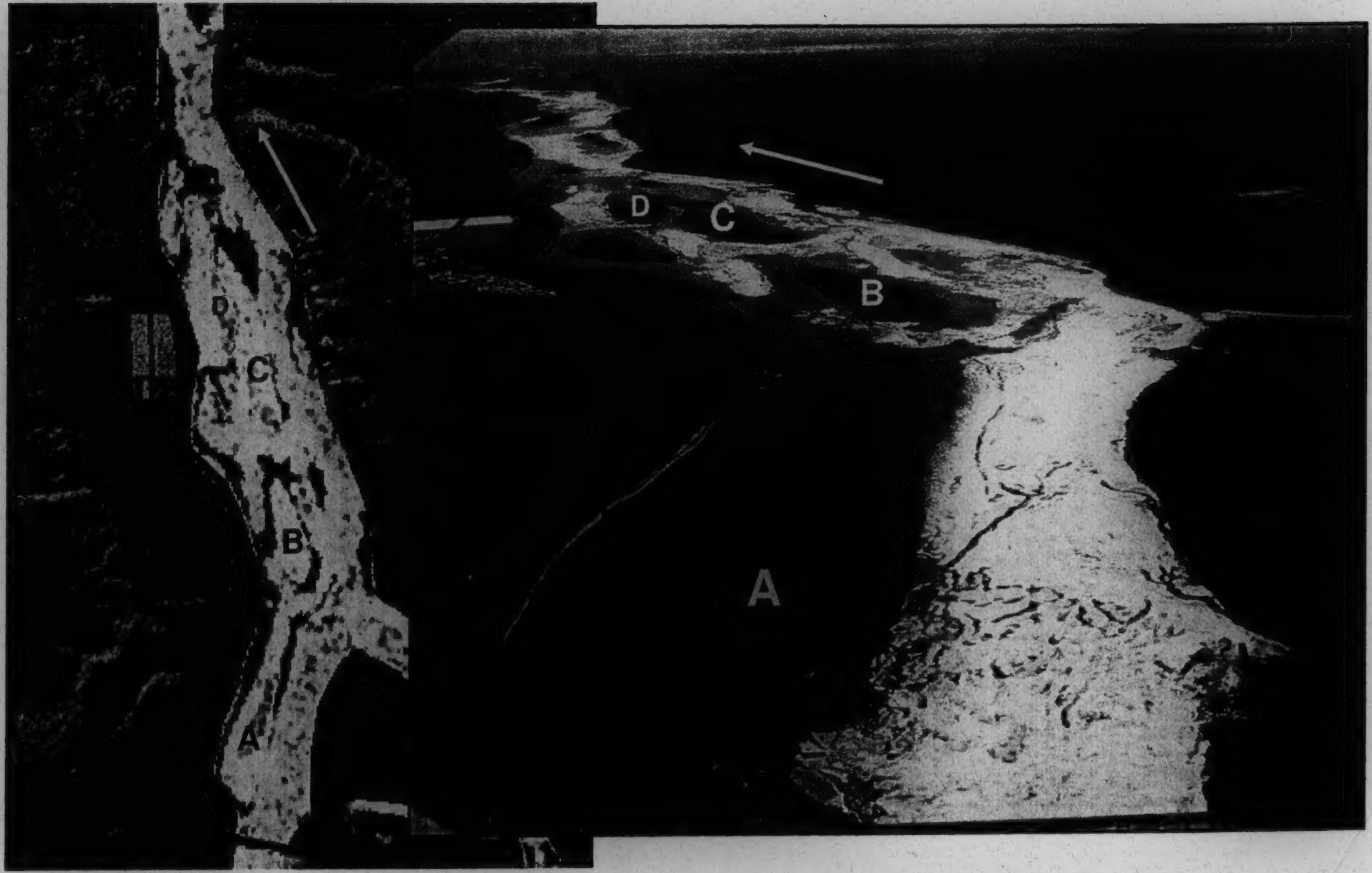

Figure 3.19 Open water development downstream of Fort McMurray (April 22, 2003).

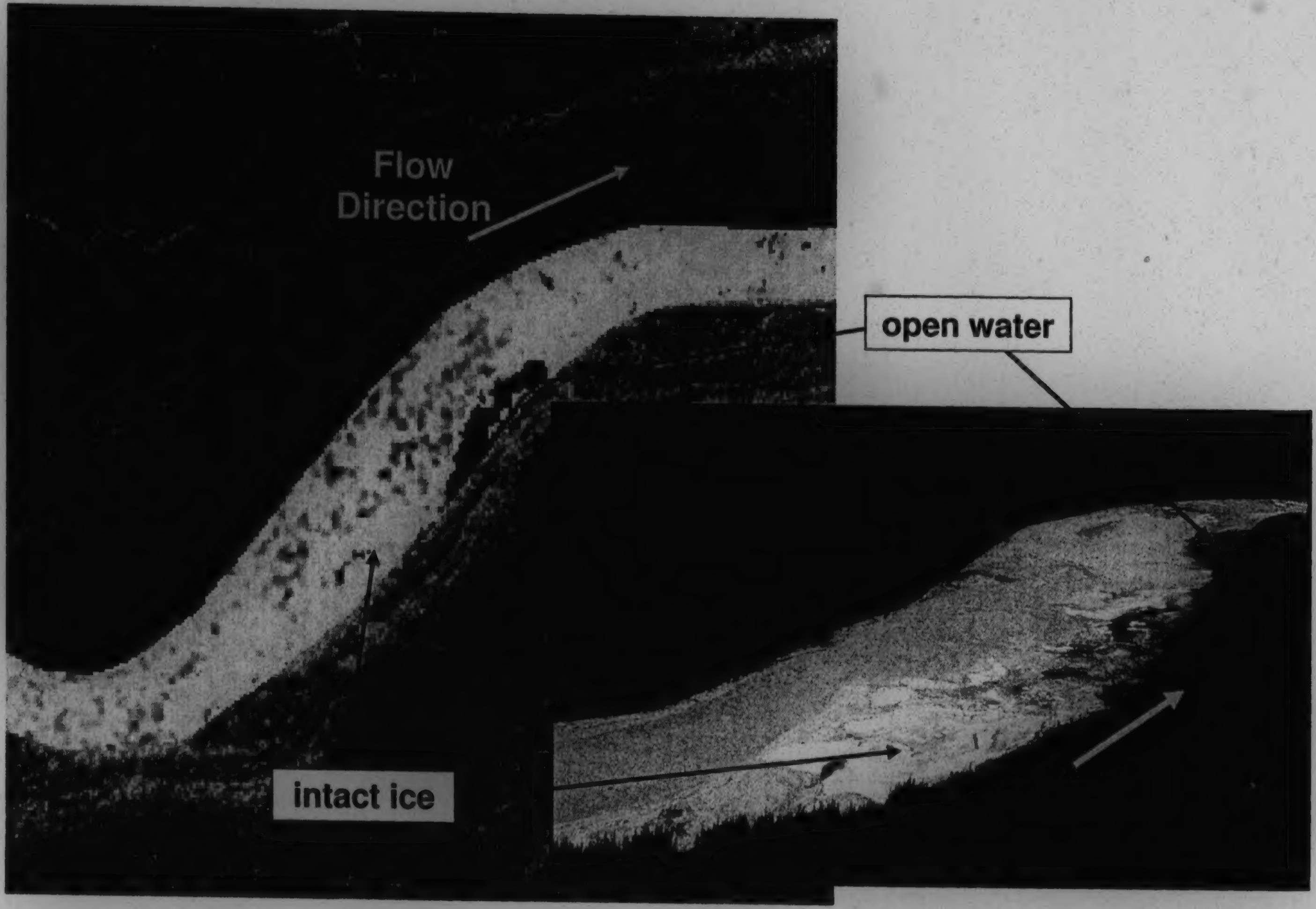
Flow
Direction
open water
intact ice

Figure 3.20 Downstream end (toe) of ice jam (April 22, 2003).

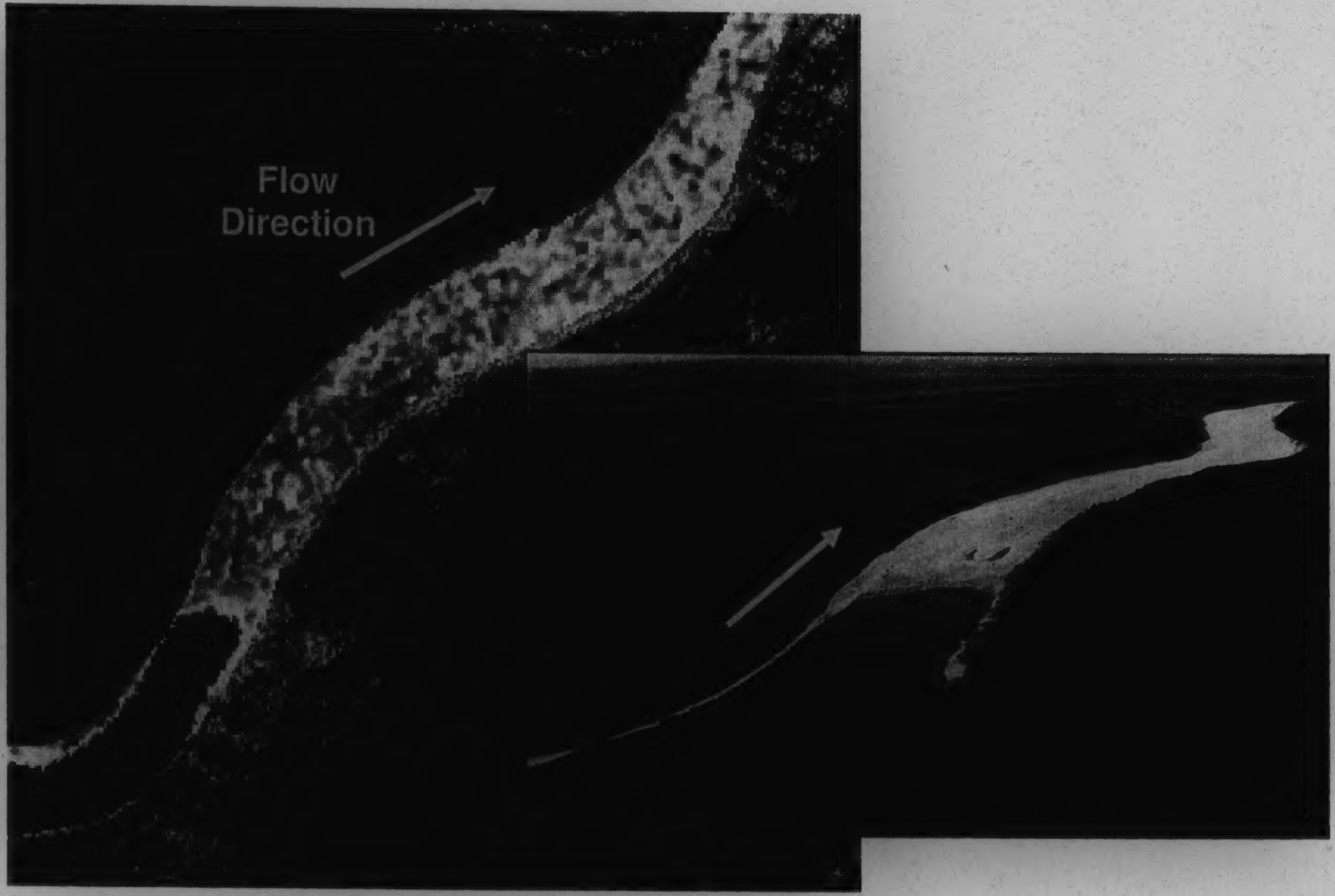
Flow
Direction

Figure 3.21 Upstream end (head) of ice jam at Mountain Rapids (April 22, 2003).

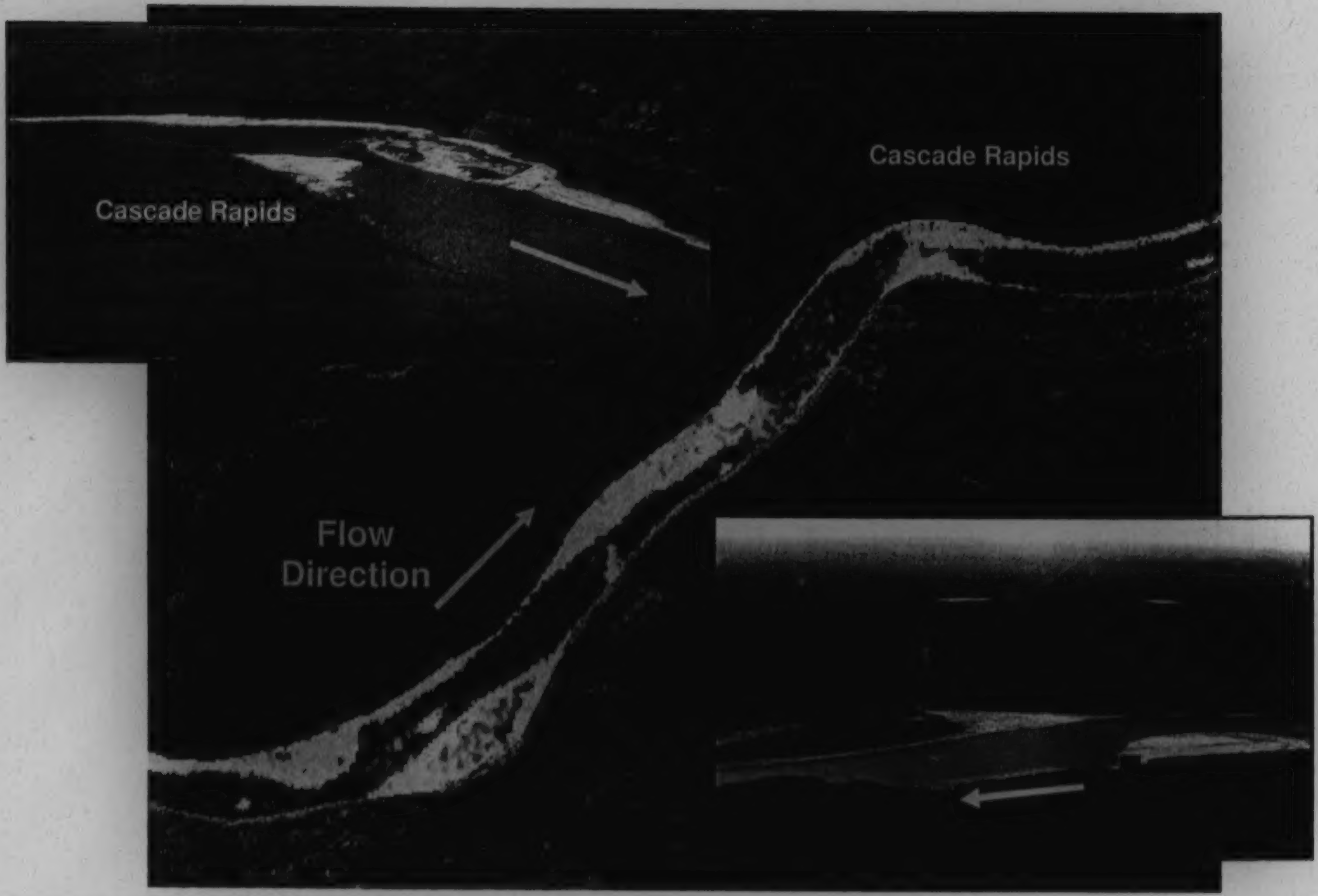
Cascade Rapids
Cascade Rapids
Flow
Direction

Figure 3.22 Residual ice at Station G140 and in Cascade Rapids (April 22, 2003).

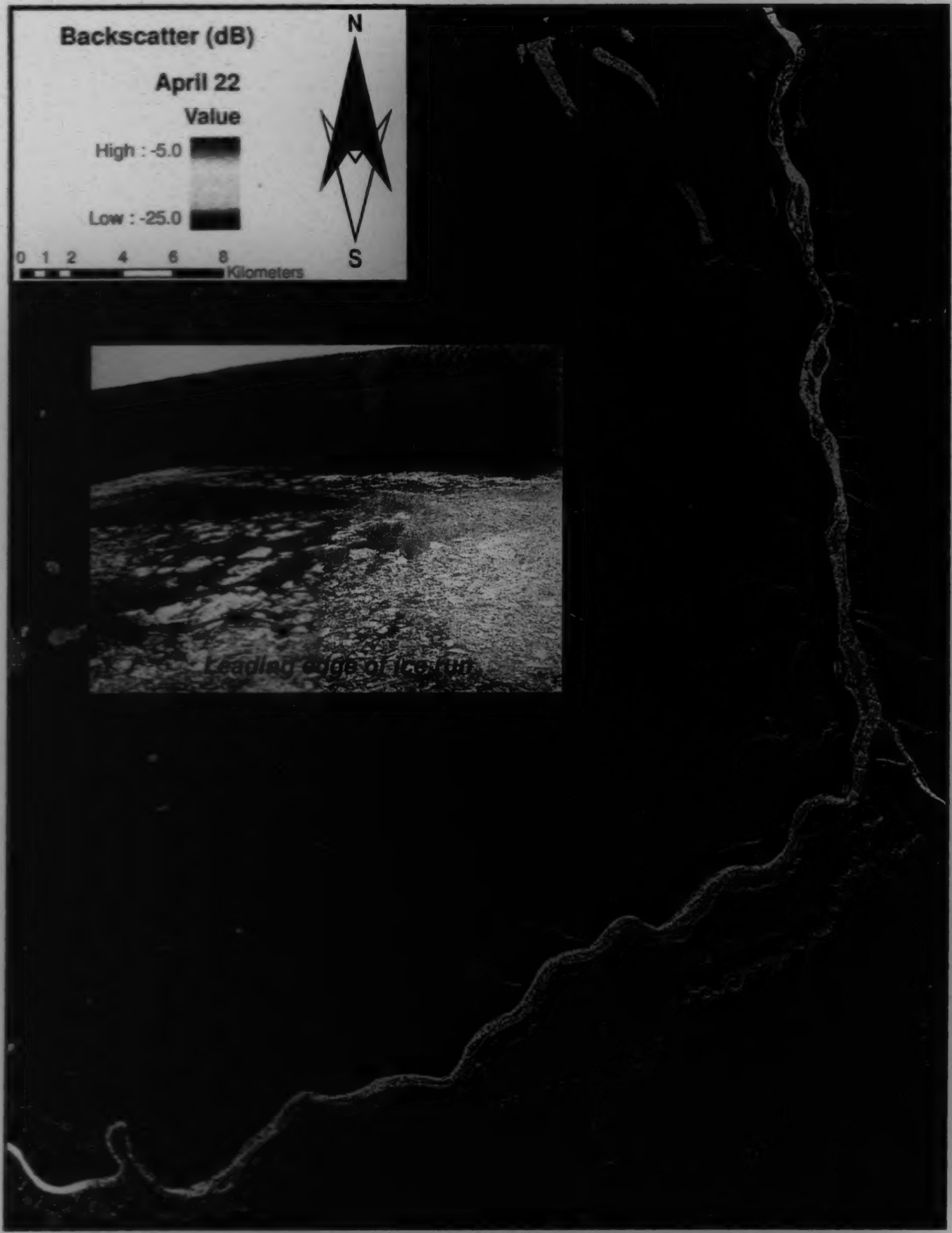
Backscatter (dB)
April 22
Value
High : -5.0
Low : -25.0
0 1 2 4 6 8
Kilometers
N
S
Leading edge of ice run

Figure 3.23 RADARSAT image product of the full study reach captured at 18:55:28 on April 22, 2003 during ice run through Fort McMurray.

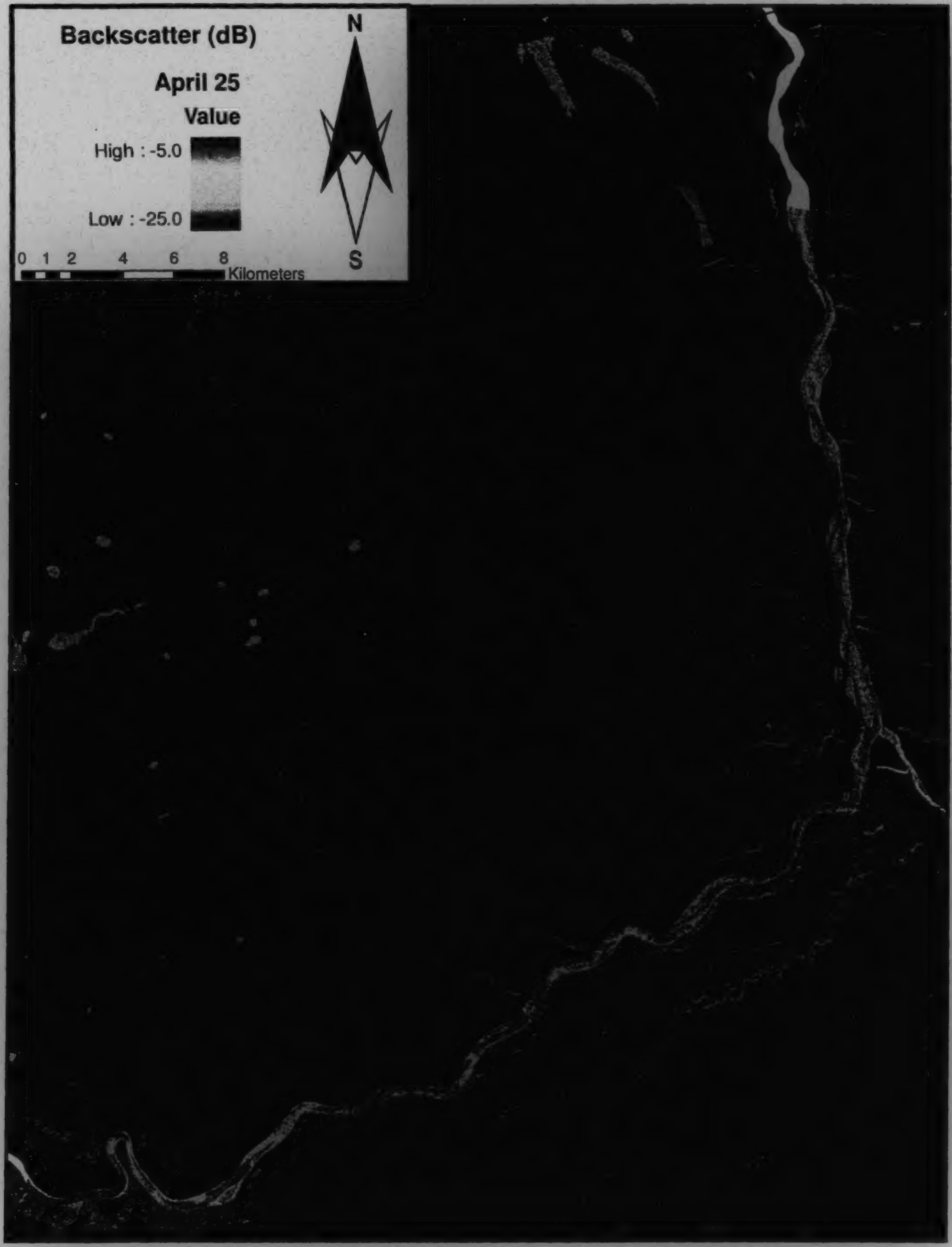
Backscatter (dB)
April 25
Value
High : -5.0
Low : -25.0
0 1 2 4 6 8
Kilometers
N
S

Figure 3.24 RADARSAT image product of the full study reach captured at 7:41:23 (local time) on April 25, 2003.

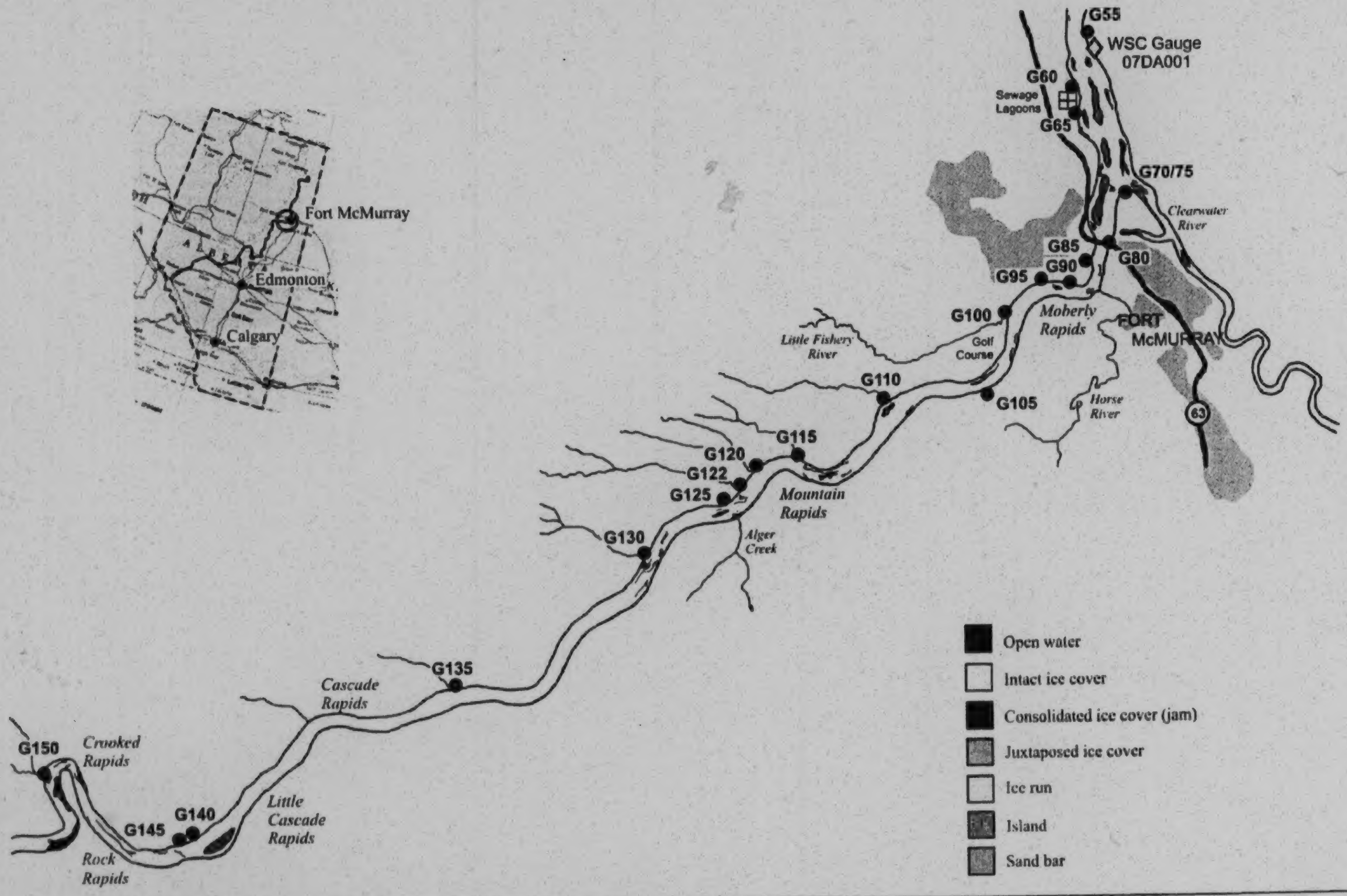
G55
WSC Gauge
07DA001
G60
Sewage
Lagoons
G65
G70/75
Clearwater
River
G85
G80
G95
G90
G100
Moberly
Rapids
FORT
McMURRAY
Little Fishery
River
Golf
Course
G110
G105
Horse
River
63
G115
G120
G122
G125
Mountain
Rapids
G130
Alger
Creek
G135
Cascade
Rapids
G150
Crooked
Rapids
G140
G145
Little
Cascade
Rapids
Rock
Rapids
Fort McMurray
Edmonton
Calgary
Open water
Intact ice cover
Consolidated ice cover (jam)
Juxtaposed ice cover
Ice run
Island
Sand bar

Figure 3.25 Ice conditions in the study reach on April 9, 2004.

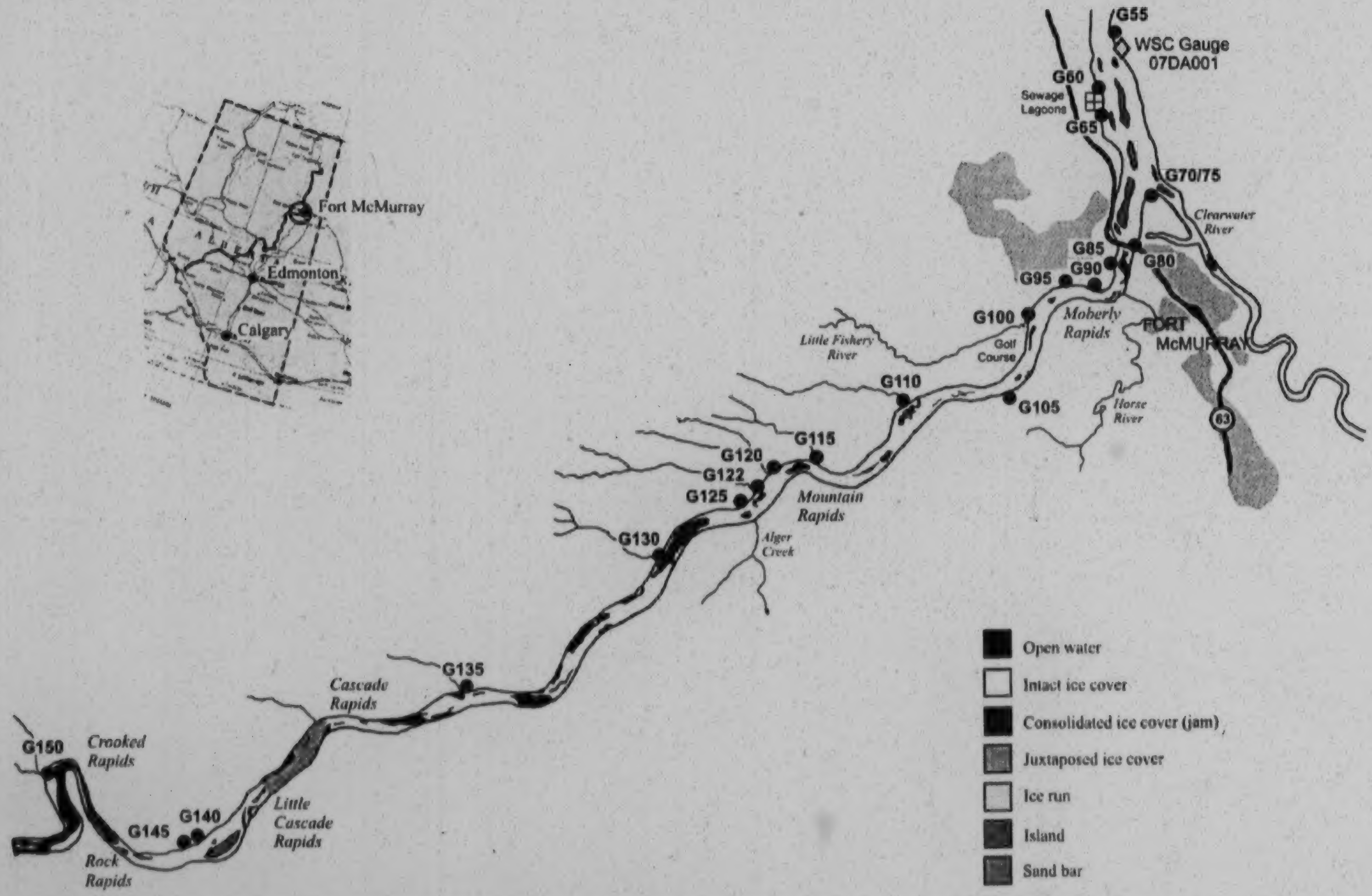
G55
WSC Gauge 07DA001
G60
Sewage Lagoons
G65
G70/75
Clearwater River
G85
G90
G80
G95
G100
Moberly Rapids
FORT McMURRAY
Golf Course
Little Fishery River
G110
G105
Horse River
63
G115
G120
G122
G125
Mountain Rapids
G130
Alger Creek
G135
Cascade Rapids
G150
Crooked Rapids
G145
G140
Little Cascade Rapids
Rock Rapids
Fort McMurray
Edmonton
Calgary
Open water
Intact ice cover
Consolidated ice cover (jam)
Juxtaposed ice cover
Ice run
Island
Sand bar

Figure 3.26 Ice conditions in the study reach on April 12, 2004.

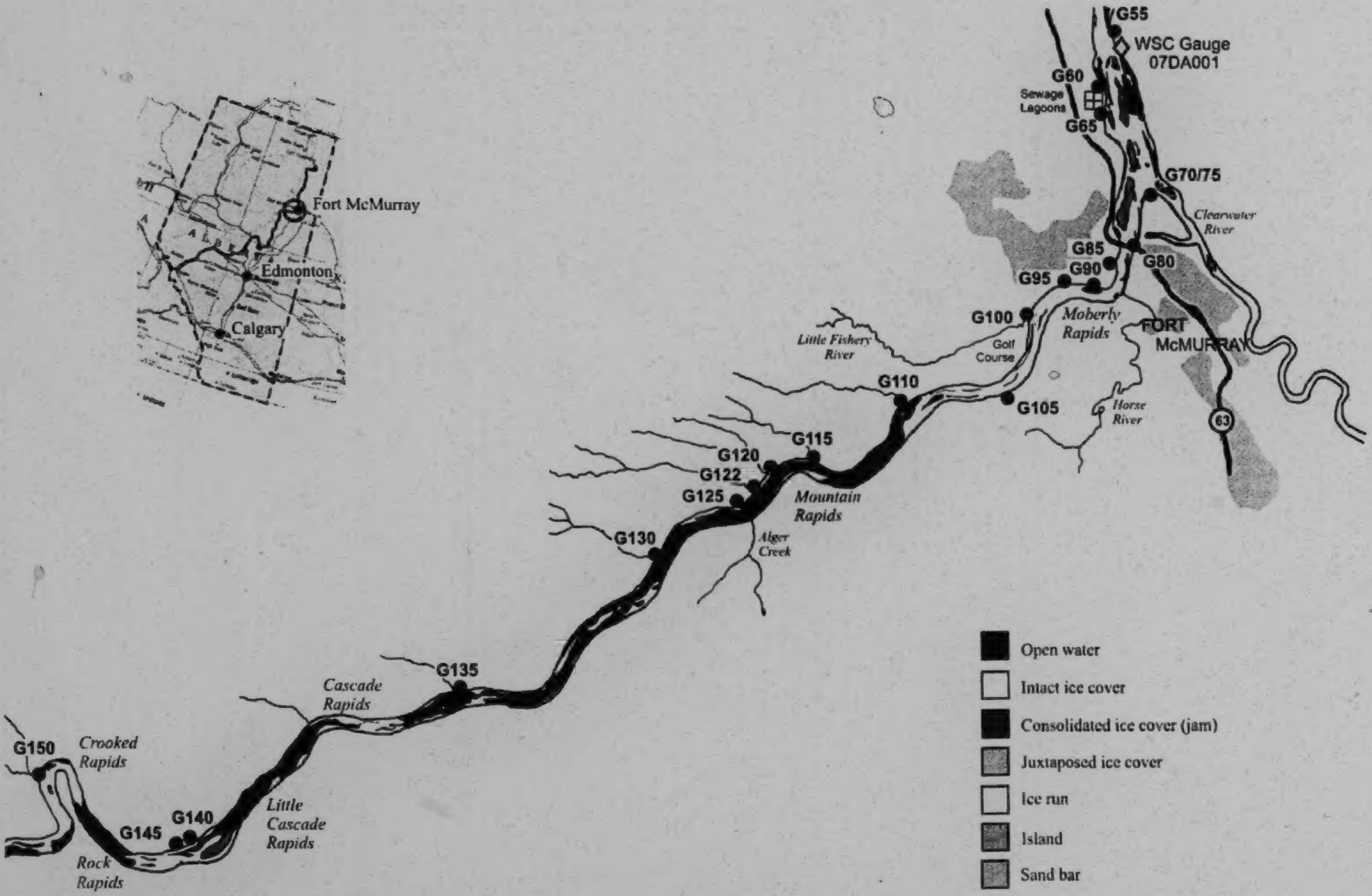
Fort McMurray
Edmonton
Calgary
G55
WSC Gauge 07DA001
G60
Sewage Lagoons
G65
G70/75
Clearwater River
G85
G80
G95
G90
G100
Moberly Rapids
FORT McMURRAY
Little Fishery River
Golf Course
G110
G105
Horse River
63
G115
G120
G122
G125
Mountain Rapids
G130
Alger Creek
G135
Cascade Rapids
G150
Crooked Rapids
G140
G145
Little Cascade Rapids
Rock Rapids
Open water
Intact ice cover
Consolidated ice cover (jam)
Juxtaposed ice cover
Ice run
Island
Sand bar

Figure 3.27 Ice conditions in the study reach on April 19, 2004.

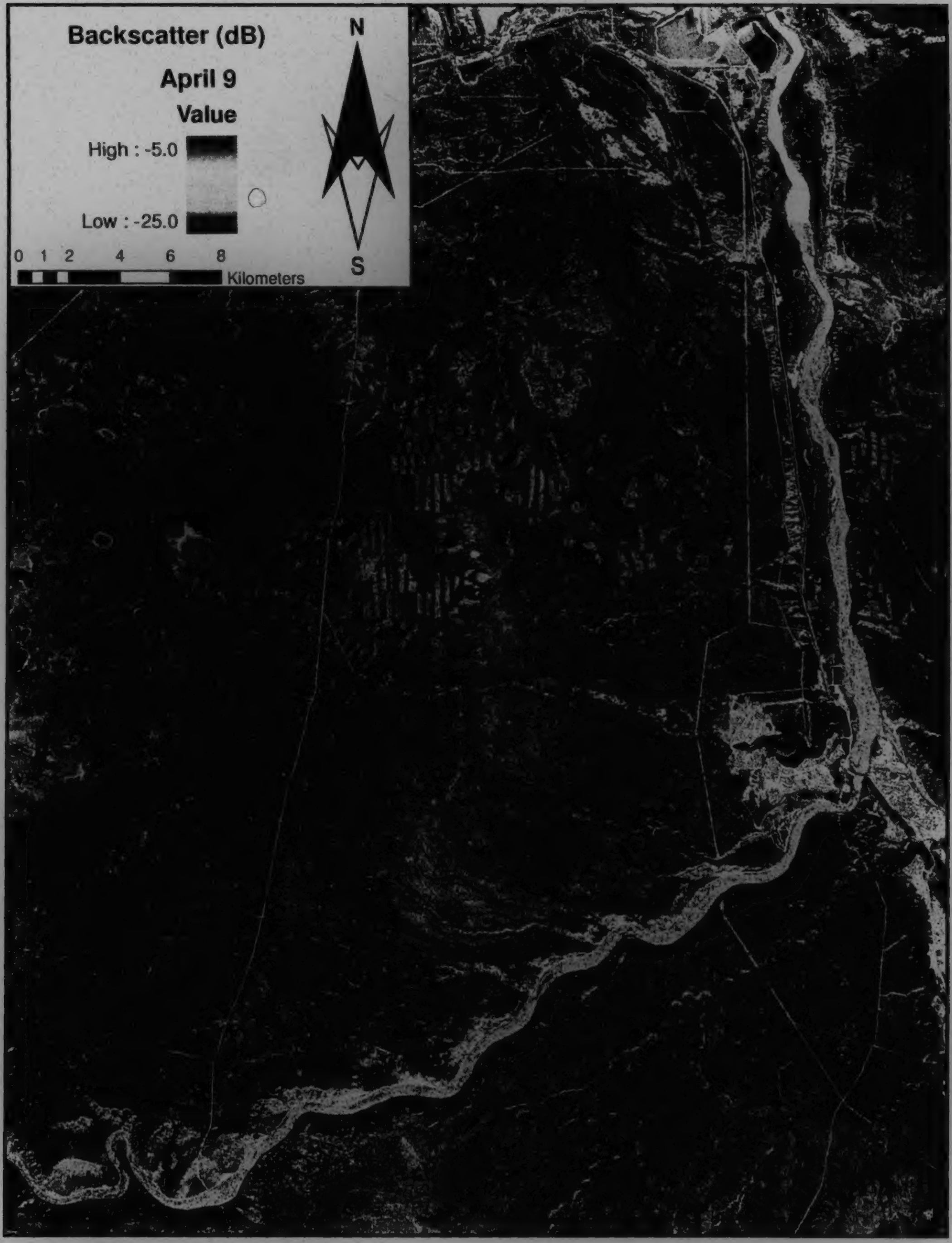
Backscatter (dB)
April 9
Value
High : -5.0
Low : -25.0
0 1 2 4 6 8
Kilometers
N
S

Figure 3.28 RADARSAT image product of the full study reach captured at 7:33:02 (local time) on April 9, 2004.

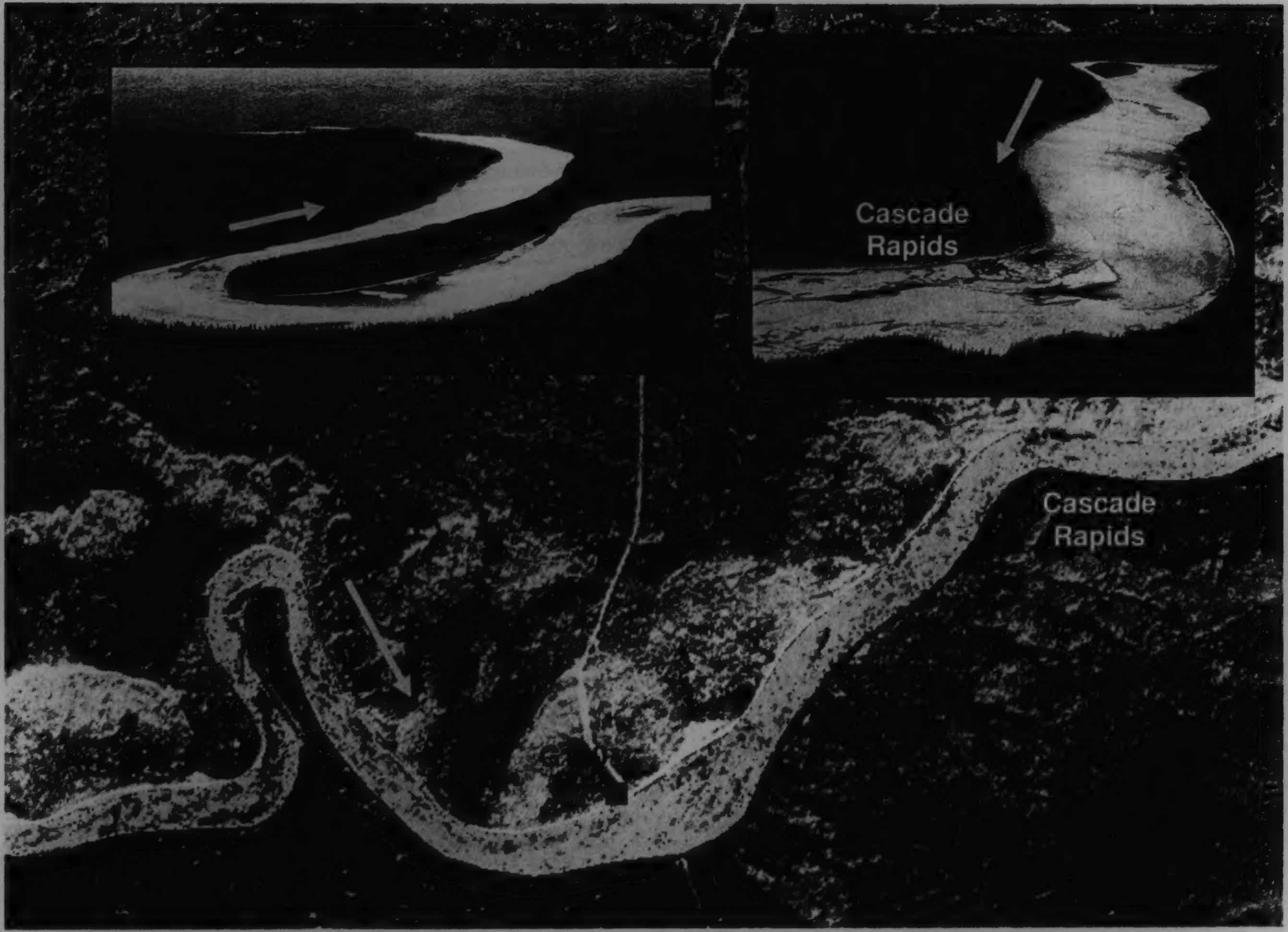
Cascade
Rapids
Cascade
Rapids

Figure 3.29 Deteriorating ice cover from Cascade Rapids to Crooked Rapids (April 9, 2004).

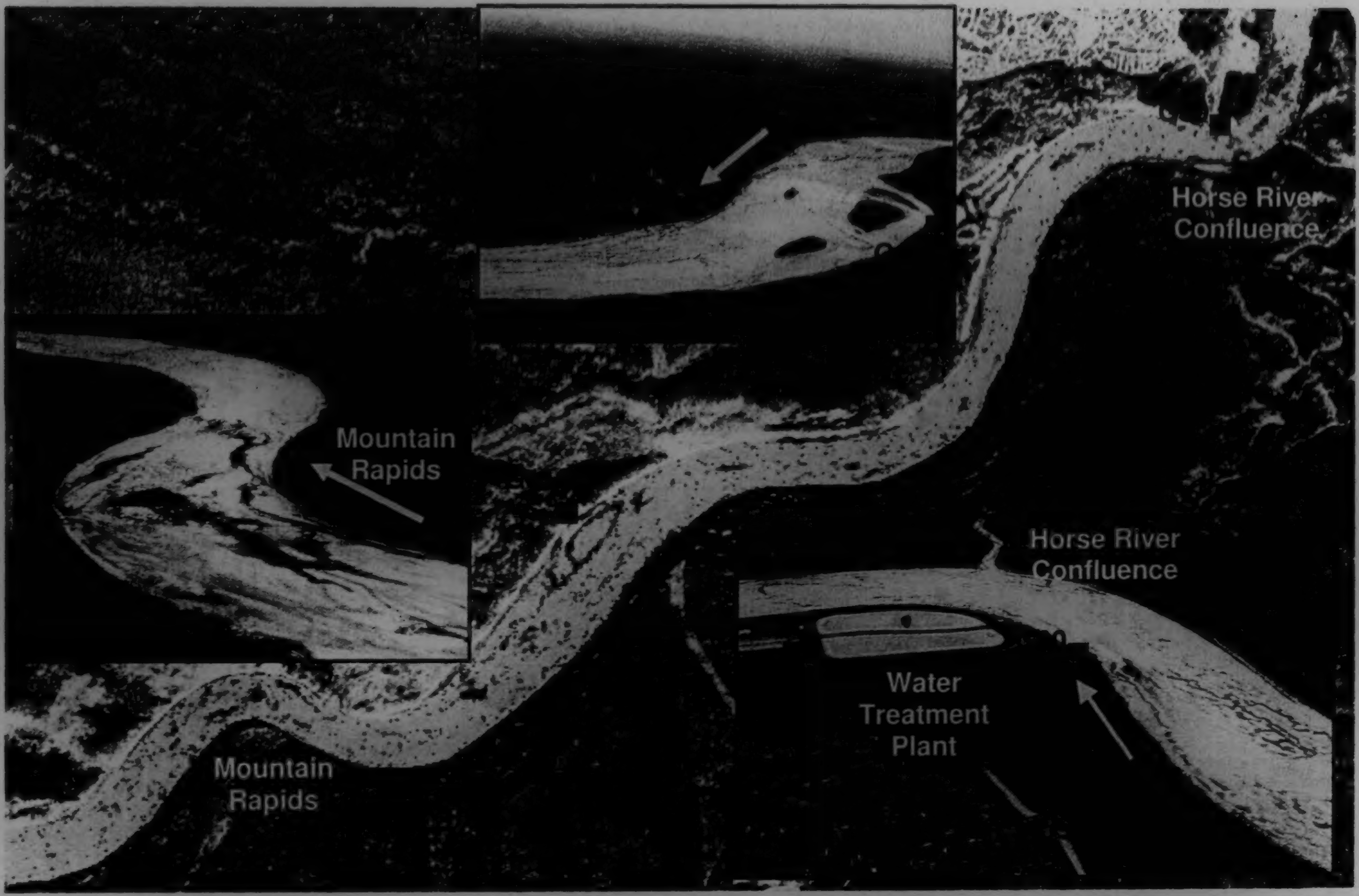
Horse River Confluence
Mountain Rapids
Horse River Confluence
Water Treatment Plant
Mountain Rapids

Figure 3.30 Open lead development at Mountain Rapids and deteriorating ice cover near bridge (April 9, 2004).

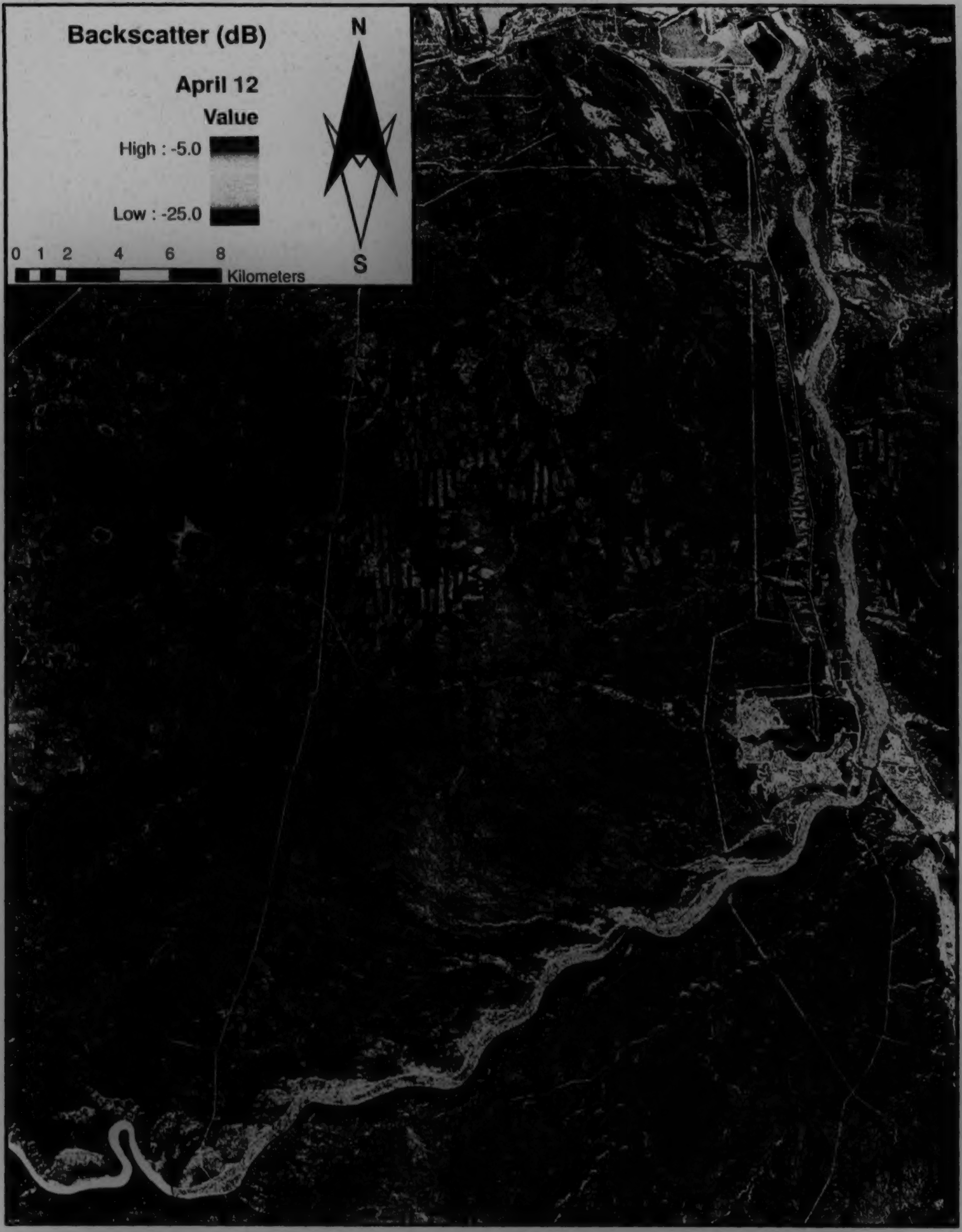
Backscatter (dB)
April 12
Value
High : -5.0
Low : -25.0
0 1 2 4 6 8
Kilometers
N
S

Figure 3.31 RADARSAT image product of the full study reach captured at 19:12:11 (local time) on April 12, 2004.

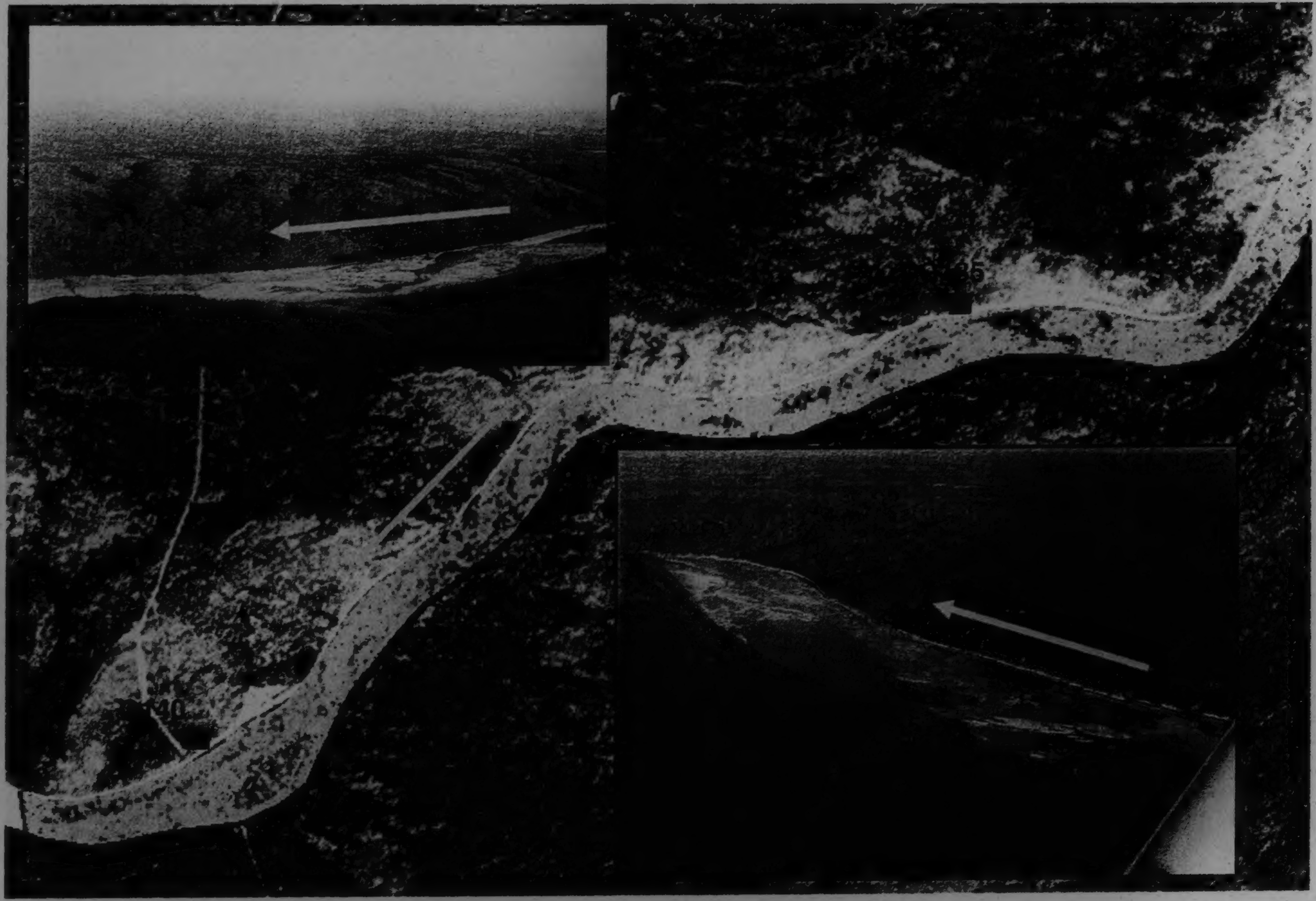

Figure 3.32 Deteriorating ice cover from G135 to G140 (April 12, 2004).

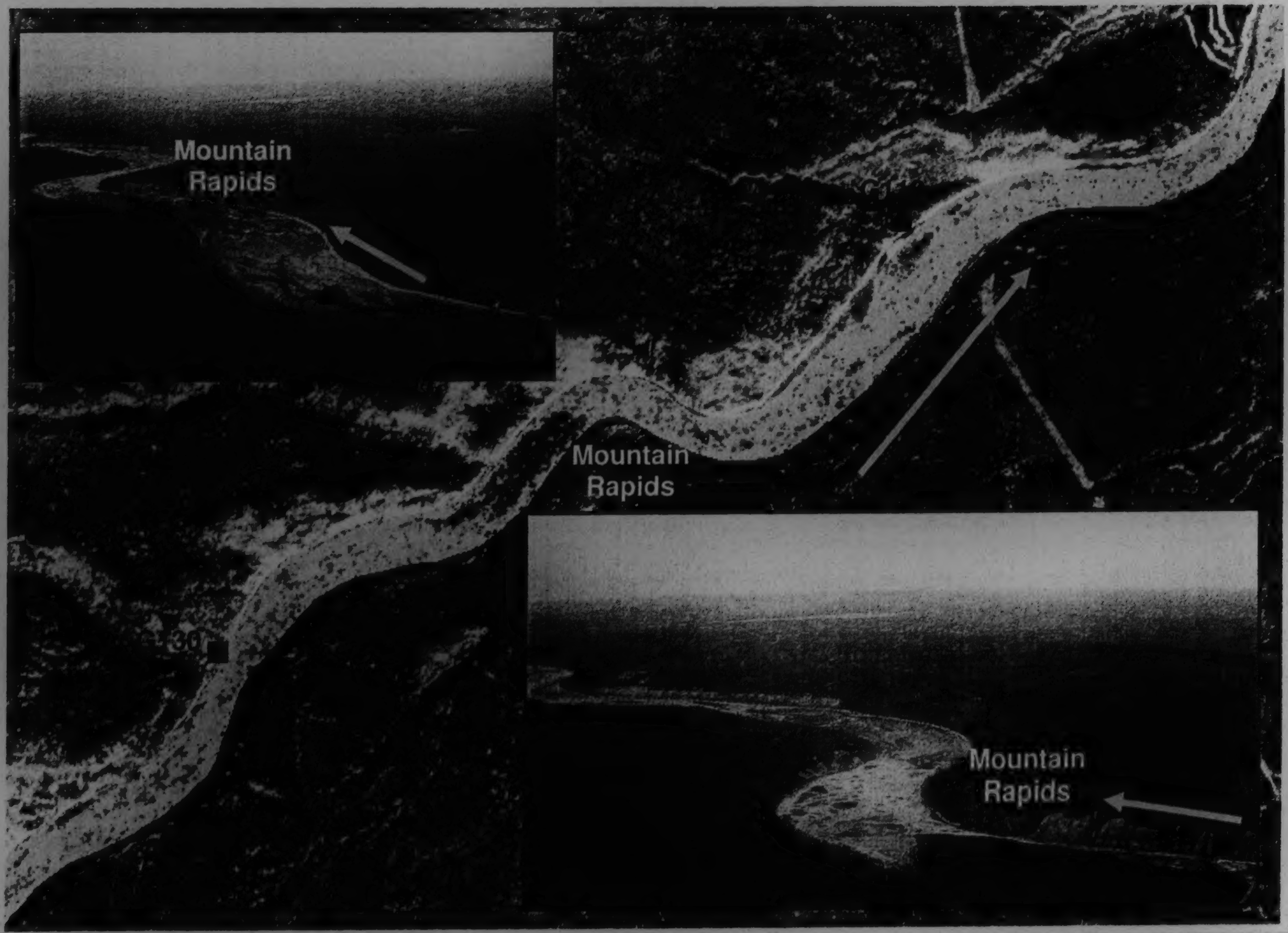
Mountain
Rapids
Mountain
Rapids
Mountain
Rapids
30

Figure 3.33 Ice accumulation at Mountain Rapids (April 12, 2004).

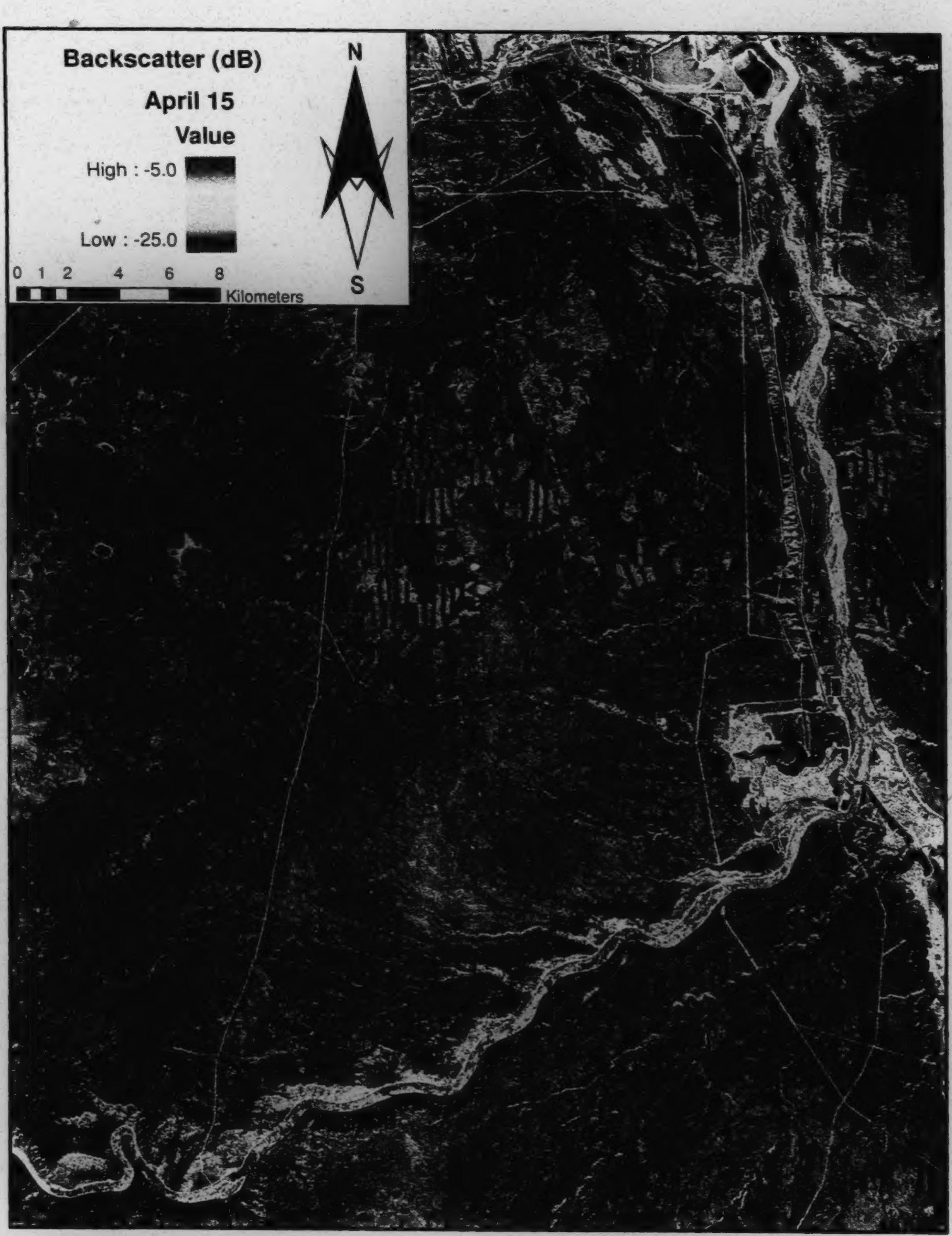
Backscatter (dB)
April 15
Value
High : -5.0
Low : -25.0
0 1 2 4 6 8
Kilometers
N
S

Figure 3.34 RADARSAT image product of the full study reach captured at 7:57:57 (local time) on April 15, 2004.

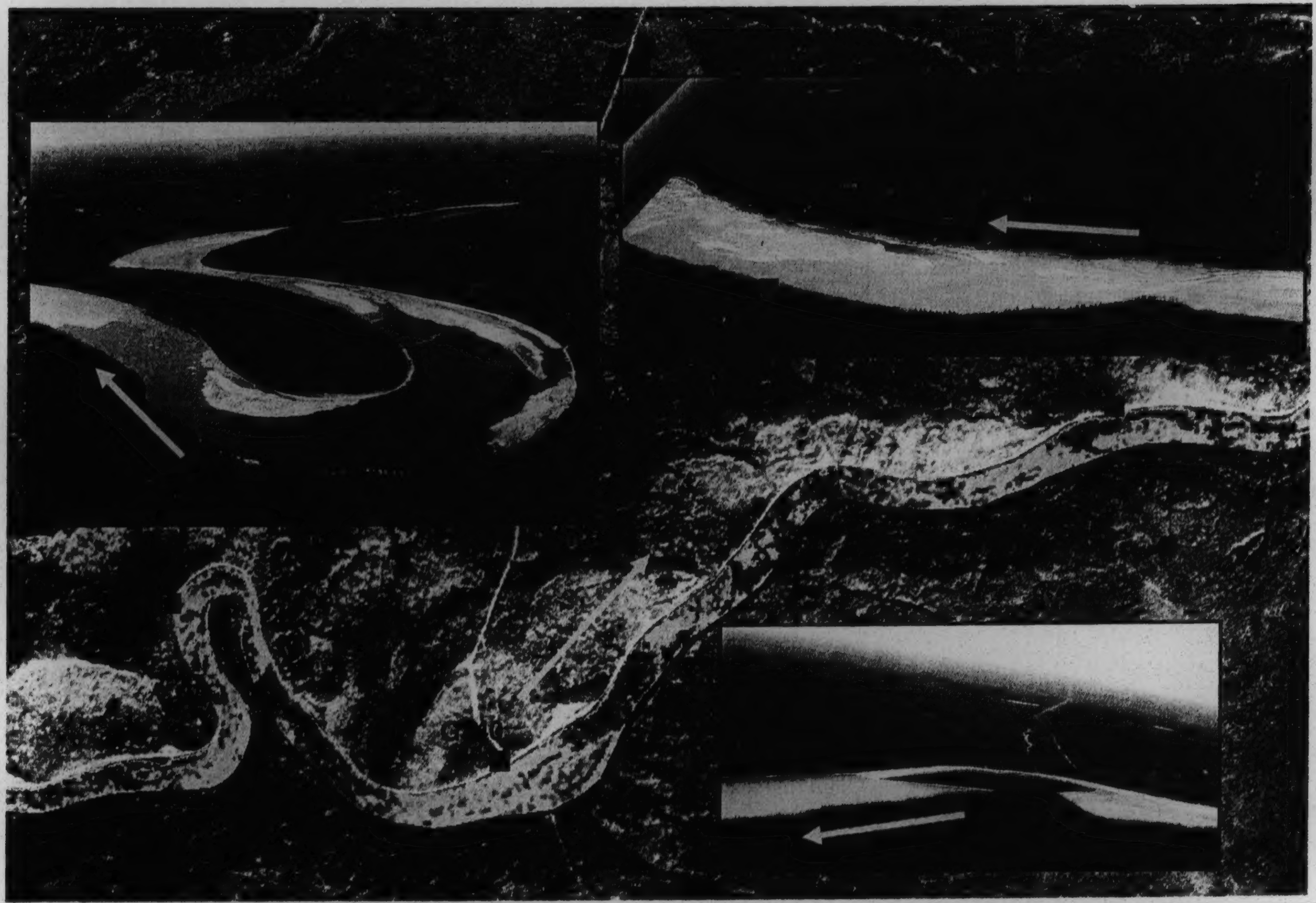

Figure 3.35 Open leads developing in study reach from G135 to G150 (April 15, 2004).

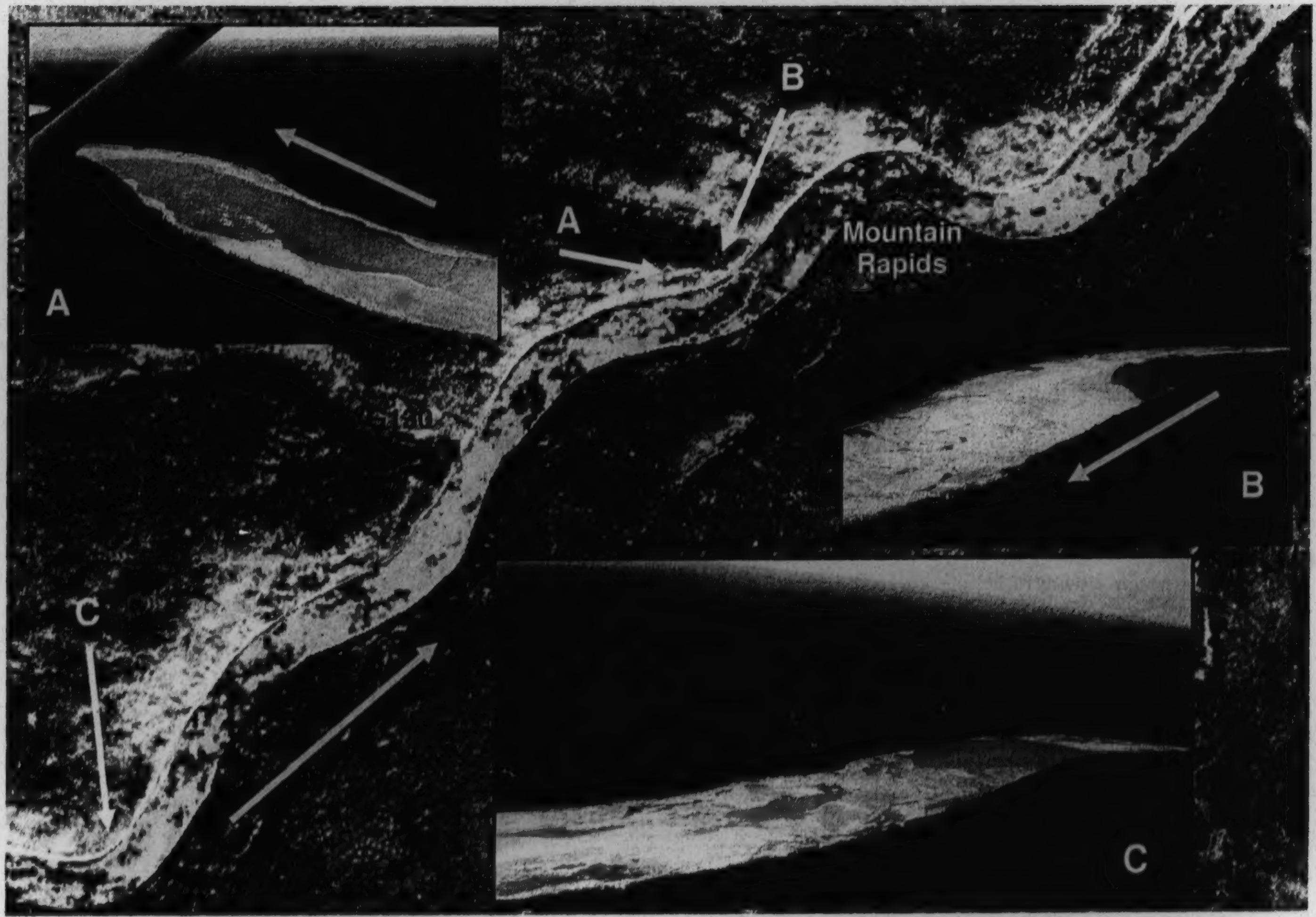
A
B
A
Mountain
Rapids
B
C
C

Figure 3.36 Open water and accumulations developing in study reach (April 15, 2004).

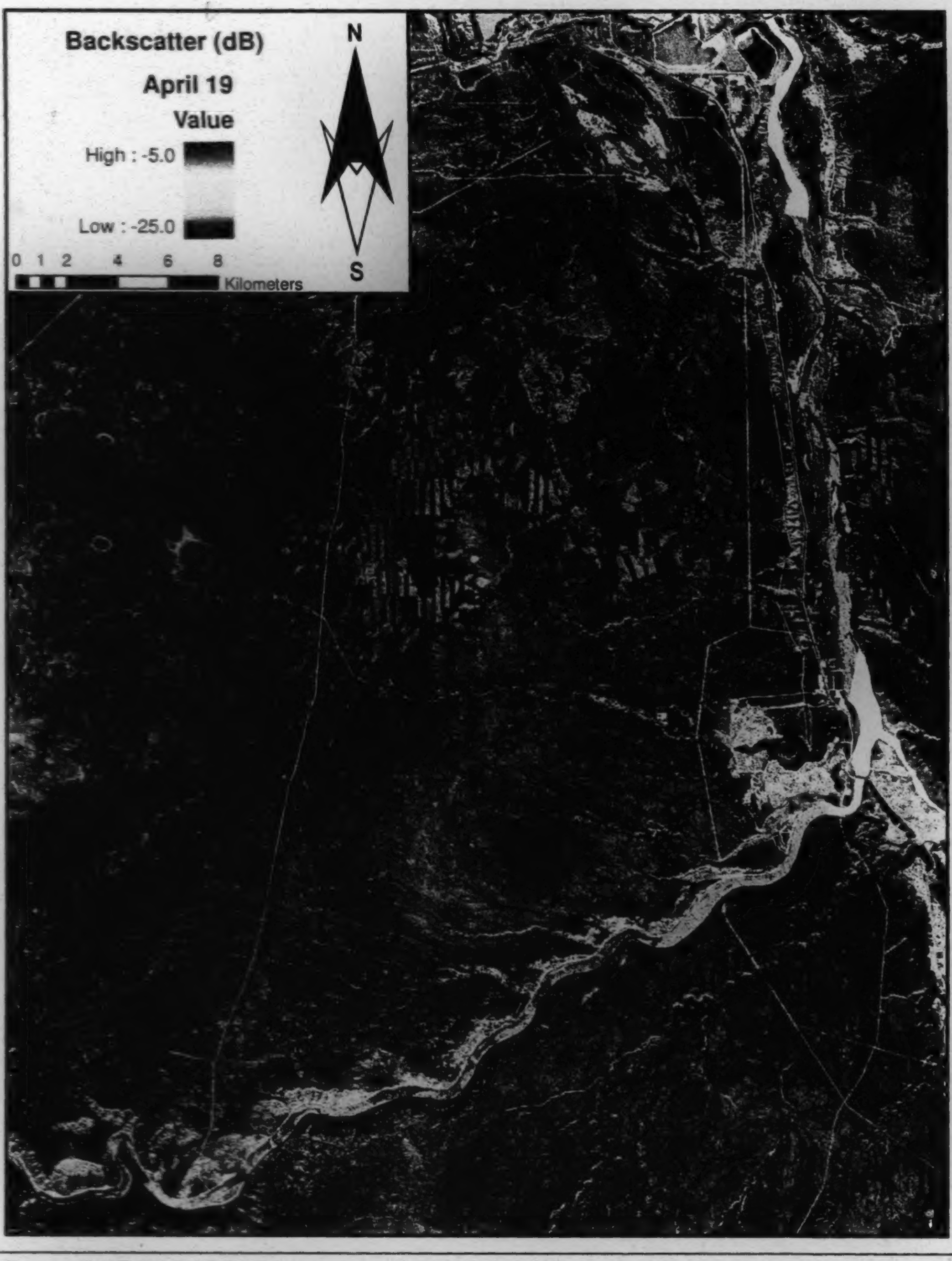
Backscatter (dB)
April 19
Value
High : -5.0
Low : -25.0
0 1 2 4 6 8
Kilometers
N
S

Figure 3.37 RADARSAT image product of the full study reach captured at 7:41:22 (local time) on April 19, 2004.

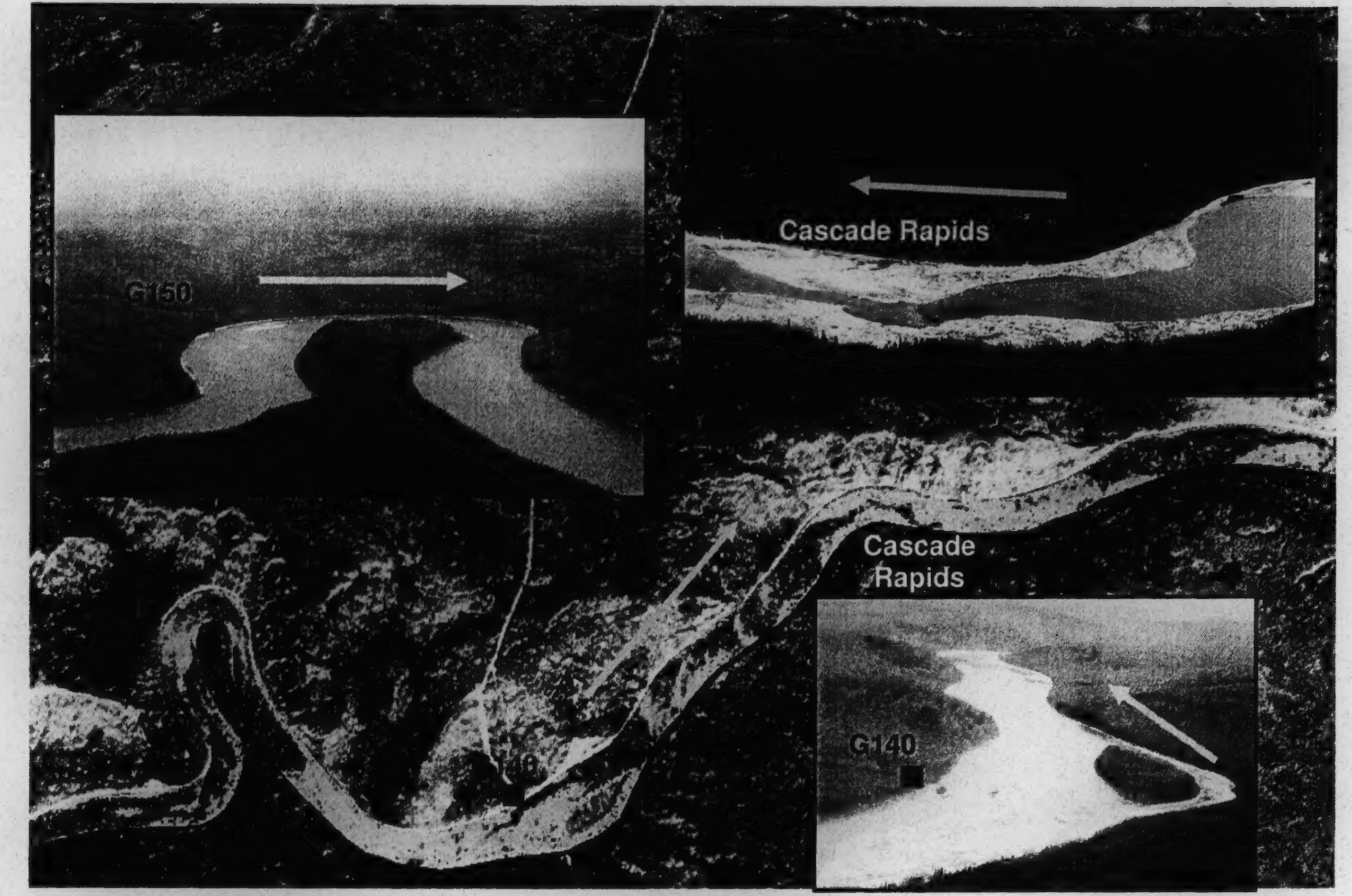
G150
Cascade Rapids
Cascade Rapids
G140

Figure 3.38 Remnant ice from Cascade Rapids to Crooked Rapids (April 19, 2004).

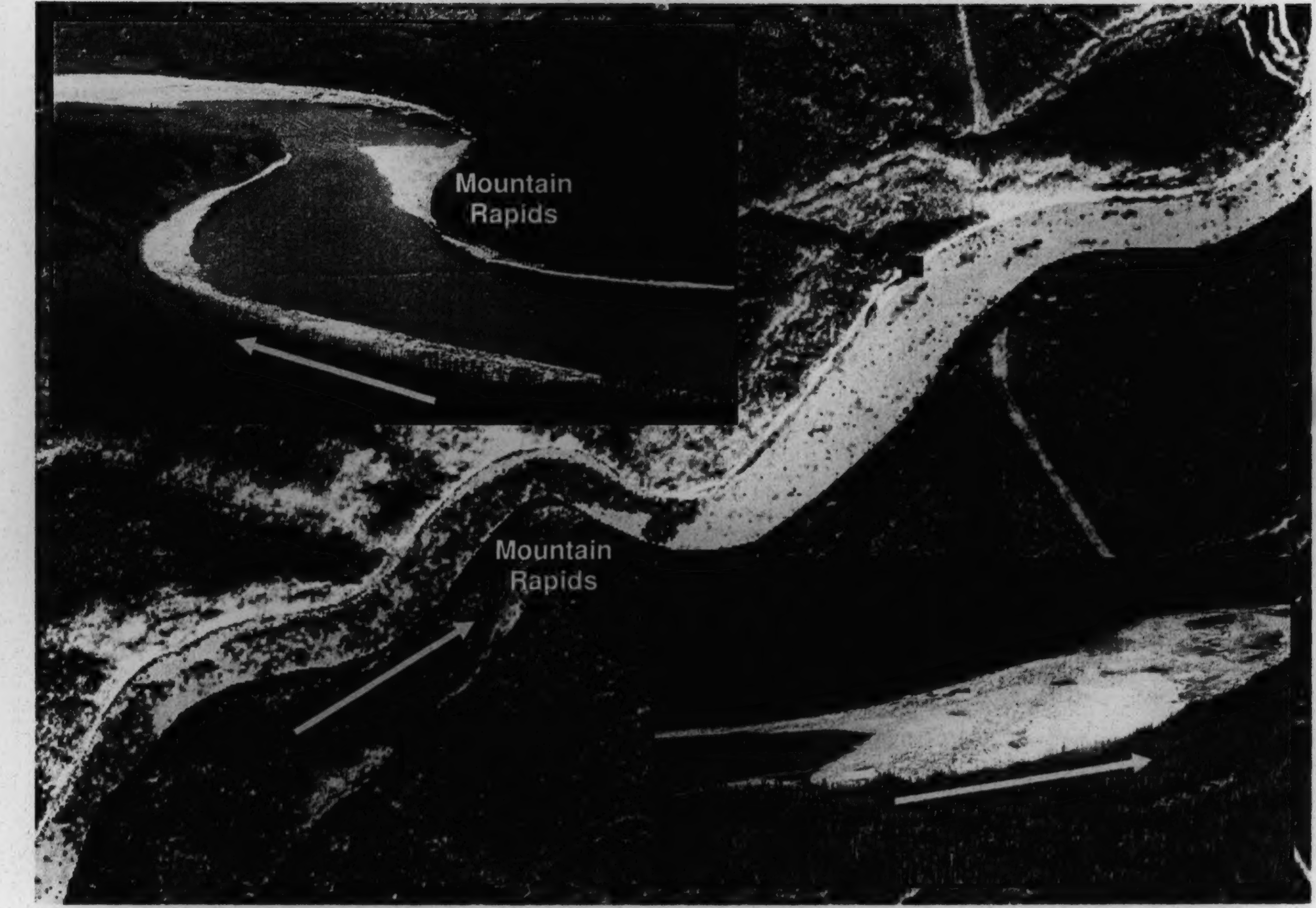
Mountain Rapids
Mountain Rapids

Figure 3.39 Deteriorating accumulation at Mountain Rapids (April 19, 2004).

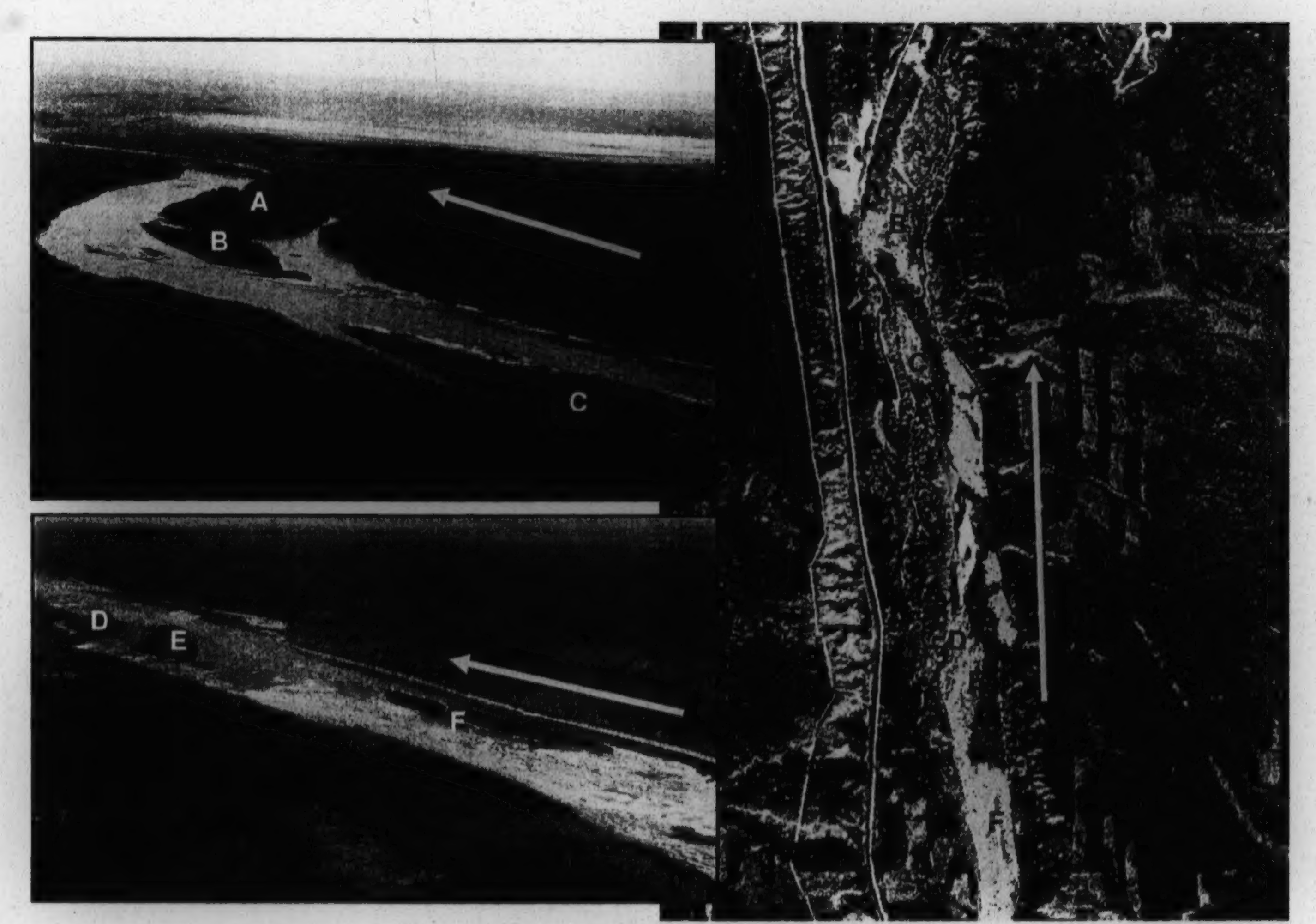
A
B
C
D
E
F
B
C
D
F

Figure 3.40 Open water and remnant ice downstream of the townsite (April 19, 2004).

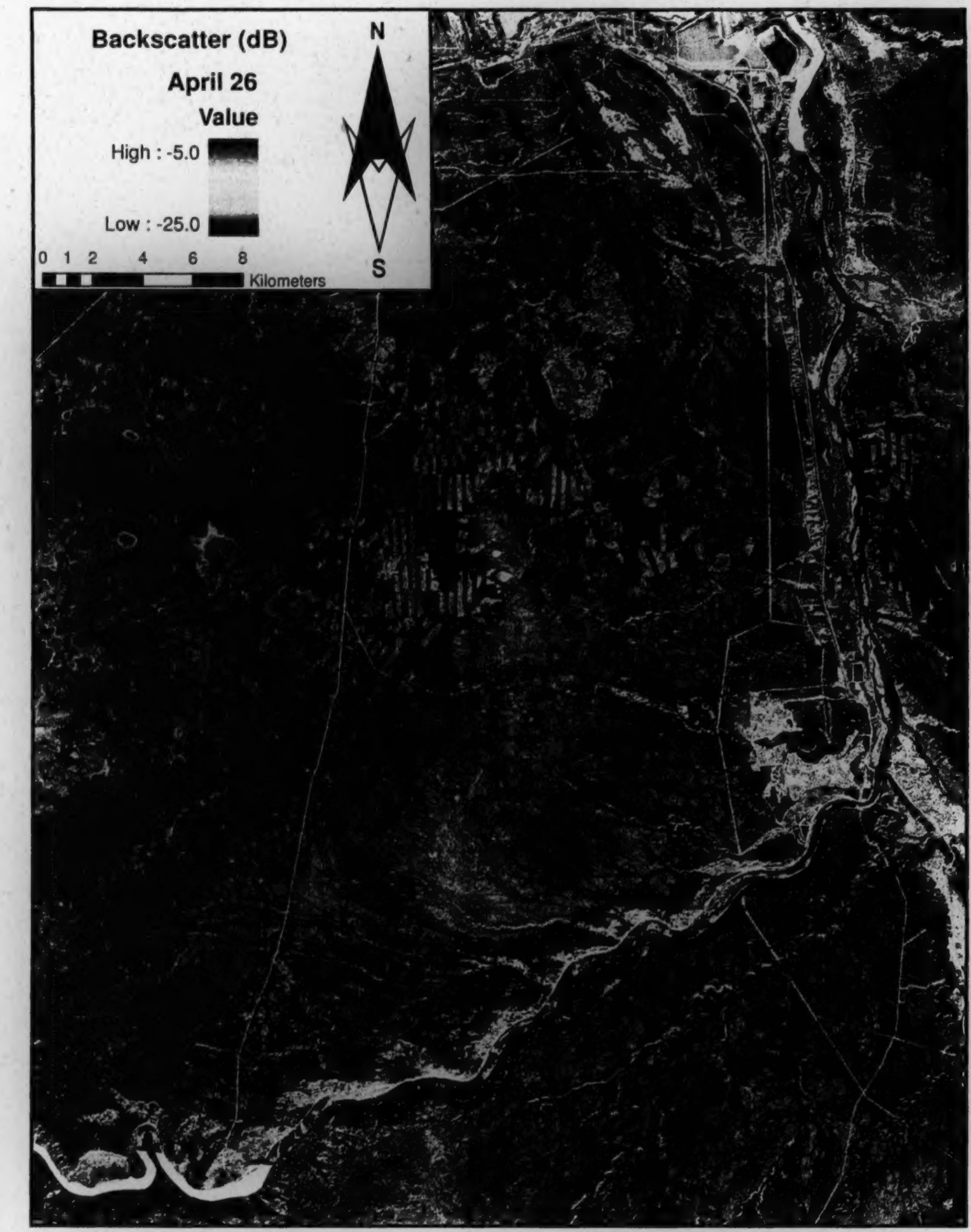
Backscatter (dB)
April 26
Value
High : -5.0
Low : -25.0
N
S
0 1 2 4 6 8
Kilometers

Figure 3.41 RADARSAT image product of the full study reach captured at 7:37:12 (local time) on April 26, 2004.

4.0 MONITORING BREAKUP: QUANTITATIVE ANALYSIS

4.1 INTRODUCTION

Despite the advantages of SAR, image interpretation remains a challenge. In addition to a suite of difficulties attributable to system parameters which are common to all SAR applications, the nature of interaction of the radar signal with river ice also introduces complications. Consequently, the results of previous studies have been predominantly qualitative in nature.

The intention of this chapter is to provide a somewhat more quantitative approach to the data, the analysis for which is comprised of two major components. The first investigation presented examines the variability of the backscatter coefficient (σ^0) during the breakup period. Because of the many factors which can affect radar return, it is difficult to assign a range of corresponding values to each ice type. The effects of melt further complicate this process, and there are additional uncertainties regarding the transferability of any classification scheme to alternate sites. The second portion of the study was specifically directed at evaluating the potential of SAR for estimating ice thickness. To this end, a preliminary field study was carried out in April 2003 and this was followed up by a more comprehensive investigation in February 2004.

The Athabasca River near Fort McMurray was again utilized as the study reach for data collection and analysis; this complements the data previously presented and was a practical choice because of the monitoring program already in place.

4.2 BACKSCATTER VARIABILITY ANALYSIS

4.2.1 Factors affecting Radar Return

As previously discussed, there are a number of factors which impact radar return. These introduce significant complications into any sort of quantitative evaluation and must therefore be acknowledged and addressed. Section 2.2 presents the major considerations in detail. Scene parameters of importance include surface wetness and texture. Water content controls the dielectric constant, which can limit penetration depth and ice texture and structure influence scattering mechanisms. Sensor parameters such as image mode and possible geometric distortions should also be considered.

4.2.2 Methods

As detailed in Table 3.1 and Table 3.2, thirteen images were collected from the RADARSAT-1 satellite during river breakup in 2003 and 2004. During image analysis, the study reach was further sub–divided into 18 zones of approximately equal river area (Figure 4.1). This facilitated a rough assessment of variability over the length of the reach. The islands were masked and, for all of the images, a mean scattering coefficient was calculated in each zone. This was then utilized to evaluate the efficacy of SAR monitoring in capturing changes to the ice cover and assess the relative importance of image mode.

4.2.3 Results

Breakup 2003

As discussed in Chapter 3, a total of eight images were acquired from the Canadian satellite RADARSAT-1 during breakup 2003. The time of acquisition, image mode and range of incidence angles for each image were detailed in Table 3.1 and the calculated backscatter coefficient for each zone is plotted in Figure 4.2. For reference, the daily mean temperature and snowfall at Fort McMurray, as recorded by Environment Canada, are presented in Figure 4.3 and Figure 4.4.

At the onset of breakup, a decreasing trend in the backscatter coefficient can be noted in the first 3-4 images. One likely explanation is that such changes may be due to snow melt on the ice cover. This results in a progressively wetter snow cover and ultimately leads to the development of a layer of liquid water on the ice surface. The increasing temperature during this period (Figure 4.3) supports this hypothesis. The presence of liquid water drastically raises the dielectric constant of the surface, thereby reducing penetration depth of the signal and causing the radar return to be dominated (to a larger extent) by surface scatter. Since intact ice has a relatively smooth surface, it would behave as a specular reflector causing less energy to be scattered back toward the radar. A comparable pattern was also noted by Gauthier et al. (2001) in an examination of the Saint-François River in Quebec.

In this context, a similar decreasing trend would also have been expected in the April 21 image; however, the exact opposite is in fact seen (Figure 4.2). Though the ice cover was intact and continuing to thermally decay, a significant increase in the backscatter coefficient is evident on this date. Probably the most likely explanation for this anomaly is the use of a different image mode (S1) on April 21. In this mode, the sensor utilizes a considerably steeper incidence angle (24-31°) than employed in the earlier images (39-47°). This effect was further investigated through an analysis of the backscatter signal for a stable distributed target (forest area) on April 21 and April 22, from which it was estimated that the offset in backscatter was in the order of 3 dB. Of these 3 dB, approximately 1.2 dB can be explained by the change in resolution cell size as a function of incidence angle. The remainder is either due to changes in scattering mechanisms, changes in environmental conditions and/or image calibration inaccuracies. While different imaging modes were also used in the previous dates, the variation in incidence angle between those cases did not represent as large a difference. It is unlikely that incidence angle could have had as significant an effect for these acquisitions.

On the subsequent day (April 22), an image was taken in S7 mode, which has an incidence angle more comparable to the earlier (pre-April 21) images (39-42° vs. 39-47°), and it is seen that the backscatter corresponding to the intact ice in this image is more consistent with those earlier values. On this day an ice jam formed in zones 6-9, and, as can be noted on Figure 4.2, the data points from this image show that the area encompassing the jammed ice had a significantly higher backscatter coefficient than the zones in that same image corresponding to intact ice. It is possible that the high scattering coefficients in this region may be attributable, at least in part, to ice characteristics. For example, the nature of a large (thick) ice jam is such that the portion of the accumulation thickness floating above the phreatic surface (~10% of the total) can be of a substantial thickness (perhaps 0.5 to 1m, or more) from which the interstitial water can readily drain, potentially lowering the dielectric constant. This would increase the penetration depth of the signal and cause volume scattering to have a greater effect on the radar return. Also, the actual surface of the ice was much rougher in these zones, compared to the intact ice. Therefore, surface reflections which do occur would tend to be more diffuse rather than specular, resulting in more radiation being directed back toward the sensor.

The image from April 23 captured the river condition once the ice jam had released, dispersed and was running downstream. The highest recorded backscatter values were obtained from this acquisition, probably due to a number of factors. First of all, as on April 21, this was an S1 image and therefore incidence angle would be again expected to play a significant role (i.e. increasing the backscatter). Additionally, though, ice characteristics were radically different on this occasion, which would alter the scattering behaviour. It was qualitatively observed that the surface roughness of the running ice was less than that seen in the stationary ice jam on the previous day. The thickness of the running ice was also known to be less (since the ice run was considerably longer than the stationary ice jam) and it is important to note that it was also less drained (i.e. more surface water apparent). This presence of surface water would lower the penetration depth of the signal, thereby reducing the volume scattering component of the radar return and causing surface scatter to govern. Since the true magnitude of the difference between the two acquisitions is marred by the change in image mode, it is unclear whether one might expect a stationary ice jam to produce a higher backscatter than running ice.

On the last day of observations, April 25 (reference Figure 3.24), the river was essentially clear of ice. Compared to the April 15 image (reference Figure 3.10), when ice was intact, some zones are seen to have a higher backscatter coefficient while others have a lower value. Note that both images were taken in F2N mode. Nonetheless, those zones with the lower backscatter coefficients are more genuinely representative of open water since considerable amounts of residual ice were observed in the zones exhibiting higher backscatter. This makes sense, since the scattering coefficient is lower under open water conditions due to specular reflections at the surface.

Breakup 2004

As discussed in Chapter 3, a total of five images were acquired from the Canadian satellite RADARSAT-1 during breakup 2004. The time of acquisition, image mode and range of incidence angles for each image were detailed in Table 3.2 and the calculated backscatter coefficient for each zone is plotted in Figure 4.5. Mean daily temperature and recorded daily snowfall at Fort McMurray are presented in Figure 4.6 and Figure 4.7 respectively.

The same general decreasing trend in backscatter coefficient during the early melt period can be noted in Figure 4.5. Again, this is likely attributable to the increasing liquid water content which raises the dielectric constant, reduces penetration depth, and increases surface scatter. Also, similar to 2003, the S1 image on April 15 exhibits significantly higher scattering than the other images within that period, suggesting that incidence angle is an important factor for this image. Unfortunately, analysis is further complicated by the drop in temperature on this date (Figure 4.6); this may also have contributed to the difference in radar return. Due to the more sparse acquisition plan during the 2004 breakup, it was not possible to detect any of the small accumulations from April 12 or the shoves which occurred on April 22 and April 23. However, as would be expected during open water conditions, the recorded scattering coefficients from April 26 are quite low.

4.3 ICE THICKNESS INVESTIGATION

To investigate whether a correlation exists between ice thickness and backscatter, it was necessary to collect field data. A preliminary study was carried out in April of 2003 which produced encouraging results. This was then followed up by a more intensive field campaign in February of 2004.

4.3.1 Methods

Taking ice thickness measurements can be a time-consuming and arduous task. Therefore, in order to maximize data acquisition, it was desirable to streamline this process as much as possible during both the preliminary and comprehensive investigations. As depicted in Figure 4.8, a 1-inch steel augur (attached to a battery-operated hand drill) was used to drill through the ice layers and make a small hole with which to measure ice thickness. The ice thickness was determined using a custom-made gauge as presented in Figure 4.9. This device was lowered into the hole by using the wire as demonstrated in the left photograph. Once it reached the bottom, it was raised back up using the measuring tape (right photograph). The weight is rotated at this stage and catches on the bottom lip of the ice cover. In this manner it is relatively simple to read the ice thickness from the measuring tape. Note that in addition to ice thickness, the snow depth, depth of flow and ice structure were also documented.

4.3.2 Limitations

As with nearly all field campaigns, some difficulties were encountered in the course of data collection. At several sites, the ice thickness could not be measured precisely using the gauge. This occurred at those points where there was a very shallow depth of flow beneath the ice cover, preventing the weight from having sufficient space to rotate. Ice thickness was therefore estimated as closely as possible when this occurred.

Another issue is that the measurement technique employed only considers solid ice and therefore the presence of any frazil ice could not be quantified. In order to do this, a larger diameter hole would need to have been drilled so that a video camera could be lowered down to observe the slush ice. This would have been time-consuming, however, and limited the overall size of the data set.

Further difficulty was also encountered at those locations where the ice cover was exceptionally rough. When an ice surface is hummocky (note Figure 4.10), it can be extremely challenging to obtain a meaningful ice thickness. In these areas it was generally only possible to measure thickness at sites which were, locally, less rough. However, this means that the thickness measured is probably not representative of a "mean" ice thickness. Additionally, in some cases, the roughness can be severe enough to make the surface too unsafe to obtain its thickness or even traverse it.

4.3.3 Preliminary Investigation, April, 2003

In April 2003, a preliminary field study examining the relationship between ice thickness and radar backscatter was conducted. Photographs along the study reach and measurements of ice thickness at key locations were taken over the course of several days from April 1 to April 3. These were then visually compared to a fine beam (F2N) RADARSAT-1 image acquired during a descending overpass on April 1 at 06:41:23. This was approximately 22 days before the breakup of the river. Figure

4.11 and Figure 4.12 display the processed image product and a view of the upstream study reach, extending from Crooked Rapids (near G150) to the Fort McMurray town site, respectively.

The ice cover appears visibly brighter along the reach from the town site to the vicinity of G110. A closer look at this sub-reach is provided in Figure 4.13, along with pictures and approximate ice thicknesses at several locations. Measurements confirmed that the ice cover was relatively thick throughout this sub-reach (1.25 m or more) as a result of a freeze-up ice jam having formed here. There did appear to be some significant variation in the backscatter within this region. Given the consolidated state of the ice cover at the time of data acquisition, though, this was not entirely surprising. The incident microwaves can be expected to penetrate the ice-air interface and be backscattered as a result of multiple reflections in the underlying ice volume and/or reflections at the rough ice-water interface. The inability of the human eye to penetrate an ice cover in a fashion similar to radar sensors increases the difficulty of interpreting these variations.

Figure 4.14 illustrates the portion of the reach in the vicinity of stations G130 and G135. As shown in the corresponding photographs, the presence of water at G130 resulted in a region of lower backscatter on the RADARSAT-1 image as compared to that at G135. Unfortunately the extent of thermal deterioration in this sub-reach made it too unsafe to gather ice thickness data.

The portion of the study reach upstream of station G135 is illustrated in Figure 4.15. Thickness measurements and photographs were taken at several locations in this section of the study reach. The first, second and fifth locations (increasing in the downstream direction), which appeared to have lower backscatter in the satellite image, were found to have thinner ice covers (0.79 m, 1.01 m and 0.93 m, respectively). Conversely, the two high backscatter areas in the satellite image were found to have relatively thick ice covers. Ice thickness was measured to be 1.30 m at Rock Rapids (third location) and 1.50 m at Cascade Rapids (fourth location). That both of these locations are near rapids is interesting. It stands to reason that this high backscatter could be due to a heavily consolidated ice cover (possible freeze-up jam) that is characterised by considerable air inclusions and a rough ice-water interface.

To the human eye, such a heavily consolidated ice cover typically presents itself in terms of a pronounced surface texture or surface roughness. Note that although location 2 is near Crooked Rapids, the ice thickness was actually measured a fair distance upstream of the rapids.

Overall, the data collected during this field trip was not sufficient to draw any firm correlation between ice thickness and the backscatter coefficient. However, results were found to be encouraging, lending some credence to the suggestion that it may be possible to infer ice thickness information from SAR imagery. To investigate this further, a more comprehensive investigation was planned for February 2004. This time of year was selected because the ice cover would likely be quite competent, thereby eliminating much of the risk associated with river ice field work and maximizing data collection potential.

4.3.4 Field Study, February 2004

For this study, field work was primarily carried out over three days from February 17th to 19th. The data collected during this period was used in conjunction with a fine beam (F2N) RADARSAT-1 image acquired on February 7th at 13:41:21 UTC (06:41:21 local time). By conducting the study when the weather is cold, meltwater on the ice or within the snow cover is generally not an issue and the variation in backscatter coefficient due to moisture is not a concern. In this case, ice thickness and roughness are the primary variables of consequence. Sites were encountered where overflow on the ice surface (but under the snow) was noted, but field data could not be collected at these sites for safety reasons.

The processed image product for February 7th is presented in Figure 4.16. Note that, because of the increased variability in the backscatter during mid-winter (chiefly in the upper range), the color scale was set to span a range from 0 to -25 decibels instead of -5 to -25 decibels as was previously used for the breakup images.

As indicated in Figure 4.17, nine transects were identified and targeted for further examination during the February field trip. These were selected as areas which covered a wide range of backscatter, potentially corresponding to a substantial variation in ice thickness. Given the relative remoteness of the study reach, all transects had to be accessed via helicopter. A series of holes was drilled across the transect to determine variation in ice thickness. Additionally, at each hole, the snow depth on the ice and depth of flow under the ice were measured. Also, ice surface characteristics were photographed and noted in order to categorize its structure (thermal, hummocky, etc). The coordinates of each hole were determined using hand-held GPS and, for further confirmation, the distance between holes was measured using a cloth tape.

4.3.5 Results

Thickness Results

A plot of the estimated and measured ice thicknesses (vs. backscatter coefficient) is presented in Figure 4.18. Note that since the weight on the ice thickness gauge is twenty centimetres long (reference Figure 4.9), the approximate error associated with the estimated values is on the order of about ten centimetres (i.e. for those cases where the weight could not be rotated fully). Error bars are displayed on the plot to denote this uncertainty. Using all of the available ice thickness data, a linear regression of the data set was performed. As is apparent, however, there was a great deal of scatter in the data, resulting in a fairly weak coefficient of determination (R^2) of only 0.356. Note that, at each site, the backscatter values were extracted after the image was filtered, but only single-pixel values were used. It is possible that a stronger correlation might be obtained if this data were re-examined using a 3x3 or 4x4 window at each sample site. Further work to explore this is planned.

As presented in Figure 4.19, there is a fair degree of variability in the thickness at each transect, but many of the data points do fall in visible groupings by transect. Therefore, the mean thickness at each transect was plotted vs. the mean backscatter coefficient for the same points in the transect. As Figure 4.20 demonstrates, this results in a stronger relationship between thickness and backscatter (R^2=0.764). This suggests that a relationship may exist between ice thickness and backscatter. However, it is important to note that, in the context of practical ice thickness ranges possible for this reach, this was a relatively limited data set in that no thicknesses in excess of one metre were actually measured. This was due in part to the logistical difficulty associated with taking measurements at hummocky locations (which is where these large thicknesses tend to occur). Therefore, more data is needed to explore this question in greater depth.

Structure Results

In addition to ice thickness, ice structure is another parameter that has been hypothesized to influence the backscatter coefficient. To investigate this, surface characteristics were photographed and documented at each hole and, using this information, the ice surface was subsequently categorized according to structure. Figure 4.18 (ice thickness vs. backscatter) was replotted according to ice structure type as shown on Figure 4.21 and from this there does appear to be a relationship between ice structure and backscatter coefficient. In fact, it is possible that ice structure is a more important parameter than ice thickness with respect to its effect on the recorded amount of backscatter. Overall, the hummocky ice cover produced the highest backscatter and thermal ice with large bubbles and/or cracks generated a stronger return than homogeneous thermal ice. There was no notable difference between homogeneous thermal ice and the juxtaposed ice cover. However, as frazil ice crystals are on the order of millimetres (or smaller), these may not be large enough to scatter the signal.

4.4 SUMMARY AND DISCUSSION

The interpretation of SAR data is complicated by many factors. An investigation into the variability of backscatter throughout the breakup period demonstrated that parameters relating to both the sensor and the target play important roles. With regard to the sensor, the consequences of image mode, and frequency of acquisition must be considered. Of particular significance, though, is the effect of image mode. In those acquisitions where the S1 mode was employed, the steep incidence angle caused a considerable increase in the calculated backscatter coefficient relative to other image acquisitions.

These effects, though, were not great enough to mask the overall progression of breakup. As the ice cover deteriorated, the significance of ice properties became apparent. Surface wetness was identified as being particularly significant as it governs the extent to which surface and/or volume scattering mechanisms contribute to radar return. Thus, an ice cover's state of thermal decay affects the scattering coefficient. Wet snow covering the ice reduces signal penetration depth, increasing the impact of surface scatter. Conversely, both volume and surface scattering (at the ice-water interface) occur when an ice cover is dry; scattering due to bubbles, impurities, water pockets and even secondary interfaces may contribute to the radar return.

A field campaign carried out early in 2004 was targeted to investigate the potential of inferring ice thickness from SAR image data. The results from this component of the study, however, were inconclusive. A correlation between thickness and radar return was found but this was not strong enough to establish a relationship between these two parameters. Further, the study also demonstrated that ice structure influences the amount of backscatter. Those locations at which the ice cover was hummocky generated significantly higher returns than areas which were cracked and/or had large bubbles. Similarly, homogeneous thermal ice and juxtaposed covers produced the lowest backscatter coefficient.

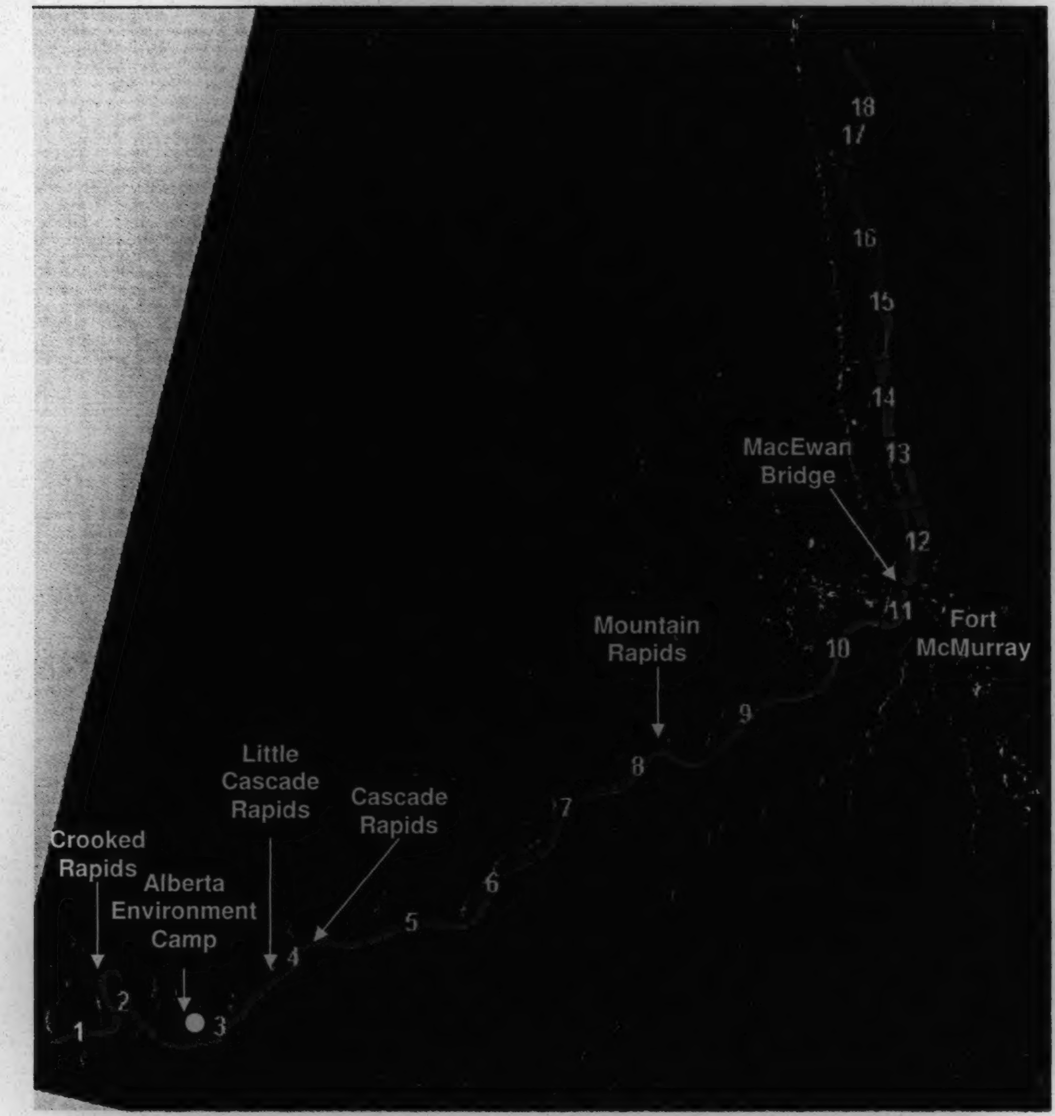
18
17
16
15
14
MacEwan Bridge
13
12
11
Fort McMurray
10
Mountain Rapids
9
8
7
Little Cascade Rapids
Cascade Rapids
6
5
Crooked Rapids
Alberta Environment Camp
4
2
1
3

Figure 4.1 RADARSAT-1 S1 mode image acquired on April 21, 2003 with the locations of zones in which mean radar backscatter was tracked.

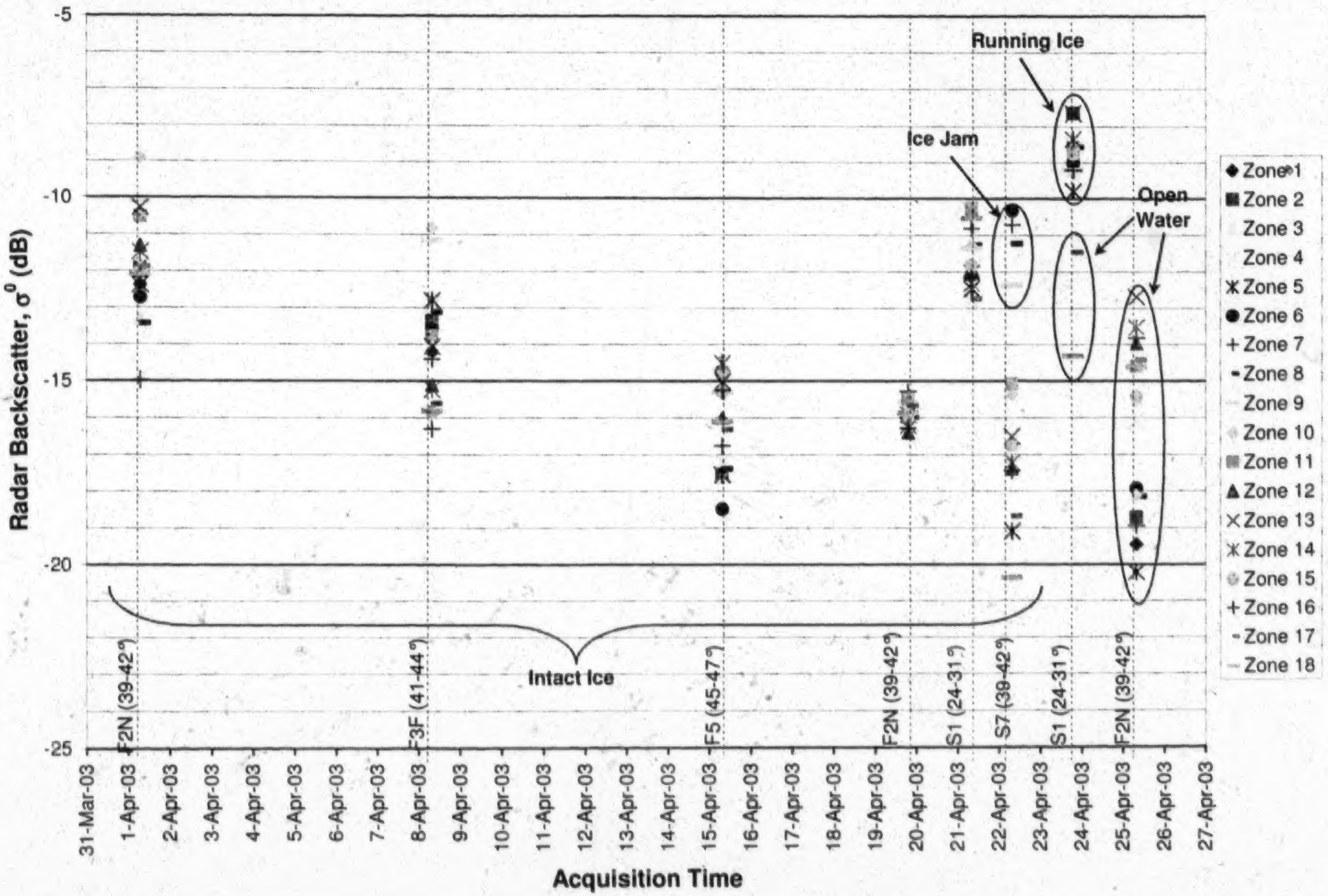

Figure 4.2 Mean radar backscatter (σ^0 in dB) during 2003 Athabasca River breakup.

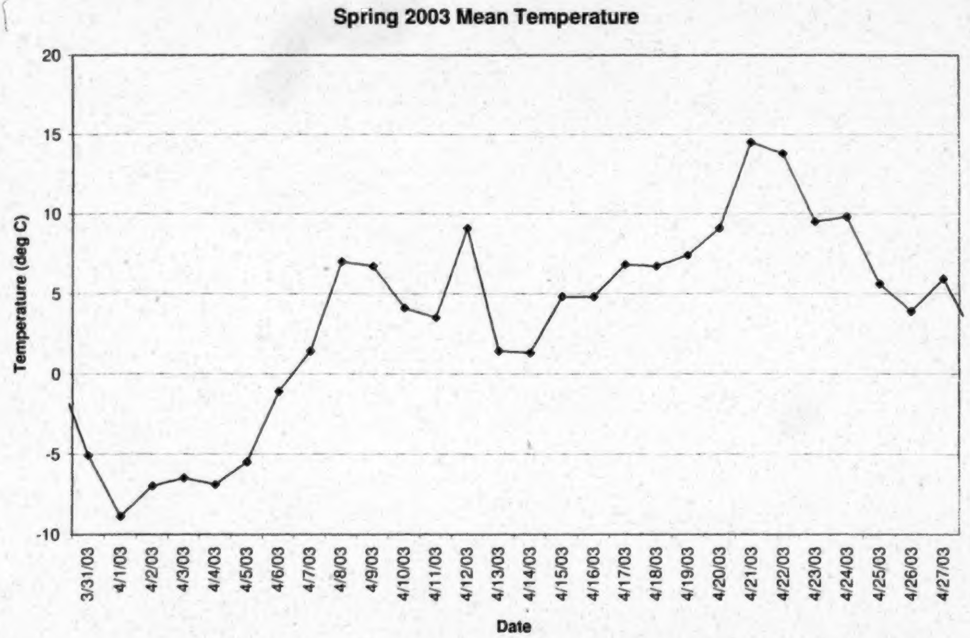

Figure 4.3 Daily mean temperature during 2003 Athabasca River breakup.

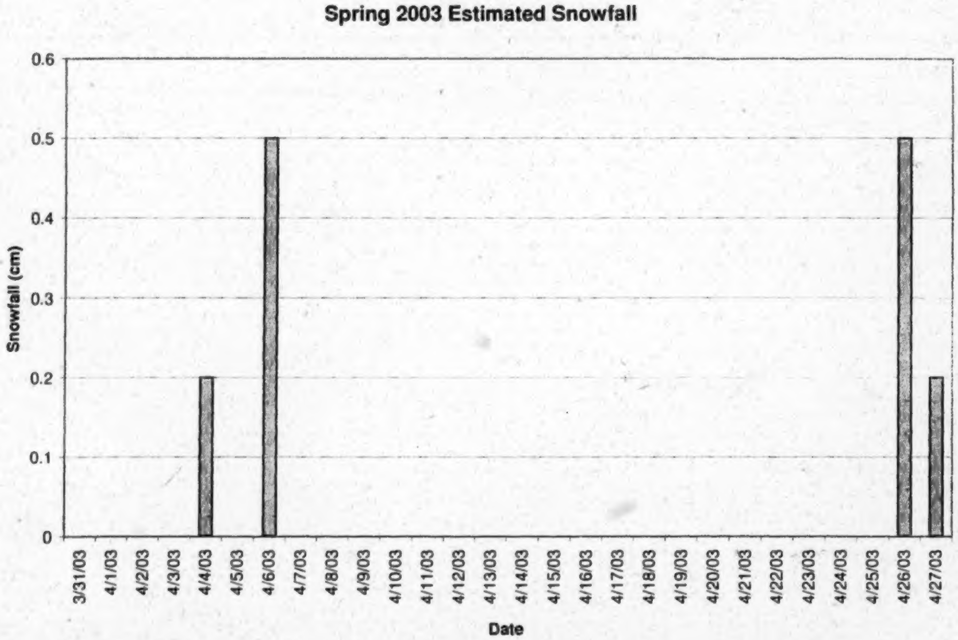

Figure 4.4 Estimated daily snowfall during 2003 Athabasca River breakup.

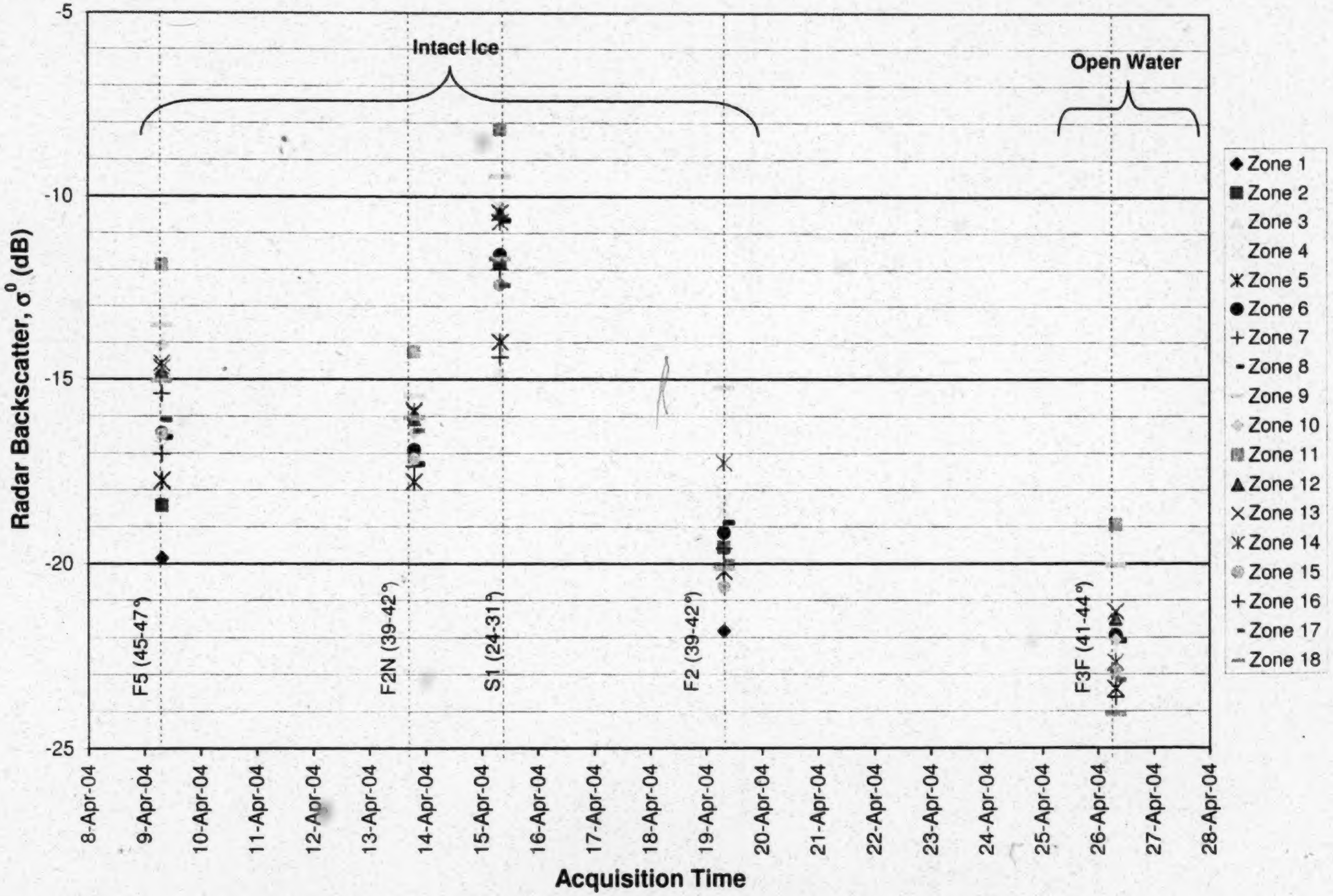

Figure 4.5 Mean radar backscatter (σ^0 in dB) during 2004 Athabasca River breakup.

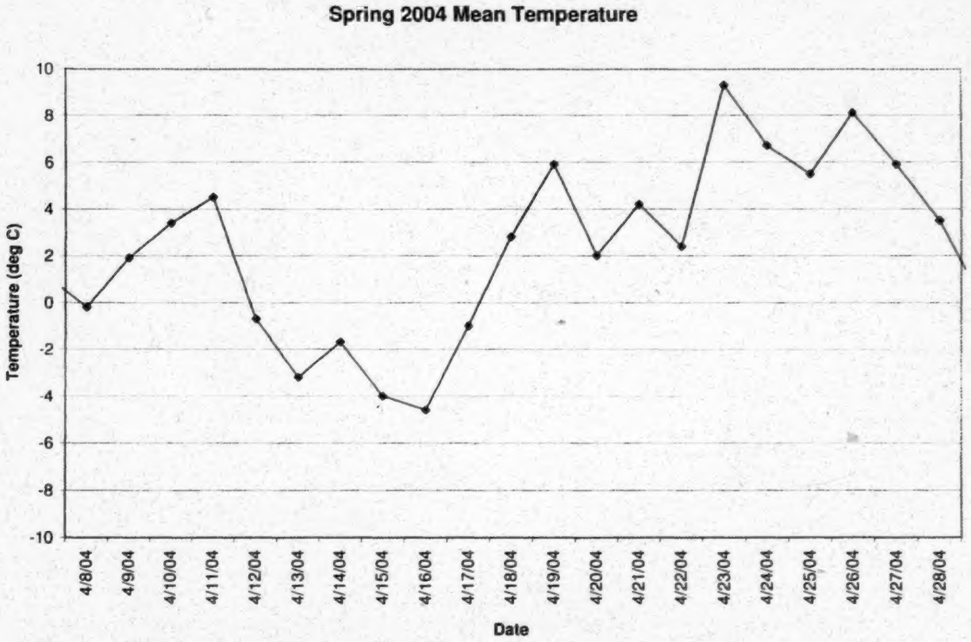

Figure 4.6 Daily mean temperature during 2004 Athabasca River breakup.

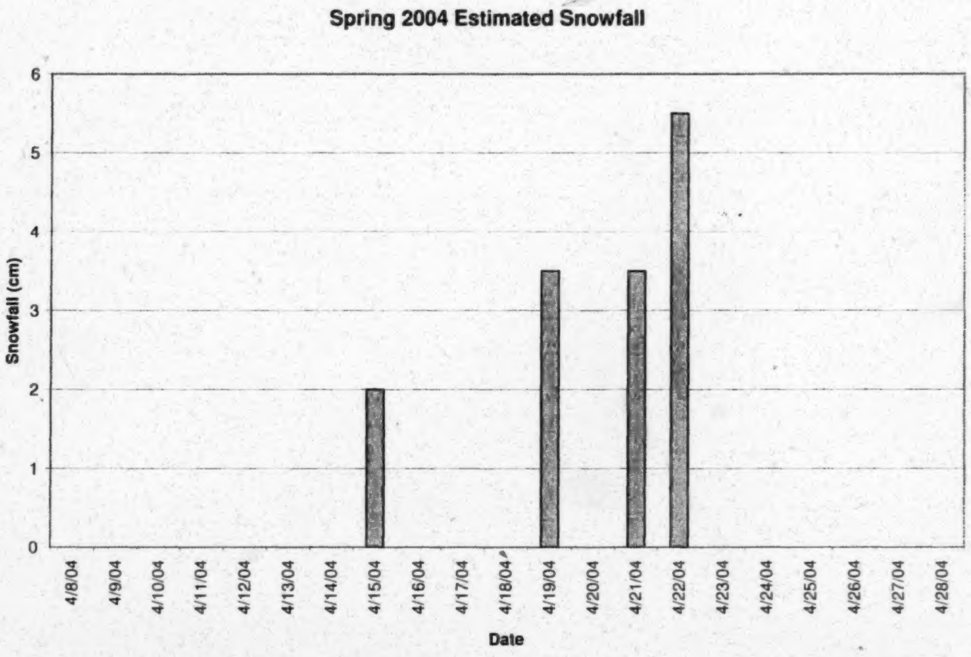

Figure 4.7 Estimated daily snowfall during 2004 Athabasca River breakup.

Figure 4.8 Drilling a hole to determine ice thickness.

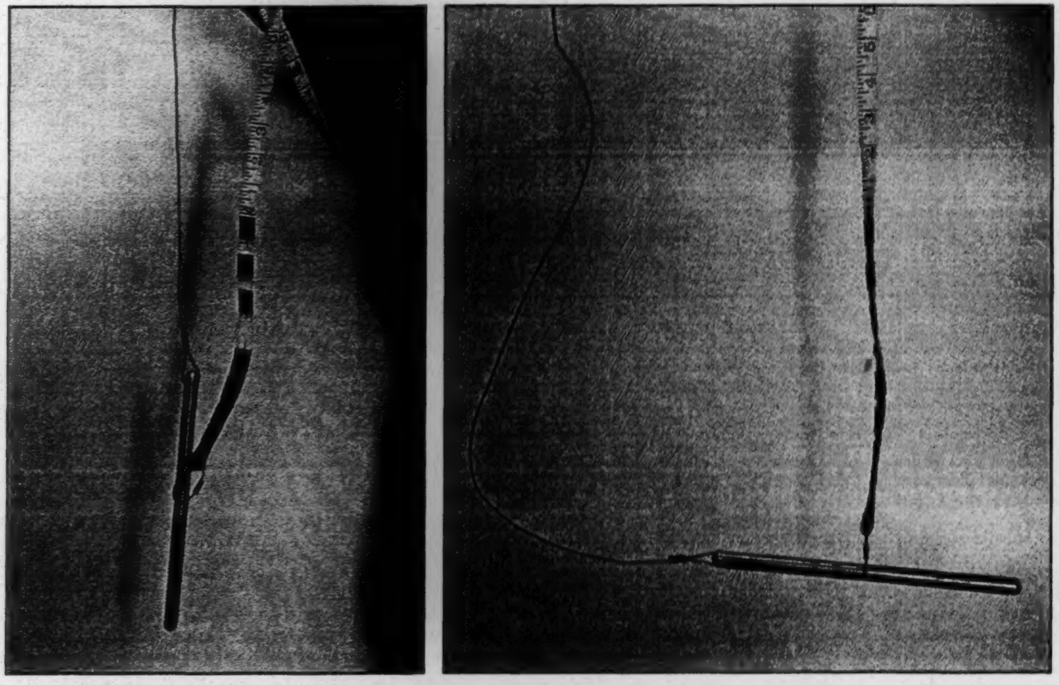

Figure 4.9 Ice thickness gauge.

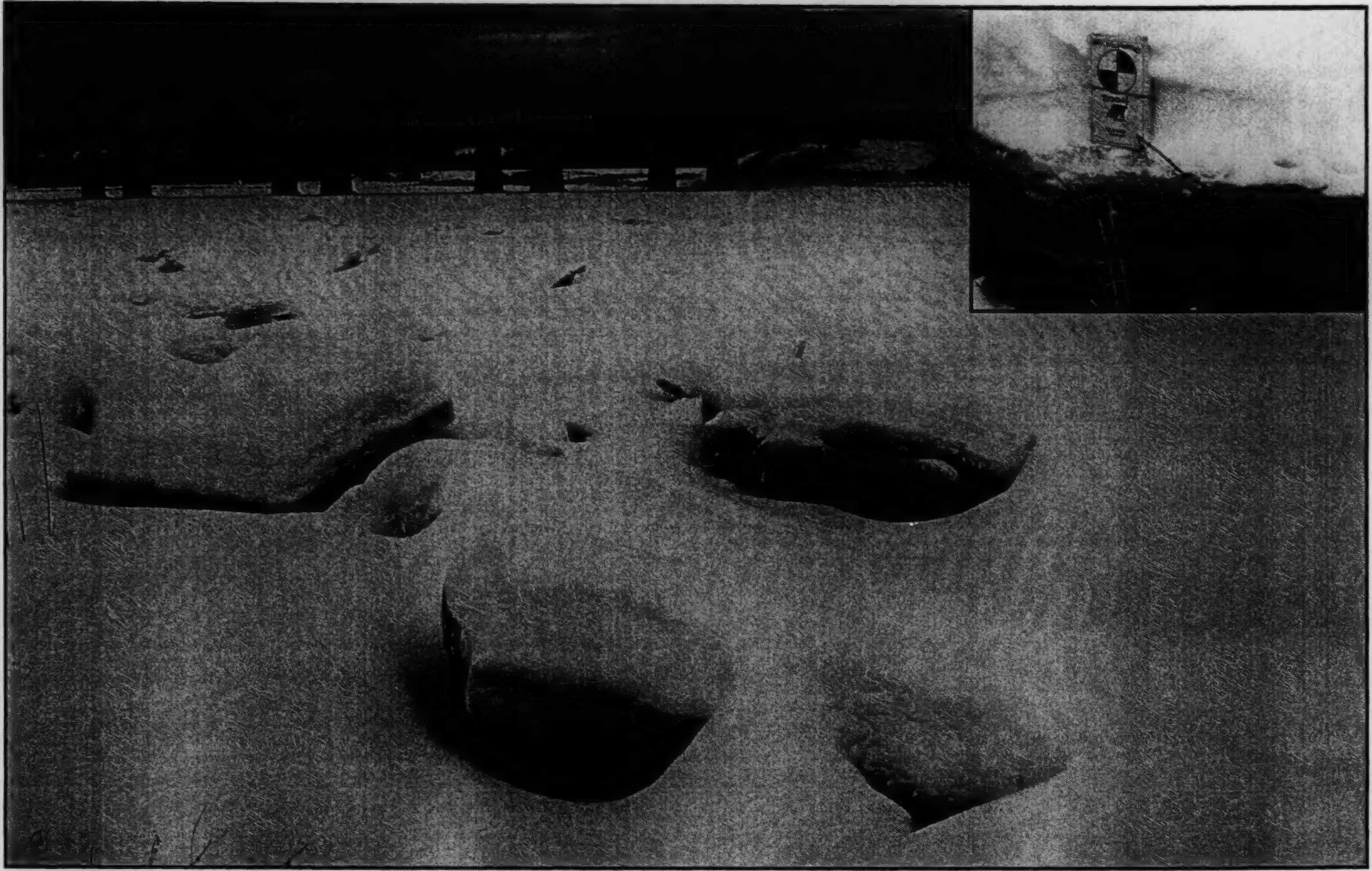

Figure 4.10 Hummocky ice surface at freeze-up jam location.

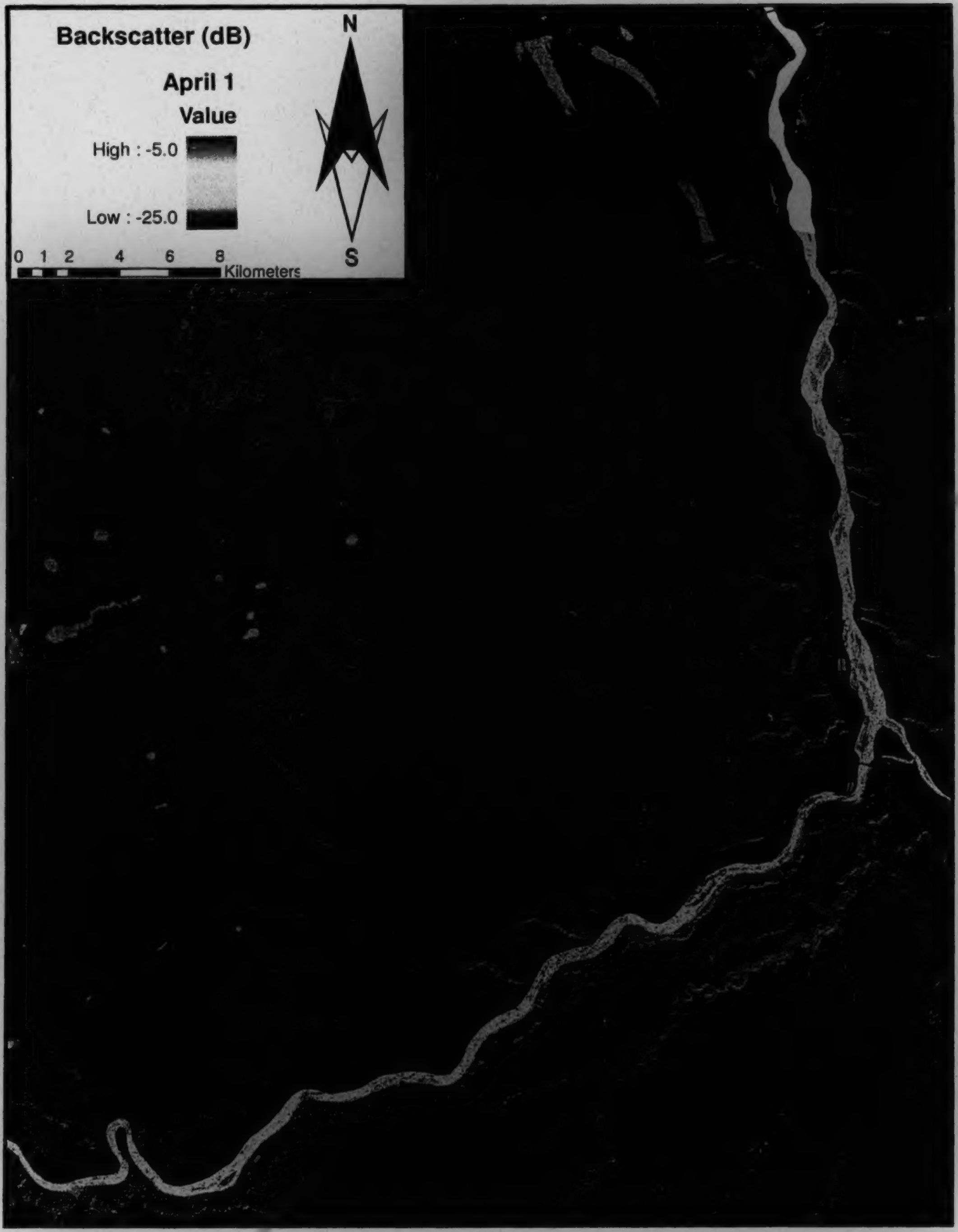
Backscatter (dB)
April 1
Value
High : -5.0
Low : -25.0
0 1 2 4 6 8
Kilometers
N
S

Figure 4.11 RADARSAT image product of the full study reach acquired at 6:41:23 on April 1, 2003.

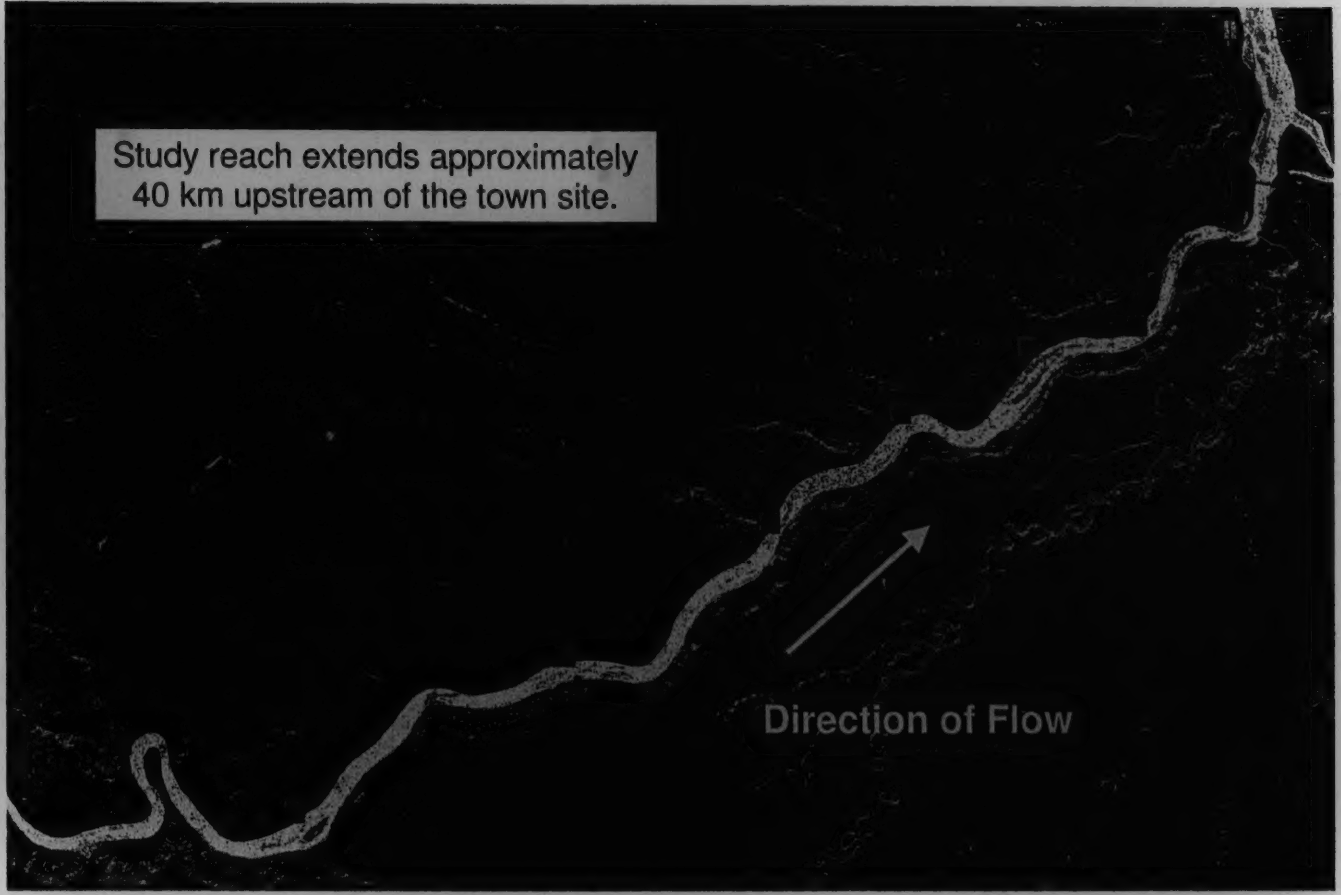
Study reach extends approximately 40 km upstream of the town site.
Direction of Flow

Figure 4.12 RADARSAT image product of the upper study reach, 22 days before breakup (April 1, 2003).

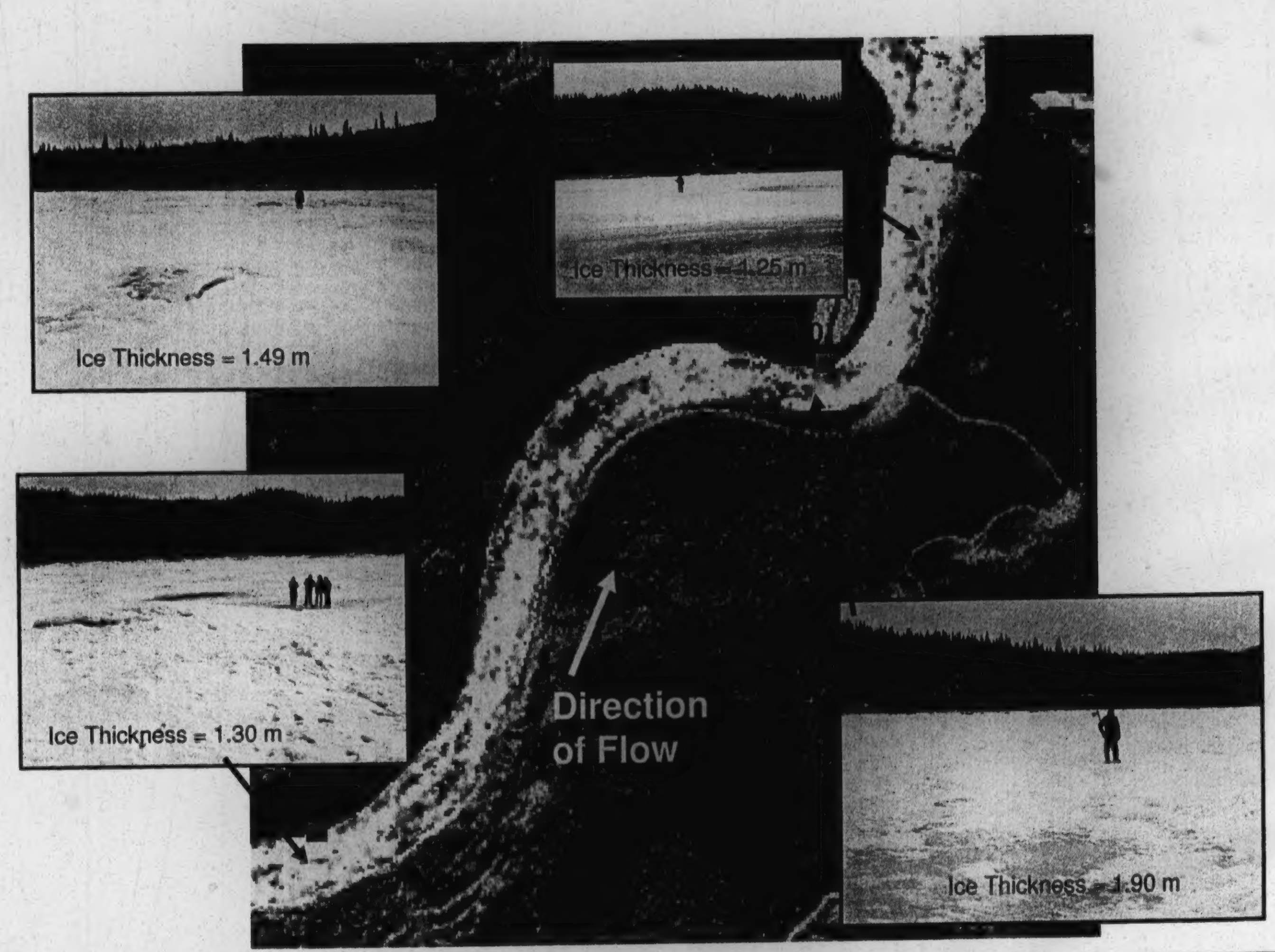
Ice Thickness = 1.49 m
Ice Thickness = 1.25 m
Ice Thickness = 1.30 m
Direction of Flow
Ice Thickness = 1.90 m

Figure 4.13 Ice conditions at four locations just upstream of Fort McMurray (April 1, 2003).

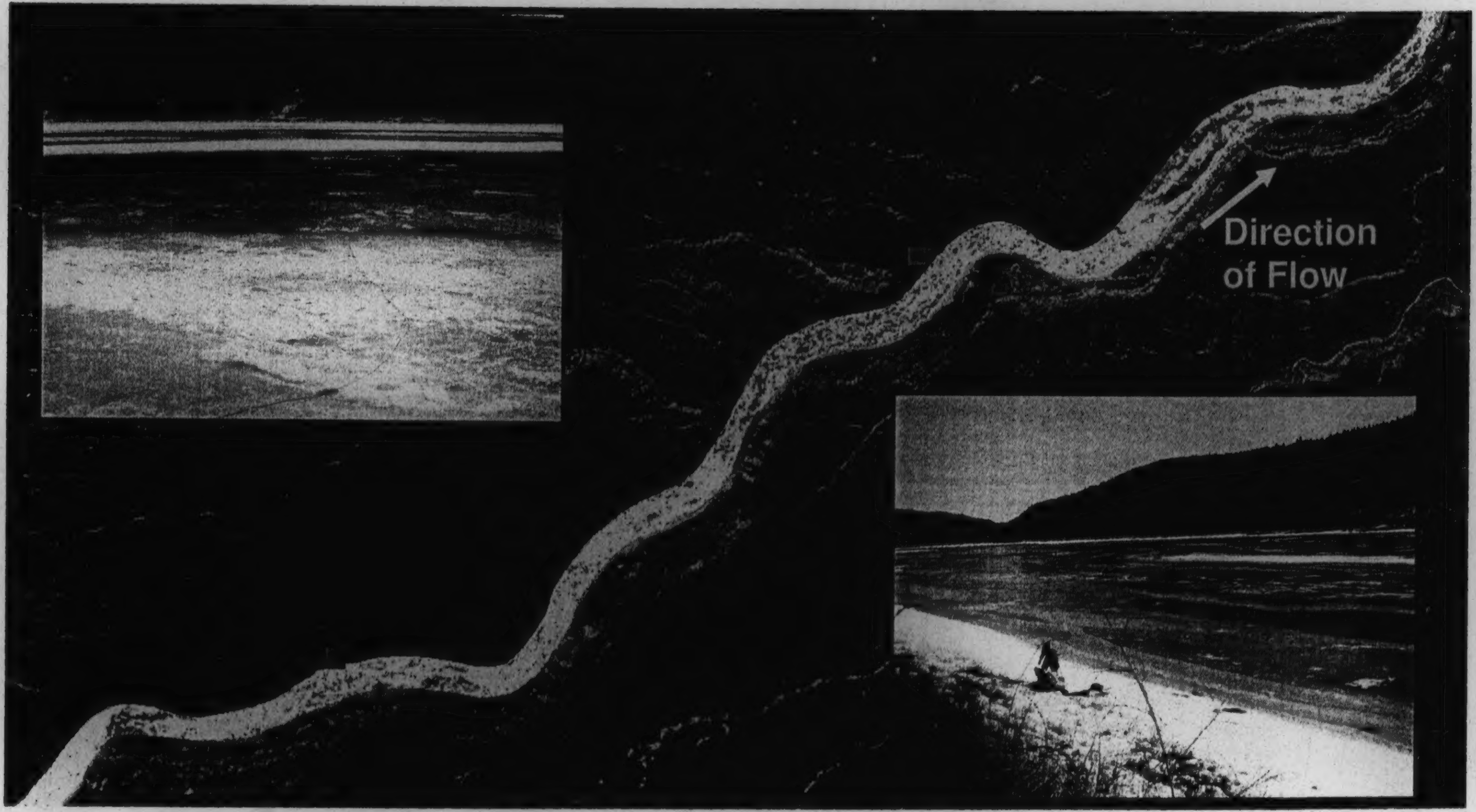
Direction
of Flow

Figure 4.14 Large extent of water present at G130 compared to the more intact ice cover at G135 (April 1, 2003).

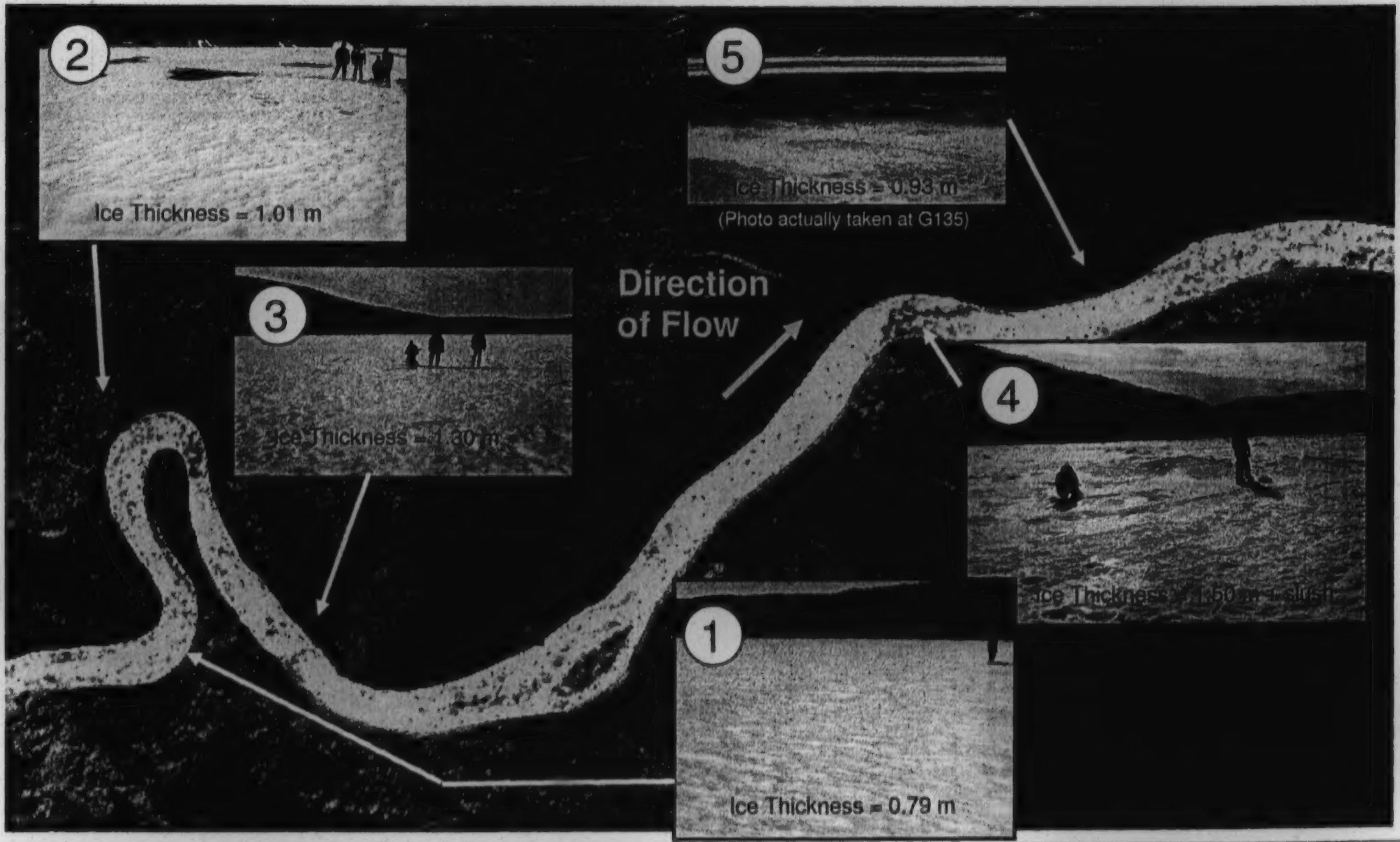
2
Ice Thickness = 1.01 m
5
Ice Thickness = 0.93 m
(Photo actually taken at G135)
3
Ice Thickness = 1.30 m
Direction
of Flow
4
Ice Thickness = 1.50 m + slush
1
Ice Thickness = 0.79 m

Figure 4.15 Ice thickness and texture at five locations in the upper portion of the study reach (April 1, 2003).

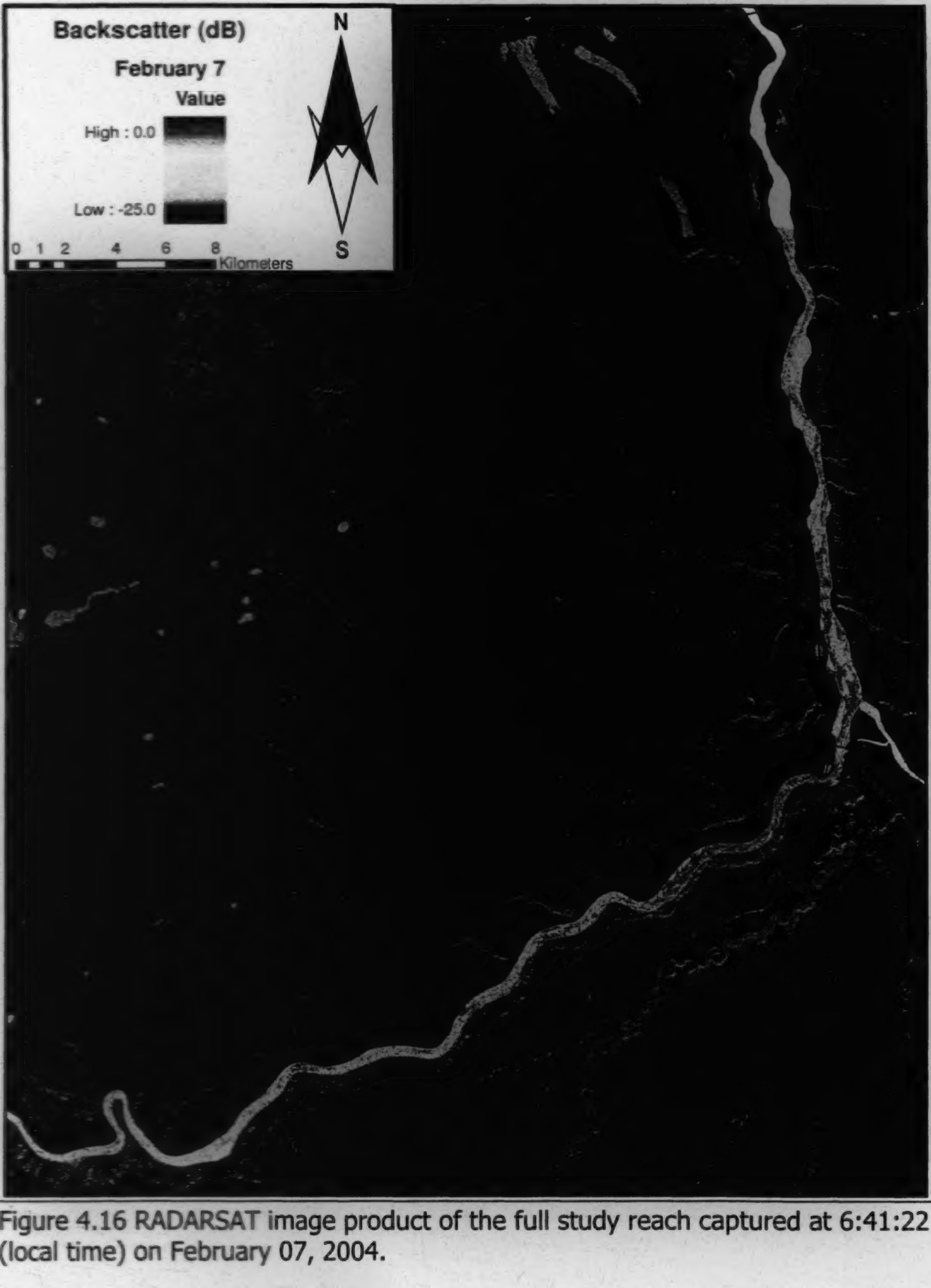
Backscatter (dB)
February 7
Value
High : 0.0
Low : -25.0
0 1 2 4 6 8 Kilometers
N
S

Figure 4.16 RADARSAT image product of the full study reach captured at 6:41:22 (local time) on February 07, 2004.

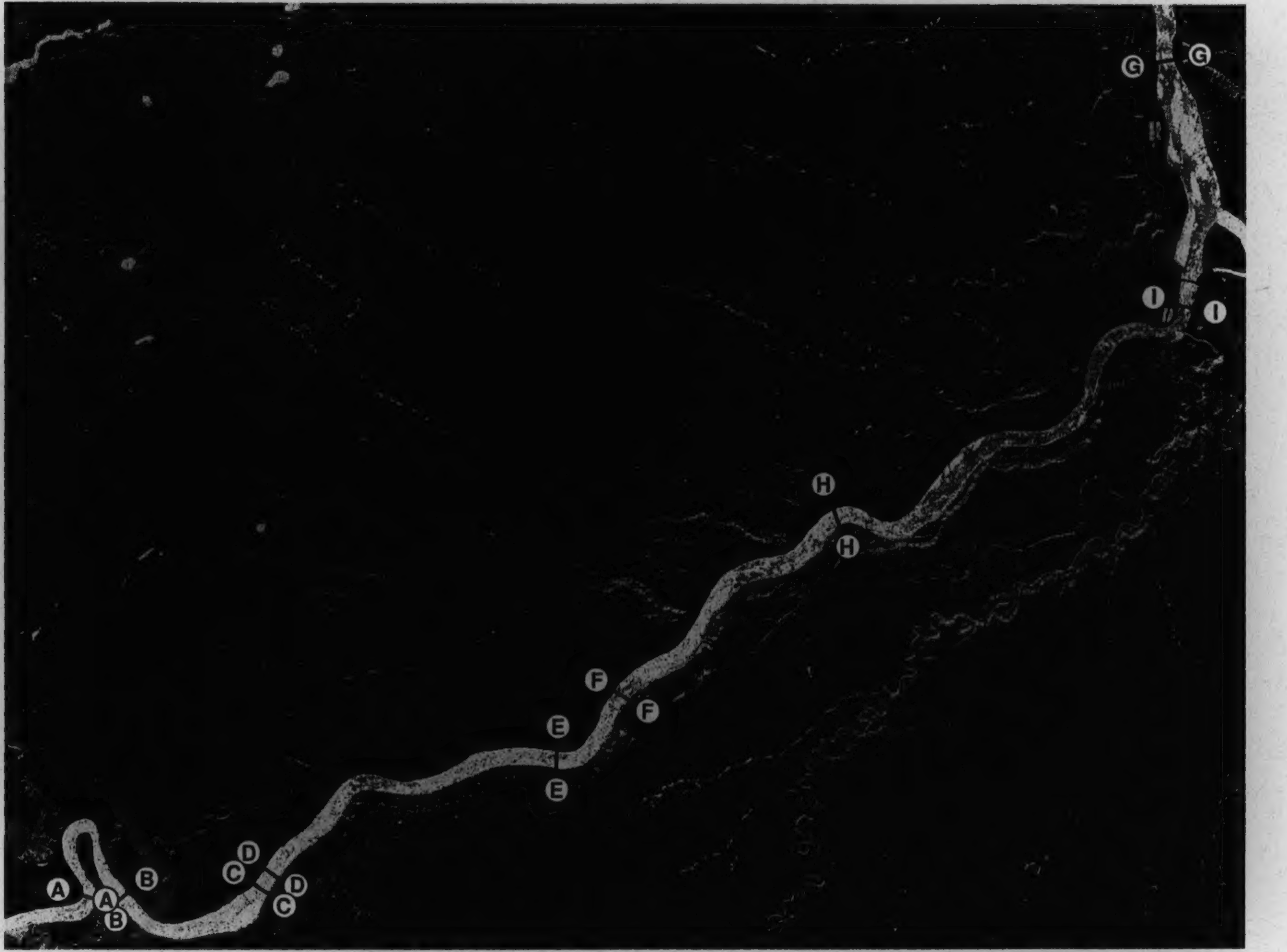
G
G
I
I
H
H
F
F
E
E
D
C
D
C
B
A
A
B

Figure 4.17 Locations of transects examined during February field study.

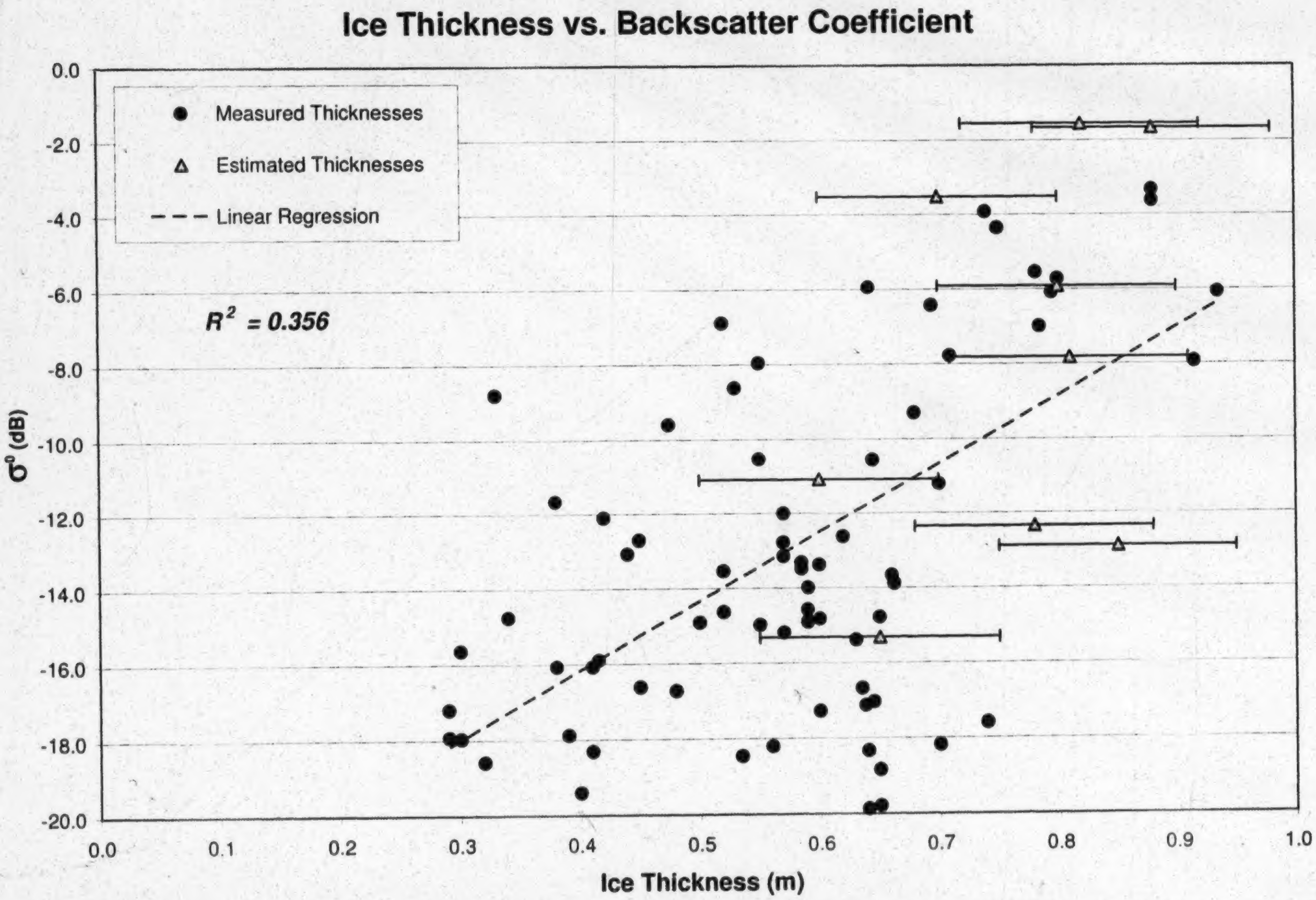

Figure 4.18 Estimated and measured ice thicknesses vs. backscatter coefficient.

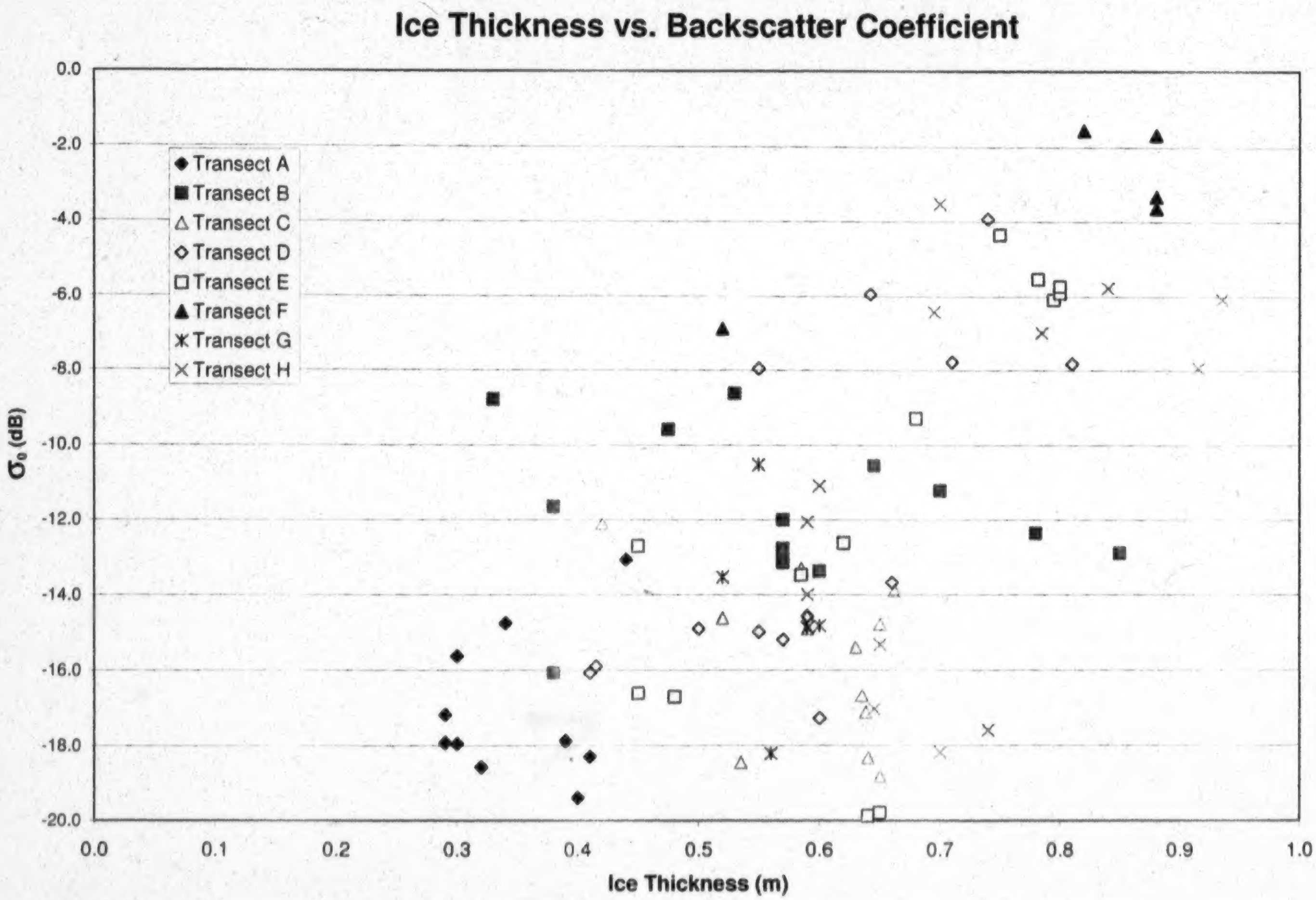

Figure 4.19 Ice thickness data plotted by transect.

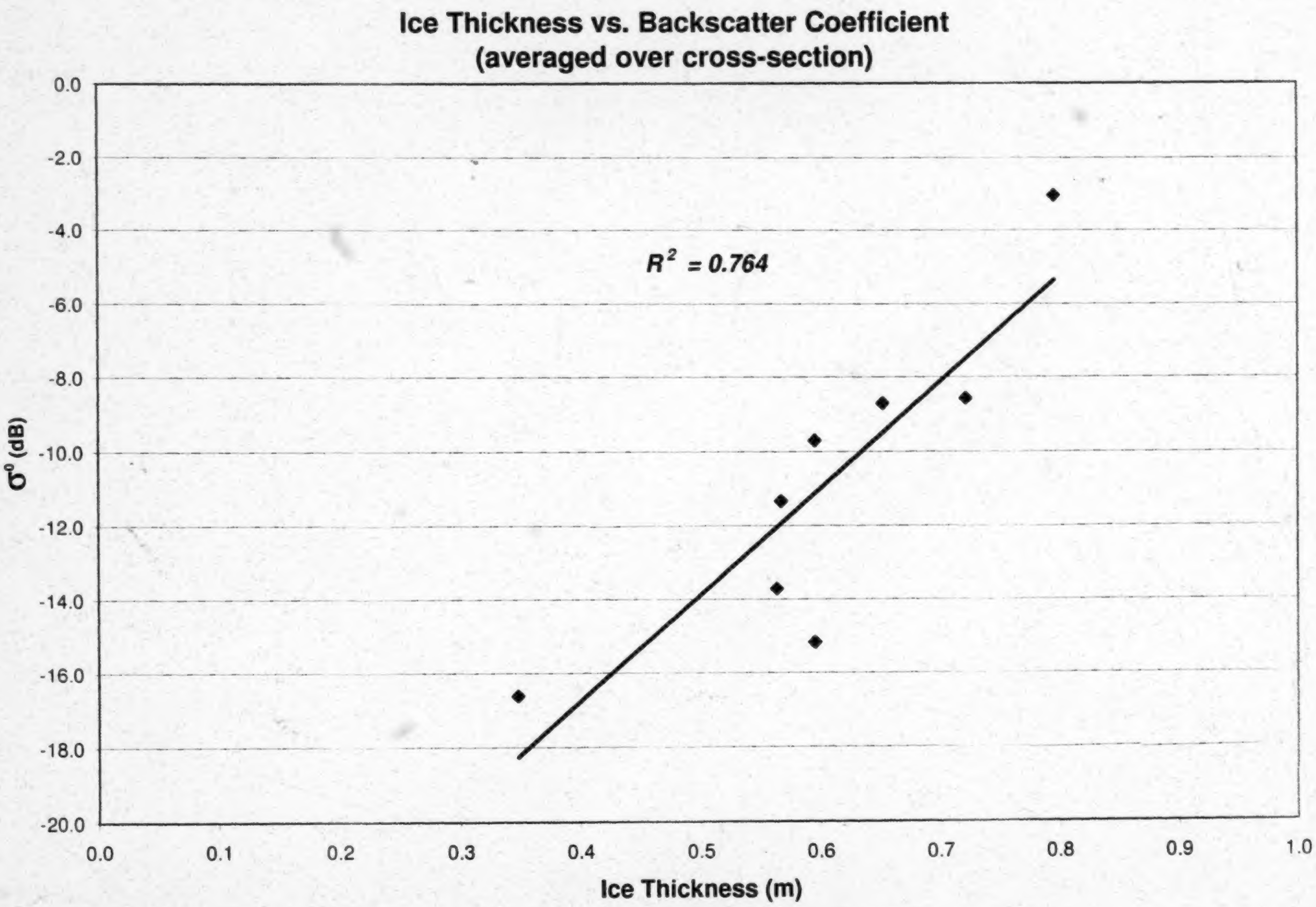

Figure 4.20 Averge cross-sectional ice thickness vs. backscatter coefficient.

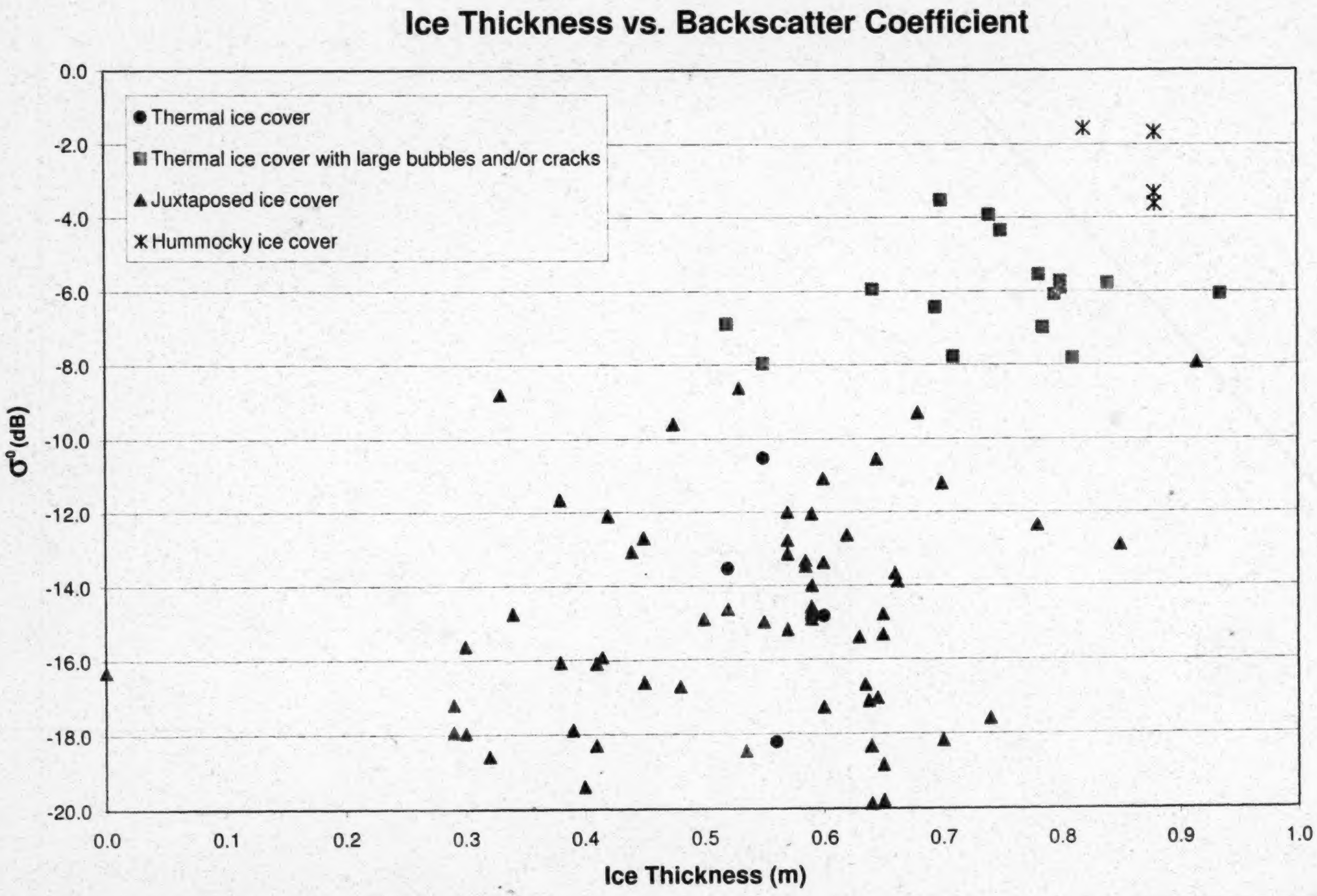

Figure 4.21 Thickness data plotted by ice type.

5.0 CONCLUSIONS AND RECOMMENDATIONS

Ice jams are a very real danger to many northern communities. These events can cause serious flood damage and occur quite suddenly, making them difficult to predict. Numerical models are being developed to facilitate forecasting, but these require reliable ice information in order to be effective. Unfortunately, the frequent inaccessibility of sites combined with the risk of working on an ice cover introduces considerable data collection challenges. The purpose of this investigation was to test the utility of SAR as a tool to monitor river breakup progression. In particular, the primary objectives were to establish whether the location and length of ice jams could be estimated and, further, to assess if more comprehensive information with regard to ice thickness or structure could be inferred.

The Athabasca River was used as a case study for this research. A 45-kilometre study reach near Fort McMurray was selected and a rigorous image acquisition schedule was adopted for the 2003 and 2004 breakup seasons. As a "first look" at the information, a purely qualitative approach was employed. Simple image processing techniques were applied to generate colourized image products: this was deemed the most comprehensible format for end users. Aerial photographs and documented observations made concurrent with image acquisitions were then used to analyze the corresponding image products. Subsequent to this approach, a somewhat more quantitative technique was applied to the data. The variability of the backscatter coefficient was explored, allowing some of the advantages and shortcomings of SAR image data to be examined. Additionally, a field investigation was carried out to determine if a meaningful correlation could be found between the backscatter coefficient and ice thickness or structure.

Several important findings were reached as a result of this investigation. These relate to the viability of SAR to monitor breakup progression as well as sensor limitations and image processing.

5.1 BREAKUP PROGRESSION

Overall, SAR data was found to be an effective means of observing river breakup. Ground truth data confirmed that it was possible to detect ice jams and estimate their approximate length. Furthermore, its usefulness at distinguishing various types of ice during breakup was demonstrated. The extent of intact ice was quite apparent and open leads could be clearly delineated. Ice roughness is an important parameter and, where present in the imagery, heavily consolidated ice could be differentiated from intact and running ice.

A field data collection program was carried out to investigate the potential of extracting more detailed information from SAR imagery. Ice thickness and structure was measured and documented at nearly 100 sites throughout the study reach. However, it was not possible to draw a strong correlation between ice thickness and backscatter. It is possible that this difference can be attributed, in part, to the limited range of ice thicknesses observed. For safety reasons, ice thicknesses could not be obtained at some (hummocky) locations and there were no measured thicknesses in excess of 1 metre. Additionally, discussion of these results with respect to previous efforts (Weber 2005) also raised the question of whether slush ice thickness could affect results.

Some support was found for the suggestion that ice structure impacts the magnitude of radar backscatter. Hummocky ice surfaces produced the highest radar return whereas locations which were cracked and/or had large bubbles in the ice surface generated a more moderate response. The lowest radar return was noted for homogeneous thermal ice covers and juxtaposed ice covers. It is probable that these two ice types do not produce a measurably different response because of the fine grained structure that is characteristic of juxtaposed ice.

The most likely inference that can be made from the mid-winter data set is that ice structure and thickness both contribute strongly to the amount of backscatter. This makes it challenging to develop a useful approach for deducing ice thickness. Fortunately, though, these two variables are not completely independent of each other. For instance, hummocky ice surfaces, which produced the highest backscatter coefficient, have a rough surface texture (on a macro scale) and composition and these ice surfaces are also normally much thicker than juxtaposed or thermal covers.

5.2 SENSOR LIMITATIONS

Various factors introduce complications to the image analysis process. Multiple image modes were utilized in order to maximize acquisition opportunities, but this made it difficult to establish a consistent basis for a meaningful quantitative evaluation. Specifically, image modes with a remarkable difference in incidence angle (as compared to that used for the majority of the images) generated the greatest degree of uncertainty. For example, as only three images were acquired using the S1 image mode, the considerably steeper incidence angle (24-31 degrees) generated an increase in backscatter. This appeared to produce a systematic difference throughout the image, relative to others collected at approximately the same time. While this did present a significant interpretation challenge, it fortunately did not prevent an examination of the overall changes to the ice cover during the breakup period.

To genuinely broaden the understanding of SAR river ice data, future investigations will undoubtedly need to address image mode considerations in greater detail. Multiple modes (and multiple sensors) will probably always be used in order for SAR data to be a viable forecasting tool. However, until this uncertainty is resolved, any quantitative assessment will continue to be limited by the unpredictability introduced by variable incidence angles. Important strides have been made in an effort to overcome this substantial roadblock (Gherboudj *et al.* 2005), but more extensive work is needed. Ultimately, a reliable and accepted methodology to "standardize" images is required.

5.3 IMAGE PROCESSING

It is not desirable to "over-process" an image, but several useful processes are necessary to make the best use of the data obtained. Due to the coherent nature of SAR image data, a speckle filter is of primary importance. Many such filters have been developed and each provides a distinct result. The selection and application of a filter should be done with care as all use an averaging process that can blur thin image details. A gamma filter used in the course of this investigation was found to provide good results.

Geocoding an image is another key process which generally needs to be performed. For the purposes of examining river ice, a rivers vector file was used to geocode the image and best results were obtained with ground control points concentrated along the length of the river (commonly at confluence locations). This is sufficient for a study of this nature. If it is preferable to select ground control points from other areas of the image or if greater precision was desired throughout the entire image area, it would be prudent to orthorectify each image using a DEM (digital elevation model).

Finally, if it is desirable to utilize an overlay in the final image product, it would be worthwhile to address the issue that channel extents will change as the water level increases and decreases. Hence, if the overlay is generated during high water conditions, there can be an obvious border along the river bank which exhibits an inconsistent backscatter coefficient. To improve clarity, the overlay should either be adaptable to varying water levels or, alternatively, it could be generated during low water conditions.

5.4 FIELD STUDIES

With regard to future field investigations, several recommendations can be made. First, site selection is a primary consideration as it will govern the quality, extent and type of data that will be collected. Scale is important and it is vital to choose a river that is of suitable size with respect to sensor resolution. It is imperative that the surrounding terrain contribute as little as possible to the radar return from the ice surface. In practice, rivers that are several hundred metres in width have been sufficient for use with both fine and standard beam imagery. A site that is easily accessible either by road or foot should ideally be chosen. This will reduce the overall cost of field work and permit more data to be gathered. Further, if breakup monitoring or ice jam detection is a key objecctive, care should be taken to select a study reach that is likely to experience a variety of ice types and thicknesses. A reach that varies in width, gradient and/or flow regime would be most appropriate.

Data collection methodology is also an important issue. To examine the effect of ice structure or thickness on radar backscatter, superior results might be acquired if target areas are selected rather than cross-sections. Due to the nature of freezeup on rivers, there can be a large degree of variability from bank to bank. Specifically, border ice normally forms before the main channel freezes and these areas can be characteristically different. As an alternative, areas exhibiting a relatively consistent backscatter coefficient could be identified beforehand. Selecting 4-5 sample sites at each such location would then be advised to obtain a representative assessment of ice conditions.

Additionally, depending on the application of the study in question, there are a number of other factors which warrant consideration. If frequency of acquisition is not a major concern, it would be prudent to select the same resolution and beam mode for each image. The data collected in the course of this study seemed to demonstrate that the S1 image mode with its relatively steep incidence angle facilitated more distinct differentiation of ice types. Slush ice below the solid ice cover is another valid concern. Therefore, it may be advisable to conduct a lab study to ascertain its impact on radar backscatter. Finally, environmental conditions should not be underestimated as liquid water content vastly alters the dielectric constant of a snow cover. When possible, collecting data during winter is preferable in order to minimize moisture effects.

6.0 REFERENCES

Brown, I.A., Kirkbride, M.P., and Vaughan, R.A. 1999. Find the firn line! The suitability of ERS-1 and ERS-2 SAR data for the analysis of glacier facies on Icelandic icecaps. International Journal of Remote Sensing, 20 (15-16): 3217-3230.

CCRS (Canada Centre for Remote Sensing). 2003. Radar Remote Sensing – Educational Resources Tutorial. Canada Centre for Remote Sensing, Ottawa, Ont. Available from *http://www.ccrs.nrcan.gc.ca/ccrs/learn/tutorials/tutorials_e.html* [accessed Mar 2004].

Drinkwater, M.R. 1989. Limex '87 ice surface characteristics: implications for c-band SAR backscatter signatures. IEEE Transactions on Geoscience and Remote Sensing, 27 (5): 501-513.

Duguay, C., Brown, R., Doucette, P., Moulton, L., and Mueller, R. Preliminary assessment of the use of SAR imagery to identify anadromous fish overwintering habitat. Canadian Journal of Remote Sensing, *In Press.*

Elachi, C., Bryan, M.L. 1976. Imaging radar observations of frozen arctic lakes. Remote Sensing of Environment, 5:169-175.

Farr, T. 2005. Radar Interactions With Geologic Surfaces, Guide to Magellan Image Interpretation. *history.nasa.gov/JPL-93-24/ch5.htm* [accessed May 2005]

Gatto, L.W. 1990. Monitoring river ice with Landsat images. Remote Sensing of Environment, 32:1-16.

Gatto, L.W. 1993. River ice conditions determined from ERS-1 SAR. Proceedings of the 50th Eastern Snow Conference, Quebec City, Quebec.

Gauthier, Y., Ouarda, T.B.M.J., Bernier, M., and El Battay, A. 2001. Monitoring the ice cover evolution of a medium size river from RADARSAT-1: preliminary results. Proceedings of the 11th Workshop on River Ice, Ottawa, Ontario.

Gauthier, Y., El Battay, A., Bernier, M. and Ouarda, T.B.M.J. 2003. An Approach Using Contextual Analysis to Monitor River Ice from RADARSAT Data. Proceedings of the 60th Eastern Snow Conference, Sherbrooke, Quebec.

Gherboudj, I., Bernier, M. and Gauthier, Y. 2005. Standardisation du Signal Radar d'Images RADARSAT-1 et ASAR pour le Suivi du Couvert de Glace en Rivière. 12ème Congrès de l'Association Québécoise de Télédétection.

Hallikainen, M., and Winebrenner, D.P. 1992. The physical basis for sea ice remote sensing. *In* Microwave remote sensing of sea ice. *Edited by* F.D. Carsey. American Geophysical Union, Geophysical Monograph 68, pp. 29-46.

Haykin, S., Lewis, E.O., Raney, R.K., and Rossiter, J.R. (*Editors*). 1994. Remote sensing of sea ice and icebergs. John Wiley & Sons, Inc., New York.

Henderson, F.M., Lewis, A.J. 1998. Introduction to radar. *In* Principles and applications of imaging radar – manual of remote sensing. 3rd ed. Vol. 2. *Edited by* F.M. Henderson and A.J. Lewis. John Wiley & Sons, Inc., New York, pp. 1-7.

Hicks, F., and Pelletier, K. 2004. 2003 Breakup Observations on the Athabasca River at Fort McMurray. Water Resources Engineering Report 2003-FH-01.

Hicks, F. 2004. Breakup 2004 Field notes.

Jasek, M., Weber, F., and Hurley, J. 2003. Ice thickness and roughness analysis on the Peace River using RADARSAT-1 SAR imagery. Proceedings of the 12th Workshop on River Ice, Edmonton, Alberta.

Kowalczyk, T. and Hicks, F. 2003. Observations of Dynamic Ice Jam Release on the Athabasca River at Fort McMurray, AB. Proceedings of the 12th Workshop on River Ice, Edmonton, Alberta.

Kowalczyk, T. 2005. Analysis of Ice Jam Release Surges on the Athabasca River at Fort McMurray, Alberta. MSc thesis. University of Alberta, Edmonton.

Leconte, R. and Klassen, D. 1991. Lake and River Ice Investigations in Northern Manitoba Using Airborne SAR Imagery. Arctic, 44 (1): 153-163.

Lewis, A.J., Henderson, F.M. 1998. Radar Fundamentals: The Geoscience Perspective. *In* Principles and applications of imaging radar – manual of remote sensing. 3rd ed. Vol. 2. *Edited by* F.M. Henderson and A.J. Lewis. John Wiley & Sons, Inc., New York, pp. 131-181.

Lopes, A., Nezry, E., Touzi, R., and Laur, H. 1993. Structure detection and statistical adaptive speckle filtering in SAR images. International Journal of Remote Sensing, 14 (9): 1735-1758.

Michel, B. 1971. "Winter Regime of Rivers and Lakes". USA Cold Regions Research and Engineering Laboratory, Springfield, Va., 131 pp.

Michel, B. and Ramseier, R. 1971. Classification of River and Lake Ice. Canadian Geotechnical Journal, 8(1): 36-45.

Moberly, H. J. and Cameron, W. B. (1929) "When Fur was King." J.M. Dent and Sons Ltd., Toronto, Canada, p. 151.

Murphy, M.A., Martini, I.P., and Protz, R. 2001. Seasonal changes in subarctic wetlands and river ice breakup detectable on RADARSAT images, Southern Hudson Bay Lowland, Ontario, Canada. Canadian Journal of Remote Sensing, 27 (2): 143-158.

Pelletier, K., Hicks, F., van der Sanden, J., and Du, Y. 2003. Monitoring breakup development on the Athabasca River using RADARSAT-1 SAR imagery. Proceedings of the 12th Workshop on River Ice, Edmonton, Alberta.

RADARSAT International. 2000. RADARSAT Data Products Specifications. *http://www.rsi.ca/products/sensor/radarsat/radarsat1.asp* [accessed May 2005]

Raney, K. 1998. Radar Fundamentals: Technical Perspective. *In* Principles and applications of imaging radar – manual of remote sensing. 3rd ed. Vol. 2. *Edited by* F.M. Henderson and A.J. Lewis. John Wiley & Sons, Inc., New York, pp. 9-130.

Robichaud, C. 2003. Hydrometeorological factors influencing breakup ice jam occurrence at Fort McMurray, Alberta. MSc thesis. University of Alberta, Edmonton.

She, Y. and Hicks, F. 2005. Incorporating Ice Effects in Ice Jam Release Surge Models. Proceedings of the 13th Workshop on River Ice, Hanover, NH.

Tracy, B.T., and Daly, S.F. 2003. River ice delineation with RADARSAT SAR. Proceedings of the 12th Workshop on River Ice, Edmonton, Alberta.

van der Sanden, J. 2004. Personal communication.

Weber, F. 2005. Personal communication.

Weber, F., Nixon, D., and Hurley, J. 2003. Semi-automated classification of river ice types on the Peace River using RADARSAT-1 synthetic aperture (SAR) imagery. Canadian Journal of Civil Engineering, 30 (1): 11-27.